DEPLOYMENT AND VALIDATION OF LOW-COST WIRELESS SENSORS FOR REAL-TIME LIFELINE CONDITION ASSESSMENT

FINAL PROJECT REPORT

by

Kelli R. Slaven
Daniel J. Borello
Oregon State University

Sponsorship
PacTrans
Oregon State University

for
Pacific Northwest Transportation Consortium (PacTrans)

USDOT University Transportation Center for Federal Region 10

University of Washington
More Hall 112, Box 352700
Seattle, WA 98195-2700

In cooperation with US Department of Transportation-Research and Innovative Technology Administration (RITA)

Disclaimer

The contents of this report reflect the views of the authors, who are responsible for the facts and the accuracy of the information presented herein. This document is disseminated under the sponsorship of the U.S. Department of Transportation's University Transportation Centers Program, in the interest of information exchange. The Pacific Northwest Transportation Consortium, the U.S. Government and matching sponsor assume no liability for the contents or use thereof.

Technical Report Documentation Page

1. Report No.	2. Government Accession No.	3. Recipient's Catalog No.	
4. Title and Subtitle DEPLOYMENT AND VALIDATION OF LOW-COST WIRELESS SENSORS FOR REAL-TIME LIFELINE CONDITION ASSESSMENT		**5. Report Date** 10/15/2016 **6. Performing Organization Code**	
7. Author(s) Kelli R. Slaven, Daniel J. Borello		**8. Performing Organization Report No.**	
9. Performing Organization Name and Address PacTrans Pacific Northwest Transportation Consortium University Transportation Center for Region 10 University of Washington More Hall 112 Seattle, WA 98195-2700		**10. Work Unit No. (TRAIS)** **11. Contract or Grant No.** DTRT	
12. Sponsoring Organization Name and Address United States of America Department of Transportation Research and Innovative Technology Administration		**13. Type of Report and Period Covered** Research **14. Sponsoring Agency Code**	
15. Supplementary Notes Report uploaded at www.pacTrans.org			

16. Abstract

The Pacific Northwest is at risk for significant seismic and tsunami events, which are capable of severely damaging lifeline transportation infrastructure, particularly bridges. As the bridges in the United States age and begin to show signs of fatigue, the risk for severe damage increases. Proper monitoring and inspection of bridges is becoming increasingly important as bridges age, especially with the high likelihood of a significant seismic event. Structural health monitoring systems can be used to evaluate the condition of bridges throughout the area, and to quickly determine the state of lifeline bridges after a disaster.

With technology advancing rapidly and making widespread monitoring possible, there exists a gap between the monitoring systems and the interpretation and presentation of recorded data. A framework needs to be developed to relay useful information to bridge owners and decision makers based on sensor readings.

Numerical models of eight prototype bridges typical to the region were developed using the OpenSees FEA package. The numerical models were subject to a suite of ground motions to simulate the demands anticipated in the Pacific Northwest. The damage state of the bridges were compared to metrics that were measurable by using wireless bridge sensors. Recommendations were developed to permit wireless sensor data to be related to bridge performance.

17. Key Words	18. Distribution Statement No restrictions.		
19. Security Classification (of this report) Unclassified.	**20. Security Classification (of this page)** Unclassified.	**21. No. of Pages**	**22. Price** NA

Form DOT F 1700.7 (8-72) **Reproduction of completed page authorized**

Table of Contents

Executive Summary……xi
Chapter 1 Introduction 1
1.1 Background 1
1.2 Structural Health Monitoring 2
1.3 Bridge Monitoring Systems 3
1.4 Project Objective 5
Chapter 2 Literature Review 7
2.1 Wireless Sensor Technology 7
2.2 OpenSees 11
2.3 Bridge Models 13
2.4 Model Analysis 19
Chapter 3 Benchmark Suite Models 25
3.1 Model Description 25
3.2 Deck Section 27
3.3 Column Sections 29
3.4 Abutments 36
3.5 Connections 37
3.6 Damping 38
Chapter 4 Structural Response 39
4.1 Gravity Load 39
4.2 Ground Motions 41
4.3 Recorders 42
4.4 IDA Plots 43
4.5 Strain Response 44
4.6 Hand Calculations for Strain 52
Chapter 5 Damage State Detection Utilizing Strain Measurements 55
5.1 Strain Limits 55
5.2 Recommendations 57
Chapter 6 Conclusions and Future Research 59

6.1 Wireless Sensor Networks 59
6.2 Future Research 60
References 63
Bibliography……..…66
Appendix A. Ground Motion Suite 67
Ground Motion Time History Plots 67
Appendix B. Strain Data 75
Maximum Strain vs Maximum Drift Plots 75
Residual Strain vs Residual Drift Plots 81
Maximum Strain Limit Values 89
Residual Strain Limit Values 91

List of Figures

Figure 2.1 Single-hop network topology (Zhou and Yi, 2013). 8

Figure 2.2 Multihop network topologies (Zhou and Yi, 2013). 9

Figure 2.3 Levels of component definition in OpenSees (Mazzoni et al., 2006). 12

Figure 2.4 Bridge Type 1 (Ketchum et al., 2004) 16

Figure 2.5 Bridge Type 11 (Ketchum et al., 2004) 17

Figure 2.6 IDA curves for a five-story steel braced frame (T1=1.8s) subjected to four different records. (Vamvatsikos and Cornell, 2002) 20

Figure 2.7 Damage state boundaries adopted by Mander, 1999. 21

Figure 3.1 Simplified bridge layout 25

Figure 3.2 Model g.eometry 26

Figure 3.3 Deck cross-section (Ketchum et al., 2004)..... 28

Figure 3.4 Deck fiber section defined in OpenSees 28

Figure 3.5 Axial push-pull behavior of the deck section. Compression (left) and tension (right).29

Figure 3.6 Moment-rotation behavior of the deck section 29

Figure 3.7 Column cross-sections..... 30

Figure 3.8 Axial push-pull behavior of Column 1A section. Compression (left) and tension (right). 31

Figure 3.9 Moment-rotation behavior of Column 1A section. 31

Figure 3.10 Axial push-pull behavior of Column 1B section. Compression (left) and tension (right). 32

Figure 3.11 Moment-rotation behavior of Column 1B section..... 32

Figure 3.12 Axial push-pull behavior of Column 11A section. Compression (left) and tension (right). 33

Figure 3.13 Moment-rotation behavior of Column 11A section. 33

Figure 3.14 Axial push-pull behavior of Column 11B section. Compression (left) and tension (right). 34

Figure 3.15 Moment-rotation behavior of Column 11B section..... 35

Figure 3.16 Modeled spring abutment longitudinal (left) and transverse (right) response in kips and inches. 37

Figure 4.1 Displaced shape of Bridge 1Ar deck under gravity load. 39

Figure 4.2 Approximate strain recorder locations 43

Figure 4.3 IDA plot for Bridge 11Ar.....44

Figure 4.4 Maximum strain vs. maximum drift for Bridge 1Ar with ground motion in the longitudinal direction. 45

Figure 4.5 Maximum strain vs. maximum drift for Bridge 1Ar with ground motion in the transverse direction. 46

Figure 4.6 Maximum strain vs. maximum drift for Bridge 11Ar with ground motion in the longitudinal direction. 47

Figure 4.7 Maximum strain vs. maximum drift for Bridge 11Ar with ground motion in the transverse direction. 48

Figure 4.8 Residual strain vs. residual drift for Bridge 1Ar with ground motion in the longitudinal direction. 49

Figure 4.9 Residual strain vs. residual drift for Bridge 1Ar with ground motion in the transverse direction. 50

Figure 4.10 Residual strain vs. residual drift for Bridge 11Ar with ground motion in the longitudinal direction. 51

Figure 4.11 Residual strain vs. residual drift for Bridge 11Ar with ground motion in the transverse direction. 52

Figure 4.12 Hand calculations for strain plotted with 1Br model data 53

Figure 4.13 Hand calculations for strain of model 1Br in elastic region 54

List of Tables

Table 2.1 Bridge type matrix (Ketchum et al., 2004) 14
Table 2.2 Column design summary for Type 1 bridge (Ketchum et al., 2004) 18
Table 2.3 Column design summary for Type 11 bridge (Ketchum et al., 2004) 19
Table 2.4 Damage states defined by Mander et al., 2007. 22
Table 2.5 Maximum column drift damage states (Mackie et al., 2008) 23
Table 2.6 Repair items for maximum column drift damage states (Mackie et al., 2008)..... 23
Table 3.1 Characteristics of eight bridge models 26
Table 3.2 Natural periods of bridge models 27
Table 3.3 Tension and compression strengths of model sections. 35
Table 3.4 Moment capacity of column sections 36
Table 4.1 Ground motion suite information. 40
Table 5.1 Maximum strain limits for Type 1 bridges 56
Table 5.2 Maximum strain limits for Type 11 bridges 56
Table 5.3 Residual strain limits for Type 1 bridges 57
Table 5.4 Residual strain limits for Type 11 bridges 57

Executive Summary

The Pacific Northwest is at risk for significant seismic and tsunami events, which are capable of severely damaging lifeline transportation infrastructure, particularly bridges. As the bridges in the United States age and begin to show signs of fatigue, the risk for severe damage increases. Proper monitoring and inspection of bridges is becoming increasingly important as bridges age, especially with the high likelihood of a significant seismic event. Structural health monitoring systems can be used to evaluate the condition of bridges throughout the area, and to quickly determine the state of lifeline bridges after a disaster.

With technology advancing rapidly and making widespread monitoring possible, there exists a gap between the monitoring systems and the interpretation and presentation of recorded data. A framework needs to be developed to relay useful information to the owners and decision makers based on sensor readings.

Numerical models of eight prototype bridges typical to the region were developed using the OpenSees FEA package. The numerical models were subject to a suite of ground motions to simulate the demands anticipated in the Pacific Northwest. The damage state of the bridges was compared to metrics measurable using wireless bridge sensors. Recommendations were developed permitting wireless sensor data to be related to bridge performance.

Chapter 1 Introduction

1.1 Background

As bridges in the United States age and begin to show signs of fatigue, monitoring and inspection is becoming increasingly important. Many interstate highway bridges were built in the 1950's or earlier and are at the end of their original design lives. Over 500 bridges partially or totally collapsed in the United States between 1989 and 2000 due to various triggering events (Zhou 2013). The Pacific Northwest is at risk for significant seismic and tsunami events, which are capable of severely damaging the lifeline transportation infrastructure, particularly bridges. Structural health monitoring systems can be used to evaluate the condition of bridges throughout the area and to quickly determine the state of lifeline bridges after such events. With such a large number of aging bridges to maintain and assess, the development of efficient monitoring systems is critical for community resilience after a disaster.

Federal requirements mandate biannual visual inspections of bridges in the U.S. Therefore, the entire inventory of more than 580,000 bridges in the U.S. are visually inspected biannually, but these inspections can be highly subjective and do not detect subsurface damage (Wang 2007). A study conducted by the Federal Highway Administration in 2001 found that 56 percent of medium to short span bridges that were given average condition ratings by trained inspectors were improperly evaluated (Zhou 2013).

Visual inspections of structures are often required after major events as well. For example, following the 1994 Northridge earthquake in California, many buildings had to be inspected before they were allowed to reopen. This resulted in buildings remaining closed for several days before inspectors were available to perform the inspections. These inspections are also very expensive. The cost of inspecting connections of steel moment frame buildings after Northridge ranged from $200 to $1000 for each welded connection (Lynch 2007).

Because of the subjective, labor-intensive, and costly nature of currently mandated visual inspections, structural health monitoring systems can be a better solution to efficiently monitor the aging infrastructure. These systems can provide facility managers with the opportunity to adopt condition-based maintenance strategies rather than just schedule-based strategies, and allow immediate evaluation of structural integrity following a seismic event (Lynch 2007).

1.2 Structural Health Monitoring

Structural health monitoring (SHM) techniques have been used for the past several decades to assist in monitoring and damage detection of civil structures, including bridges. Global health monitoring methods determine whether damage is present in the structure, but not necessarily the exact location or extent of the damage, and have traditionally been used for bridges. Once damage has been detected, further examination of the structure can lead to the determination of the severity and exact location of the damage.

Most of these global monitoring methods focus on detecting changes to a structure's dynamic properties, such as mode shapes or natural frequencies. Damage to structural members can cause these parameters to shift. However, changes in temperature or other environmental factors can also produce shifts in the dynamic characteristics of a bridge. Early studies found that the loss of a single structural member can result in changes in the natural frequency of 1 to 30 percent. If a member that is damaged is not excited in the fundamental mode, the loss of that member would not affect the fundamental frequency or mode shape. While these global methods are useful in detecting significant damage to the overall structure, they may not be effective in sufficiently assessing or characterizing damage that is inherently a localized phenomenon.

Local health monitoring methods include non-destructive evaluation methods to detect local damage, such as cracking in a member. These methods provide more detailed information

on the location and severity of damage, but they are often much more expensive and time consuming than global methods. This makes it necessary to use both global and local health monitoring methods. Recently, many research projects have been funded to improve health monitoring methods and technologies and allow more complete and accurate data to be collected. As new sensors and technologies are developed, improved structural health monitoring methods are becoming increasingly feasible (Chang et al. 2003).

1.3 Bridge Monitoring Systems

Traditionally, wired systems have been used to monitor bridges. These systems can be very expensive and difficult to install, and they usually need to be installed during construction. The installation of a commercial cable-based system often exceeds a few thousand dollars per sensing channel (Wang et al. 2007). For example, the Bill Emerson Memorial Bridge had an average cost per channel of over $15,000, including installation costs, for its 84 accelerometer channels (Jang 2013). Additionally, the wires can obstruct the function of the structure and may limit the number of sensors that can be installed.

As technology advances, the disadvantages of these wired monitoring systems become more apparent, and the development of wireless systems becomes more critical. Some of the disadvantages to wired structural health monitoring systems that can be addressed by wireless systems are high cost, low efficiency, susceptible disturbance, and inflexibility (Zhou 2013).

Jang (2013) proposed a wireless system to instrument the Bill Emerson Memorial Bridge that would cost less than $500 per channel, including solar panels, as compared to the $15,000 per channel cost of the wired system. Wireless systems can also be much more flexible than wired systems, since new channels will not need to have cables run to new locations. For these

reasons, research is being conducted by numerous researchers to develop effective wireless sensors for structural monitoring applications.

Because of the relatively low cost of wireless sensors, a higher number of sensor channels per structure becomes plausible. This dense sensor deployment would allow for detailed local health monitoring in addition to the global monitoring already possible with wired systems, and would provide much greater insight to the structure's behavior (Lynch 2007). According to Zhou (2013), "bridge health monitoring using a network of wireless sensors is one of the most promising emerging technologies and is seen as the next generation of SHM."

Strain gauges are widely used as the sensors for structural health monitoring. They are relatively inexpensive and easy to install, and they are sensitive enough to detect small changes in a structure. Because strain gauges have commonly been used in traditional wired systems, the technology has become advanced and there is a large amount of knowledge on interpreting strain data (Choi et al., 2008). These advantages make strain gauges a very suitable choice for use in wireless sensor networks.

While the technology for structural health monitoring is becoming increasingly advanced, there still remains the need for a framework to make decisions based on the data obtained. The data from these sensors should be used to instruct bridge inspection and maintenance. At this point, there is a gap between the advanced monitoring technology and the useful application of the data collected. Work must be done to determine how best to process the data and produce information that will be directly useful to bridge inspectors and owners and will allow them to make informed decisions.

1.4 Project Objective

The objective of this project was to develop and use OpenSees bridge models to determine a relationship between strain data and damage states that could provide a useful framework for decision making. These models are used to determine how sensor readings can be directly related to the condition of a bridge and provide meaningful information for decision makers. Based on sensor readings, the state of a bridge can be quickly assessed, and recommendations for the maintenance or repair of a bridge can be made. This will allow bridge officials to quickly assess the condition of lifeline bridges after a natural disaster and to relay that information to first responders who need to know the most efficient routes. This report discusses background information on wireless sensor networks for use in bridge monitoring and focuses on the OpenSees models that have been developed.

Chapter 2 Literature Review

This section includes a literature review of articles and topics relevant to this research. This review will provide important context and background information.

2.1 Wireless Sensor Technology

Wireless sensors for structural health monitoring were first proposed in 1998 by Straser and Kiremidjian, who studied the integration of wireless radios into sensor networks to reduce the high cost. Several researchers have investigated the use of wireless sensors and the development of wireless sensor networks since this first study (Lynch 2007). However, wireless sensors for SHM have often leveraged proprietary platforms. Technology has advanced rapidly in recent years, and there are many new and advanced off-the-shelf components that can be used in wireless sensor networks.

Zhou and Yi (2013) identified the key issues and components of wireless sensor networks used in bridge health monitoring as the wireless sensor, network topology, data processing technology, power management, and time synchronization. The wireless sensors are the data acquisition nodes, which include the structural sensing element (such as a strain gauge), onboard microprocessor, and wireless communication element. There are two methods typically used to create high performance wireless sensors. The first is to combine commercially available platforms with customized sensor boards, while the second is to use both customized platforms and sensor boards.

A network topology is used to organize the wireless sensors in the network and enable them to cooperate with each other. Commonly used topologies can be classified into single-hop and multihop networks. The single-hop network places the central server at the center of the network, and data are transmitted from each wireless sensor to the base station server by a single

hop, as shown in figure 2.1. The limited range of most wireless radios, combined with long spans, makes single-hop network topologies impractical for many bridge monitoring applications, and multihop networks become a more practical alternative. Multihop networks transfer data between nodes and to the base station by multihop communication. The data are transmitted to the end point using intermediate nodes. Multihop networks can become very complex, and each node must determine the most efficient route to send data to the server. There are four categories that multihop networks can be classified into: mesh-type networks, tree networks, linear multihop networks, and random multihop networks, as shown in figure 2.2 (Zhou and Yi 2013).

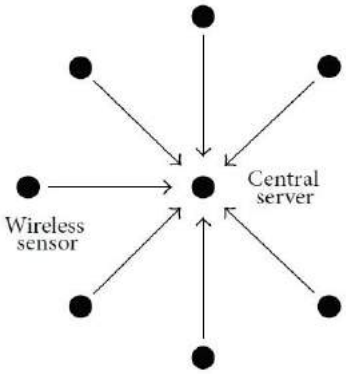

Figure 2.1 Single-hop network topology (Zhou and Yi, 2013).

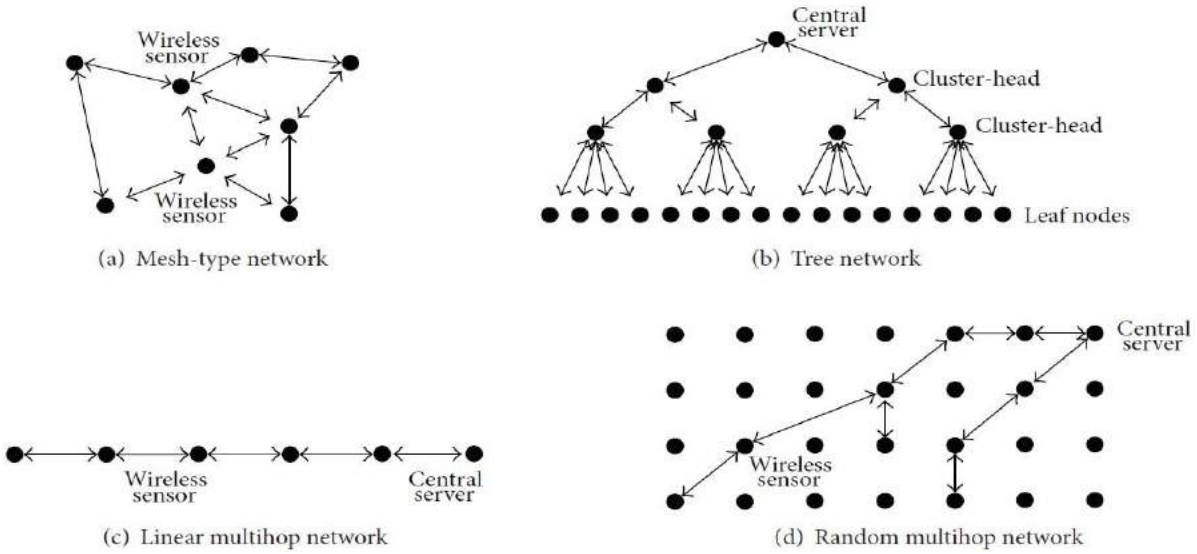

Figure 2.2 Multihop network topologies (Zhou and Yi, 2013).

The next component discussed by Zhou and Yi is the data processing technology. Since the low cost of wireless sensors allow for a dense array of nodes, a very large amount of data are generated by the wireless monitoring system. The data processing technology used to handle all of these data becomes an important part of a successful wireless sensor network. The main strategies for data processing are centralized and distributed processing. With a centralized data processing strategy, all data are sent back to a central server for further processing. This is the strategy used in traditional wired monitoring systems. However, there are huge power and bandwidth requirements involved in sending all data from the sensors to the central server, and it is not a highly efficient strategy. Distributed data processing involves locally processing data at the sensor node using the onboard microprocessor before sending information to the central server. This allows for unnecessary information to be eliminated, and the amount of data sent to the server to be reduced. (Zhou and Yi 2013)

The final components discussed by Zhou and Yi (2013) are power management and time synchronization. Wireless sensors are typically battery powered, which provides a limited

capacity. Once all of the power from the battery has been consumed, replacement can become very expensive and possibly impossible because of the location of the sensor node. Since these sensor networks are typically designed for long deployments, power management becomes one of the biggest considerations for deployment of a large-scale bridge monitoring wireless sensor network. Three ways to manage power within a wireless sensor network are through low power consumption hardware, power efficiency (such as using sleep mode and network optimization), and power harvesting through techniques such as solar panels. Based on research in the field, harvesting solar energy may be one of the most effective choices to power a network.

Time synchronization is also a concern in wireless sensor networks. An error with time synchronization can cause inaccuracies in the data, especially with mode shape construction of higher modes. This error is caused by the delay of radio transmission or by internal clock drift. Time synchronization has been one of the most addressed issues in wireless sensor networks, and several protocols have been developed. Two of the most promising are the flooding time synchronization protocol and the timing-sync protocol (Zhou and Yi 2013). Strain gauges do not have the same time synchronization issues that other sensor types, such as accelerometers, have.

With these components and issues in mind, certain requirements and characteristics have been laid out for wireless sensor networks used in bridge health monitoring. Zhou and Yi (2013) defined requirements including high resolution, high frequency, high speed, high reliability, long lifetime, time synchronization, various signal formats, long distance transmission, and fixed sensor locations. Many of these requirements are not necessary for the traditional wired system, and some create unique issues with wireless sensor network design. Some critical issues identified by Jang et al. (2010) include power management, energy harvesting, fault tolerance, autonomous operation, and environmental hardening. Environmental concerns are generally addressed by placing the sensor node in an environmentally hardened enclosure with the antenna

mounted externally (Jang et al. 2010). Power consumption is a critical issue that still needs to be fully addressed. Work must be done to create wireless sensors with hardware designed to allow for long-term deployments. Power harvesting technologies will be the solution, but there is still much work to be done to advance these technologies and make them more efficient. There are technologies under development that might offer power harvesting from ambient structural vibrations, which could be a very efficient solution for bridge monitoring systems (Lynch 2007).

As technology becomes more advanced, increasingly efficient and powerful wireless sensor systems will be developed. However, the application of the data from theses sensors to instruct bridge inspection and maintenance is still in its initial stages. A gap exists between the structural health monitoring technology and a useful application of the data collected. With the appropriate data processing, structural health monitoring could be used to provide direct information to bridge inspectors and owners (Ko and Ni 2005). Bridge models can be used to understand the data that might be collected from sensors and how to apply those data in a way that could be useful in determining the state of a bridge.

2.2 OpenSees

OpenSees, Open System for Earthquake Engineering Simulation, is an open source structural analysis program used to simulate the seismic response of structures (Mazzoni et al., 2006). It is capable of modeling and analyzing nonlinear responses using a wide range of material models, element types, and solution algorithms. OpenSees is based on the finite element method, which is the most adaptable approach for modeling the response of structures. Therefore, OpenSees is well-suited for a wide range of applications, including bridge modeling (Scott et al 2008).

The string based Tool Command Language (Tcl) is used to build models and run analyses in OpenSees. The Tcl scripting language supports commands to define geometry, loading, and

solution strategies for the model to allow users to combine software building blocks for their customized applications (Scott et al 2008). Each component of a model can be defined at a number of levels. The first is the element level, which defines the force-deformation model. The section level describes the moment-curvature model, and the fiber level defines the material stress-strain model. Figure 2.3 shows these levels and their relation to the component they describe (Mazzoni et al 2006). These levels of definition allow users to create complex models with the accurate behavior they are aiming to model. The recorder command can be used to record responses at each of these levels at user defined points. Using this command at critical points can help users to understand the behavior of the structure, and obtain information about the specific characteristics they are interested in.

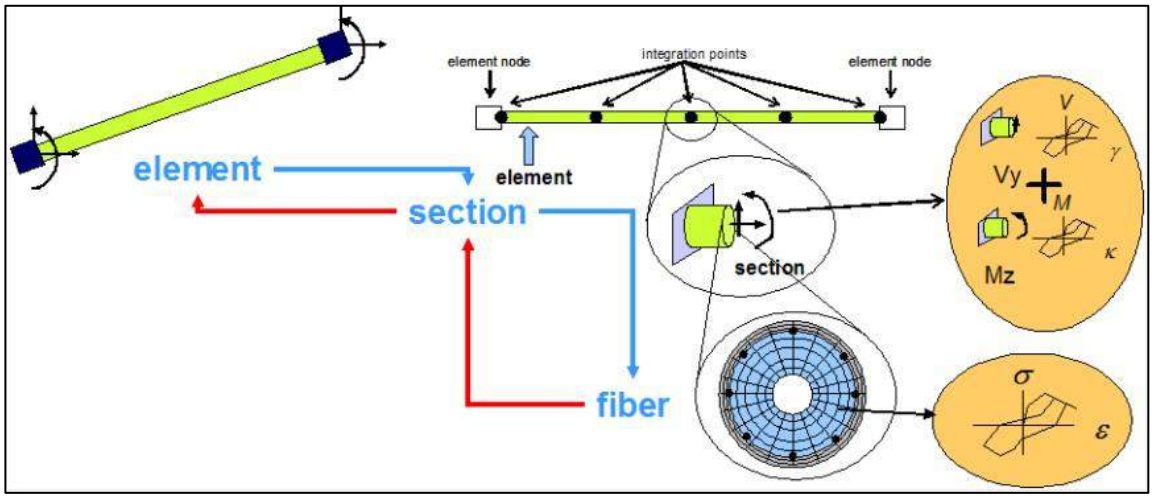

Figure 2.3 Levels of component definition in OpenSees (Mazzoni et al., 2006).

Many different types of elements can be defined in OpenSees models, depending on the desired behavior of the element. Elastic and nonlinear elements can be combined in a model, allowing users to focus on the members they are concerned with. According to literature about bridge modeling, certain components should be considered as nonlinear, including piers,

abutments, expansion joints, bearings, and soil-structure interactions. The superstructure remains elastic in most cases, and does not necessarily need to be modeled as nonlinear (Simon 2010).

OpenSees offers many options to customize a model and the analysis of that model, so it is a very powerful tool for modeling structures. Finite element analysis software and highpowered computers are becoming more advanced, which has allowed three-dimensional finite element analysis to become popular for even straightforward bridge analyses (Chung and Sotelina, 2006).

2.3 Bridge Models

The concrete box girder models used for this project were based on a study on benchmark reinforced concrete bridges (Mackie et al., 2008). These models were taken from an earlier paper by Ketchum et al. (2004) and are classified as "ordinary standard bridges" by the Caltrans Seismic Design Criteria (Caltrans, 2004). To be classified as an ordinary standard bridge, a bridge must meet certain criteria, including being of standard concrete construction, having less than 90-meter span lengths, and having no eccentricities or special bearings. Ketchum et al. (2004) selected 11 of the most prevalent ordinary construction types for a study on bridge construction cost and generated designs conforming to the Seismic Design Criteria. Out of these 11 bridge types, two continuous, five-span, straight, post-tensioned, cast-in-place, box girder bridges on monolithic piers were selected for the study by Mackie et al. (2008).

The 11 bridge types selected by Ketchum et al. (2004) were based on the dominant types of highway bridges in California. It was found that the four most prevalent types of bridges were post-tensioned cast-in-situ box girders on monolithic piers, pre-tensioned pre-cast concrete Igirders on bearings supported by piers, concrete slabs on pile extensions, and steel plate girders on bearings supported by piers. Of these four types, the concrete box girder and concrete I-girder bridges are most common. According to the 2005 National Bridge Inventory, 85 percent of all

bridges are made of concrete or prestressed concrete, and 90 percent of all Caltrans bridges are either concrete box girder or I-girder bridges (Ketchum et al 2004.) Because of this fact, the study focused on these two bridge types only and eliminated slab on pile extensions and steel plate girder bridges from consideration in the study.

The bridge type matrix, shown in Table 2.1 below, describes each of the benchmark bridge configurations studied by Ketchum et al. (2004). Four of the eleven bridge configurations were not considered and are not included in the bridge type matrix. The characteristics of each of the bridge configurations were chosen to represent typical statewide bridge construction. Each of the bridges was designed with some simplifications in comparison to real structures in order to remove complexities that might obscure results (Ketchum et al 2004).

Table 2.1 Bridge type matrix (Ketchum et al., 2004)

Bridge Type	Structure Type	Geometry	Deck Width	Deck Depth	Span Arrangement	Bent Columns	Column Height
1	CIP/PS box	Straight	39'	6'	120'+150'+150'+150'+120'	1	22'
3	CIP/PS box	Straight	39'	4'	80'+100'+100'+100'+80'	1	22'
4	CIP/PS box	Straight	68'	4'	80'+100'+100'+100'+80'	3	22'
6	PC/PS girder	Straight	68'	5'-2"	80'+100'+100'+100'+80'	3	22'
9	CIP/PS box	1000' radius	27'	6'	120'+150'+150'+150'+120'	1	22'
10	CIP/PS box	30° skew	68'	4'	80'+100'+100'+100'+80'	3	22'
11	CIP/PS box	Straight	39'	6'	120'+150'+150'+150'+120'	1	50'

Each bridge in the bridge type matrix was designed in compliance with Caltrans standards for “ordinary bridges.” This includes the design philosophy of weak column/strong beam. In a severe earthquake, the columns should yield and dissipate energy while the superstructure and foundation remain essentially elastic (Ketchum et al. 2004).

Mackie et al. (2008) selected the two continuous, five-span, straight, post-tensioned, castin-place, box girder bridges on monolithic piers for their study, which are bridge Type 1 and

Type 11 in the bridge type matrix. These same benchmark bridge models were adopted by all of the research teams within the Pacific Earthquake Engineering Research (PEER) bridge group.

Geotechnical teams at the University of Washington (Kramer et al., 2008) and the University of California, Berkeley (Ledezma and Bray, 2008) used bridge Type 1A to analyze certain site condition responses. Bridge types 1 and 11 were used by a structural team from Stanford (Lee and Billington, 2008) to examine performance-enhanced materials and elements. Several ongoing PEER and Caltrans projects also use these benchmark bridges (Mackie et al 2008).

The two bridge types chosen were identical except for their column heights. They both had 39-foot wide decks with a common prestressed deck section. They had five spans, with two external 120-foot spans and three internal 150-foot spans, for a total bridge length of 690 feet. The superstructure of each of the bridge types 1 and 11 was supported on neoprene bearing pads under each of the three webs of the box girder (Mackie et al., 2008). The elevation view and column geometry for bridge types 1 and 11 are shown below in figure 2.4 and figure 2.5.

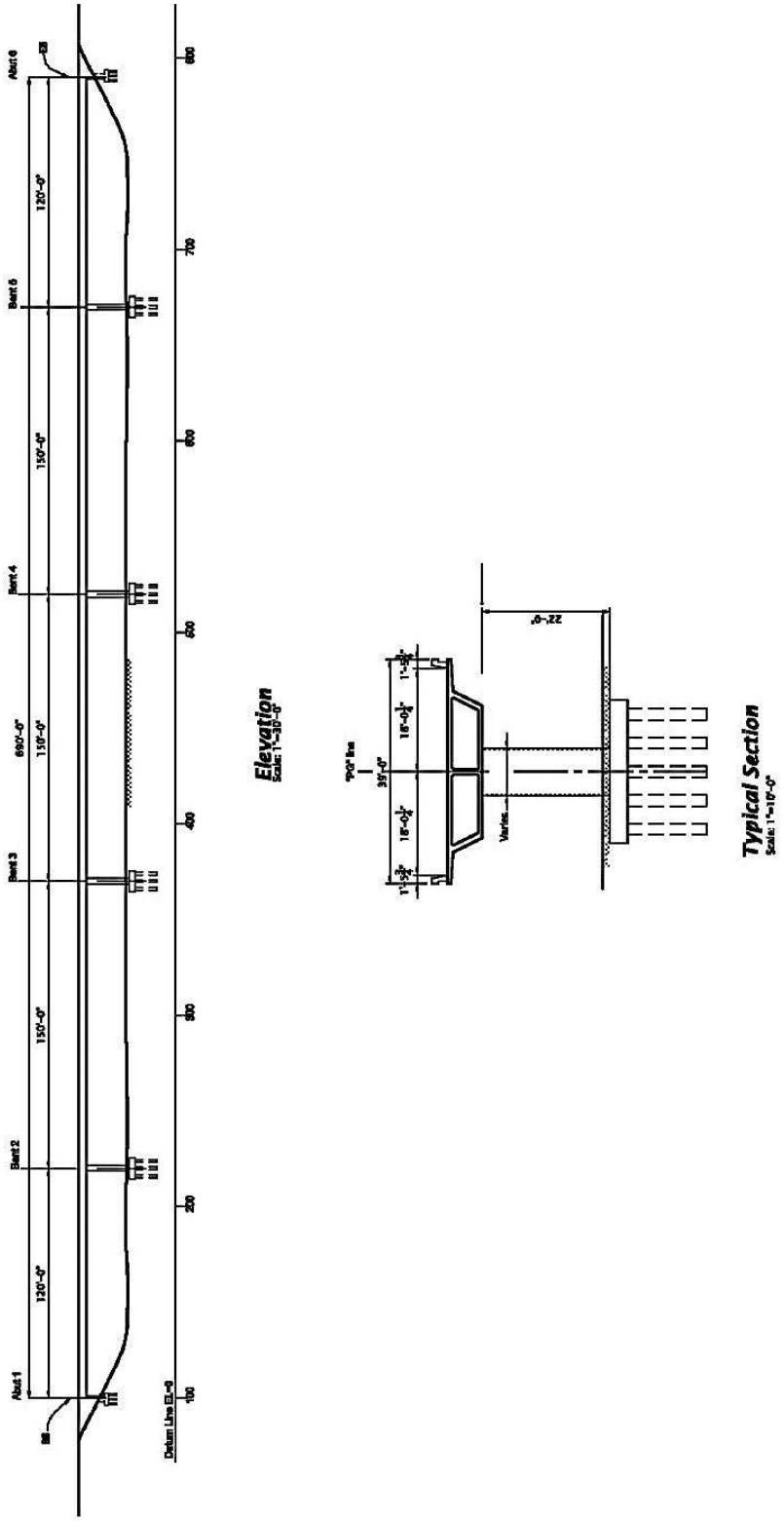

Figure 2.4 Bridge Type 1 (Ketchum et al., 2004)

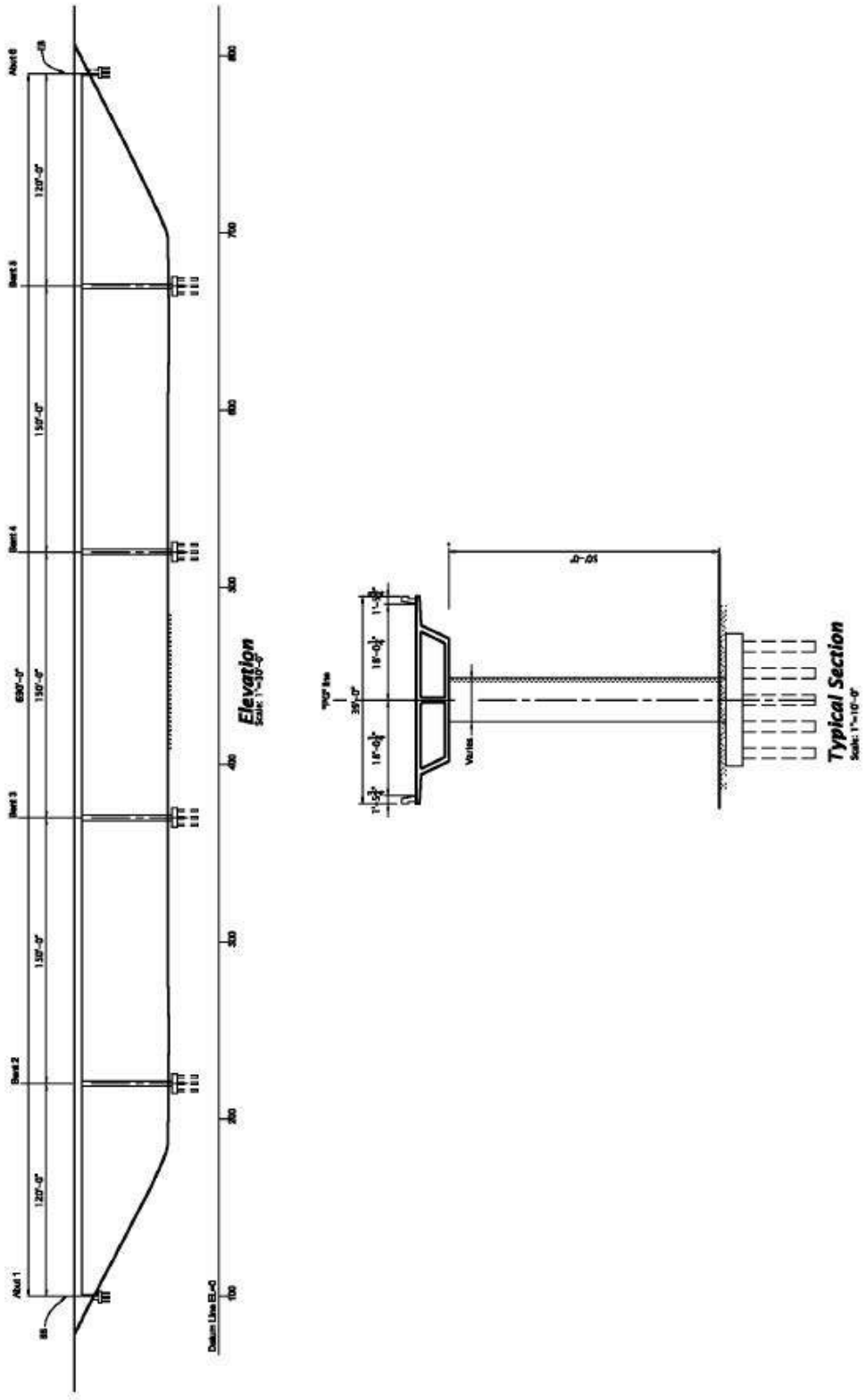

Figure 2.5 Bridge Type 11 (Ketchum et al., 2004)

For the study described in Mackie et al. (2008), each of the two chosen bridge types had 12 different designs. These designs were based on different dimensions for the columns and foundations. Table 2.2 shows the different options for the column design of the Type 1 bridge, and table 2.3 shows the options for the Type 11 bridge.

Table 2.2 Column design summary for Type 1 bridge (Ketchum et al., 2004)

Column Type	Dimensions	Longitudinal Steel
1A	4' Circular	Bundled #10 total 28 (14 bundles)
1B	4' Circular	Bundled #10 total 42 (21 bundles)
1C	5' Circular	#11 total 18
1D	4' x 6' Oblong	#10 total 24
1E	4' x 6' Oblong	Bundled #10 total 48 (24 bundles)
1F	4' x 6' Oblong	Bundled #10 total 72 (36 bundles)
1G	5' Circular	Bundled #11 total 36 (18 bundles)
1H	6' Circular	#11 total 26
1I	7' Circular	#11 total 36
1J	5'-6" x 8'-3" Oblong	#11 total 36
1K	5'-6" x 8'-3" Oblong	Bundled #10 total 72 (36 bundles)
1L	7"' x 10'-6" Oblong	#11 total 58

Table 2.3 Column design summary for Type 11 bridge (Ketchum et al., 2004)

Column Type	Dimensions	Longitudinal Steel
11A	4' x 6' Oblong	Bundled #10 total 72 (36 bundles)
11B	6' Circular	Bundled #11 total 52 (26 bundles)
11C	6' Circular	Bundled #11 total 78 (39 bundles)
11D	7' Circular	#11 total 36
11E	7' Circular	Bundled #11 total 72 (36 bundles)
11F	8' Circular	#14 total 32
11G	5'-6" x 8'-3" Oblong	#11 total 36
11H	5'-6" x 8'-3" Oblong	Bundled #11 total 72 (36 bundles)
11I	5'-6" x 8'-3" Oblong	Bundled #11 total 108 (54 bundles)
11J	7"' x 10'-6" Oblong	#14 total 40
11K	7"' x 10'-6" Oblong	Bundled #14 total 80 (40 bundles)
11L	7"' x 10'-6" Oblong	Bundled #14 total 120 (60 bundles)

OpenSees models were developed for each bridge type, and the models were analyzed to determine measures such as repair costs for the study by Mackie and his research team.

2.4 Model Analysis

There are many ways to use models to analyze the expected behavior of a structure. One approach is to use an Incremental Dynamic Analysis (IDA). IDA allows engineers to estimate responses in terms of different engineering demand parameters (EDP), such as maximum deflection or drift, with respect to chosen intensity measures (IM), such as peak ground acceleration. An IDA curve is formed by running ground motion records on a model, each scaled to several IM levels. The IM levels are chosen to force the structure from its elastic response all the way to collapse (Mander et al., 2007). A single-record IDA will not fully represent the behavior that a structure might display in future events because the IDA can depend heavily on which ground motion record has been chosen. This means that a suite of ground motion records must be chosen to perform an IDA that will capture the full range of expected behaviors (Vamvatsikos and Cornell 2002).

There are several objectives for performing an IDA, as discussed by Vamvatsikos and Cornell (2002). The first of these objectives is to obtain an in-depth understanding of the behavior of a structure under a range of ground motion records with varying levels of intensity. The second is to achieve a better understanding of the effects of more severe and less common ground motion levels. A third objective is to explore the behavioral changes in the structural response as the ground motion becomes more and more intense. The final objective discussed is the ability to estimate the dynamic capacity of the global structure.

Figure 2.6 shows IDA curves for a five-story steel braced frame under four different ground motion records. The response of the structure ranges from a gradual collapse to a weaving behavior. The structure behaves very differently with each ground motion record and at different intensities. This illustrates the importance of running a suite of ground motions when

performing an IDA to fully understand the behavior of a structure (Vamvatsikos and Cornell 2002).

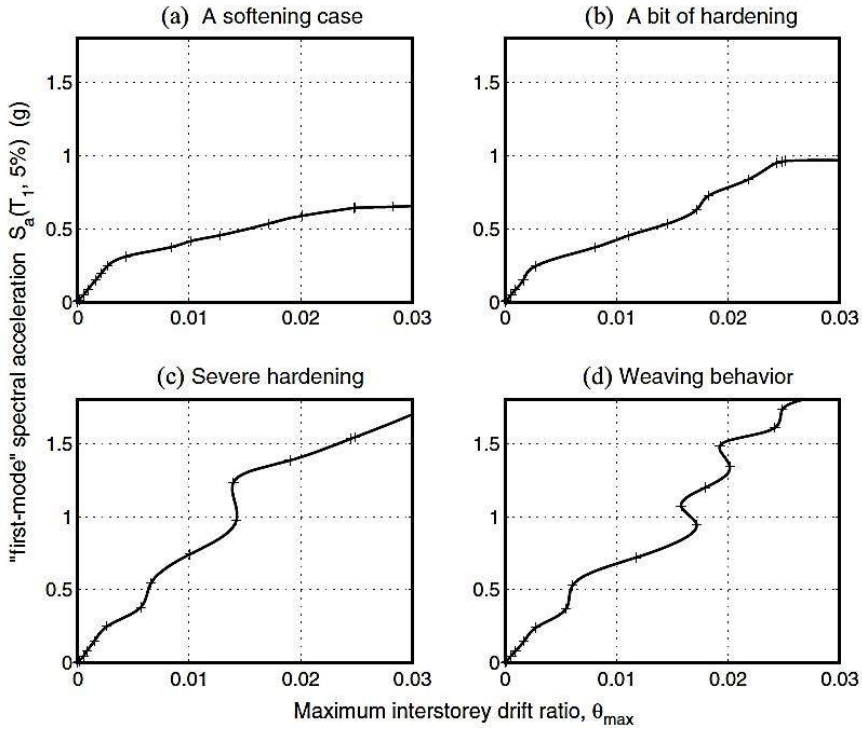

Figure 2.6 IDA curves for a five-story steel braced frame (T1=1.8s) subjected to four different records. (Vamvatsikos and Cornell, 2002)

Once an IDA has been performed, information can be obtained about the structure to define damage limit states. In order to use these limit states, they must be clearly and quantitatively defined. Figure 2.7 shows the damage states defined by Mander (1999) on an idealized curve for moment versus drift. These damage states can be used to estimate repair costs and provide recommended actions for bridge repair. The first damage state (DS1) is defined as the onset of damage, which is at the computed yield drift. DS5, the final damage state, is defined as the point where the structure has become unstable and collapse is initiated. The definitions for the other three limit states are a bit more subjective. A level of damage that requires repairs

defines the boundary between DS2 and DS3, while the boundary between DS4 and DS5 is defined as the point where the structure has inflicted irreparable damage.

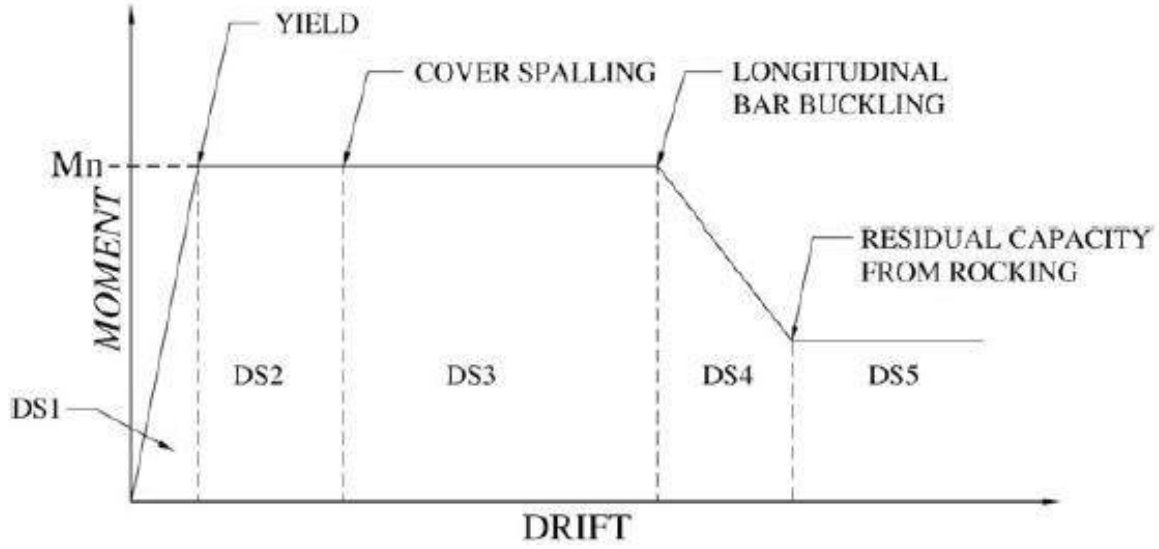

Figure 2.7 Damage state boundaries adopted by Mander, 1999.

Numerical values for the damage states illustrated in figure 2.7 were calculated, and are shown in table 2.4. The yield limit for DS1 was calculated by using yield curvature and elastic deformation of the pier. Cover spalling was represented by a compressive concrete strain of 0.008 to calculate the limit between DS2 and DS3. Longitudinal bar buckling onset was calculated on the basis of a buckling model developed by Barry and Eberhard (2005). The final damage state, DS5, was assumed to occur at $\mu DS5 = \mu DS4 + 2$, where μ is defined as the drift divided by the yield drift. The limit state definitions for this study were experimentally verified using 30 percent scale models of bridge piers (Mander et al., 2007).

Table 2.4 Damage states defined by Mander et al., 2007.

	Damage State	Failure Mechanism	Repair Required	Outage	Caltrans Drift Limit (%)
DS1	None	Pre-yielding	None	None	-
DS2	Minor/Slight	Minor spalling	Inspect, patch	< 3 days	0.53
DS3	Moderate	Bar buckling	Repair components	< 3 weeks	1.90
DS4	Major/Cracking	Bar fracture	Rebuild components	< 3 months	5.10
DS5	Complete/Collapse	Collapse	Rebuild structure	> 3 months	6.16

Mackie et al. (2008) also defined damage states for the benchmark bridges they modeled. Since the models used typical, spiral reinforced, concrete columns and the same benchmark designs were used by several groups, a large number of data were available that allowed for the definition of specific performance levels. Four damage states were defined, and the median drift ratio for each is shown in table 2.5. The repair items corresponding to each damage state can be seen in table 2.6.

Table 2.5 Maximum column drift damage states (Mackie et al., 2008)

	Damage State Limit Description	Drift Ratio for Limit State	λ	β
DS0	Negligible damage with initial cracking	Drift ratio associated with cracking moment Mcr	0.23	0.30
DS1	Cover concrete spalling	Δsp equation from Berry and Eberhard (2003)	1.64	0.33
DS2	Longitudinal reinforcing bar buckling	Δbb equation from Berry and Eberhard (2003)	6.09	0.25
DS3	Column failure	Δff equatino from Mackie and Sojadinovic (2007)	6.72	0.35

Table 2.6 Repair items for maximum column drift damage states (Mackie et al., 2008)

Damage State	Repair Item
DS1	Seal cracks and minor removal and patching of concrete
DS2	Seal cracks, major patching
DS3	Replace column

These damage state definitions can be helpful in relating wireless sensor data to bridge maintenance or inspection actions. Recommendations for action can be made on the basis of which damage state level a sensor reading signals.

Chapter 3 Benchmark Suite Models

OpenSees models for this project were created on the basis of the benchmark concrete box girder bridges designed by Ketchum et al (2004). This chapter describes these models and their validation.

3.1 Model Descriptions

Eight OpenSees models were created for this work, based on the Type 1 and Type 11 benchmark bridges. Each bridge had two external spans of 120 feet and three internal spans of 150 feet, with a pre-stressed box girder deck. Figure 3.1 shows a simplified layout of the bridge elevations. Type 1 models had 22-foot tall columns, and Type 11 models had 50-foot columns. For each bridge type, two different column designs and two different abutment types were modeled. The column designs for the Type 1 models were designated as 1A and 1B columns, and the columns for the Type 11 models were designated as types 11A and 11B. Each of the column bases was constrained in all six degrees of freedom, to represent a fixed foundation condition. The two abutment types used for the models in this project were the roller abutment and the spring abutment, both as described in more detail below. Table 3.1 shows the characteristics of each of the eight bridge models.

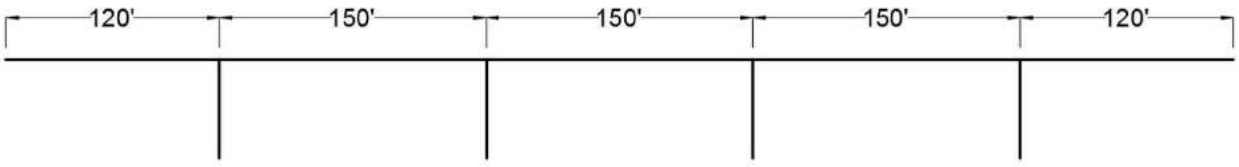

Figure 3.1 Simplified bridge layout

Table 3.1 Characteristics of eight bridge models

Bridge Designation	Abutment Type	Column Height	Column Cross Section	Column Reinforcement
1Ar	Roller	22’	4’ Circular	Bundled #10 total 28 (14 bundles)
1As	Spring	22’	4’ Circular	Bundled #10 total 28 (14 bundles)
1Br	Roller	22’	4’ Circular	Bundled #10 total 42 (21 bundles)
1Bs	Spring	22’	4’ Circular	Bundled #10 total 42 (21 bundles)
11Ar	Roller	50’	4’ x 6’ Oblong	Bundled #10 total 72 (36 bundles)
11As	Spring	50’	4’ x 6’ Oblong	Bundled #10 total 72 (36 bundles)
11Br	Roller	50’	6’ Circular	Bundled #11 total 52 (26 bundles)
11Bs	Spring	50’	6’ Circular	Bundled #11 total 52 (26 bundles)

A single flexibility-based element with five integration points was used for the column, and 69 flexibility-based elements were defined along the deck. The deck and column sections were described by fiber models, as explained later in this chapter. Vertical loads were placed at each deck node to model the self-weight of the bridge, and each node was given a nodal mass based on the self-weight in all six degrees of freedom. Figure 3.2 shows the geometry of the nodes, elements, and gravity load for the model.

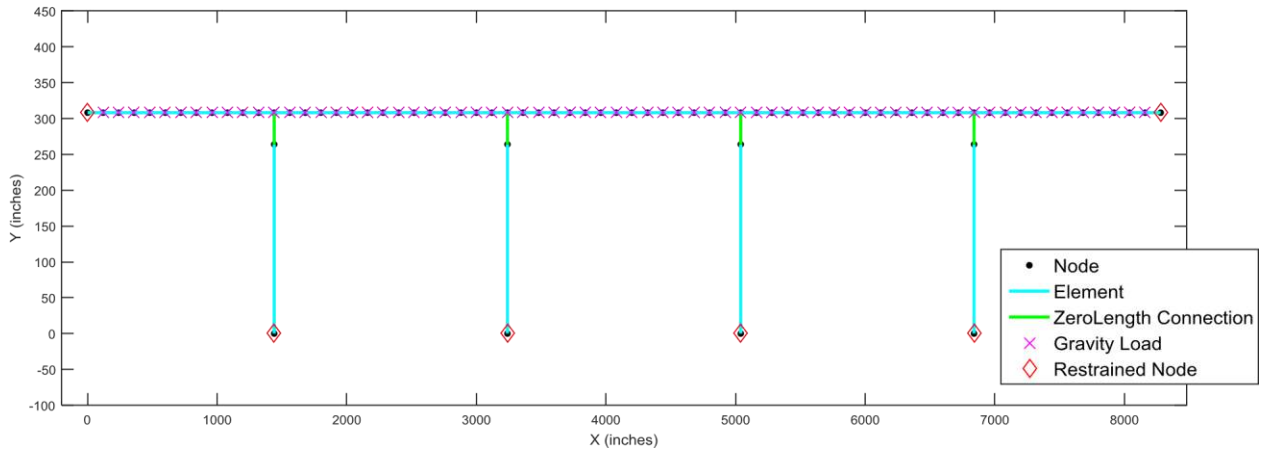

Figure 3.2 Model geometry

To validate these models, the compressive and tensile strengths of each element were calculated and compared to strengths obtained from OpenSees. Bending behavior was also

investigated, and the model was checked for symmetry in the response and conservation of forces. The first natural period of each of the eight models is shown in table 3.2. While Mackie et al. (2008) provided natural periods for each of the models, comparison was not applicable because there were several differences among the models. One of the major differences was that the models used in that effort had a rigid element connecting the columns to the deck. The connections for the models in this work used the stiffness of the neoprene bearings, so they were not rigid connections.

Table 3.2 Natural periods of the bridge models

Bridge Type	**1Ar**	**1As**	**1Br**	**1Bs**	**11Ar**	**11As**	**11Br**	**11Bs**
Natural Period (sec.)	1.49	1.05	1.46	1.03	2.88	1.70	1.97	1.30

3.2 Deck Section

The deck section was identical for both Type 1 and Type 11 bridges, so only one fiber section was defined for the deck. Figure 3.3 shows the deck design used in these models. The deck was 39 feet wide and 6 feet deep. Longitudinal reinforcing steel is not shown in the figure, but two layers of reinforcing bars were placed in the deck, soffit, and girders. The section was defined in OpenSees by combining concrete and steel fibers, using the Kent-Scott-Park concrete (concrete01) and Giuffre-Menegotto-Pinto strain-hardening steel (steel02) materials. The concrete material was given a specified compressive strength of 5.2 ksi, and the steel strength was defined as 60 ksi. The 7,000 kips pre-stressing force was added as an axial load on the deck at the end nodes. Figure 3.4 shows the simplified section defined in the OpenSees model.

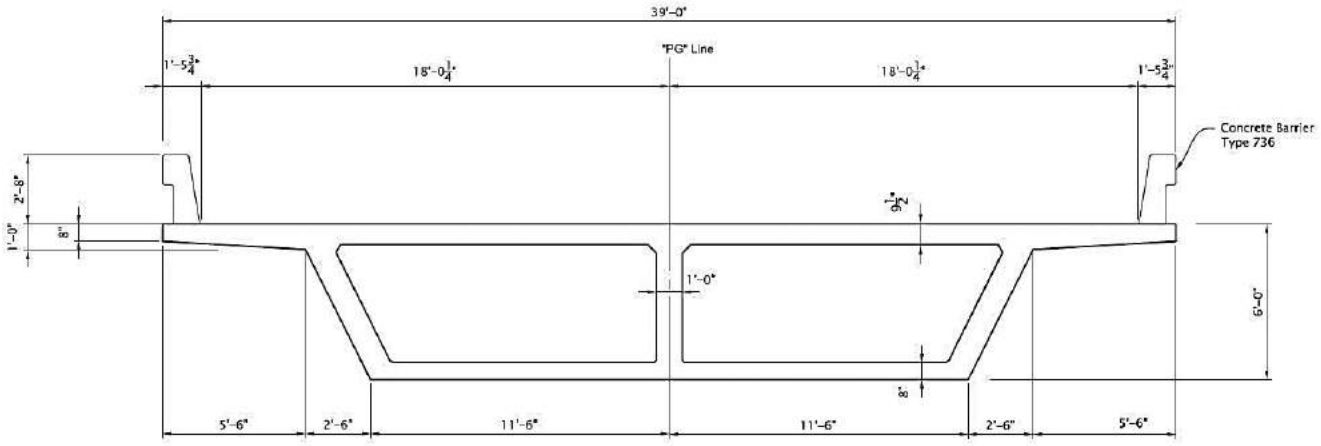

Figure 3.3 Deck cross-section (Ketchum et al., 2004)

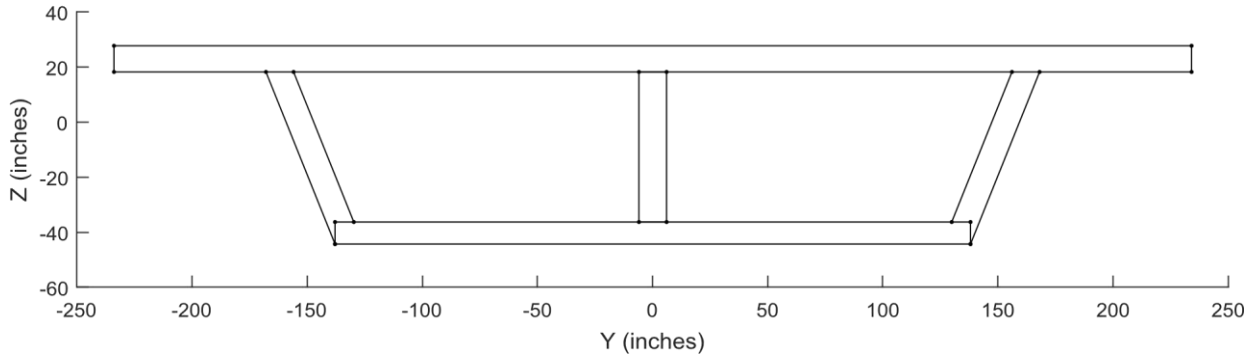

Figure 3.4 Deck fiber section defined in OpenSees

On the basis of the material strengths of the concrete and steel models used, the compressive and tensile strengths of the deck section were calculated to be -52,387 kips and 7,584 kips. Figure 3.5 shows the force vs displacement plots obtained from an axial push-pull test of the deck element. From OpenSees, the compressive strength was -51,650 kips and the tensile strength was 7,278 kips. The moment-rotation behavior for the deck section is shown in figure 3.6, with different levels of axial force applied to the element. A reinforced concrete

column analysis software program, Response-2000, was used to validate the moment capacity for the column sections but could not be used for the deck section (Bentz, no date).

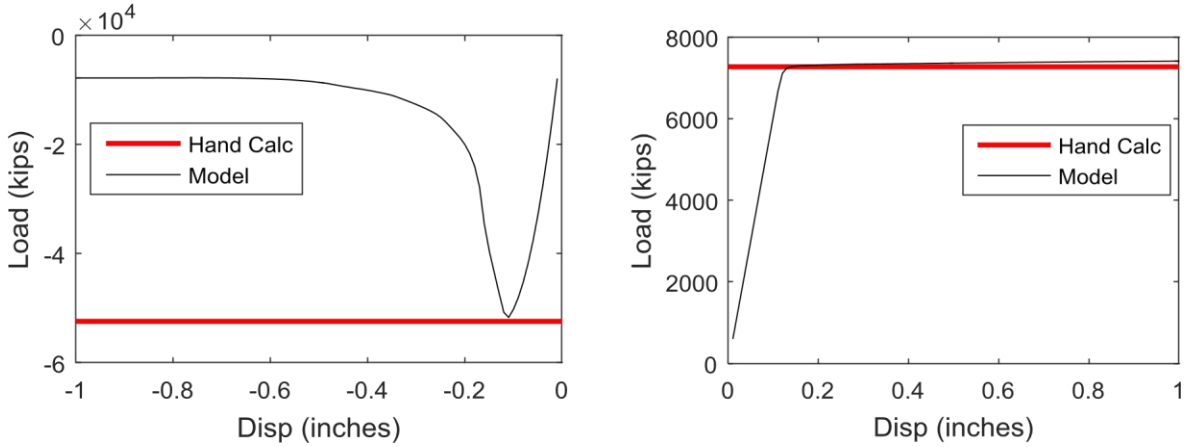

Figure 3.5 Axial push-pull behavior of the deck section. Compression (left) and tension (right).

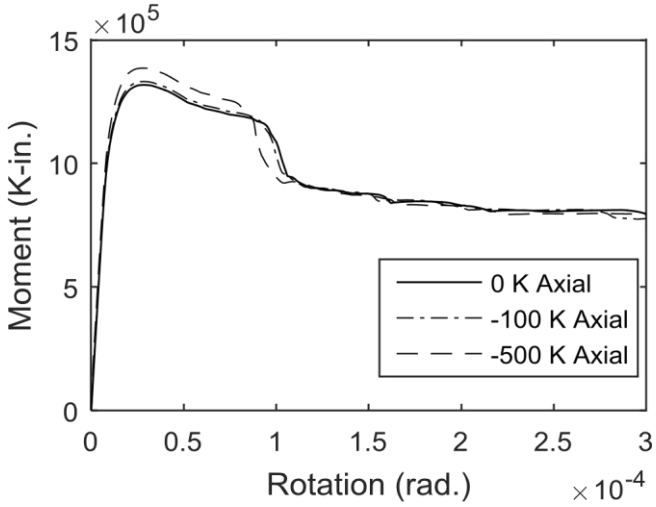

Figure 3.6 Moment-rotation behavior of the deck section

3.3 Column Sections

Each of the four column fiber sections was modelled by using the same material definitions as the deck. The columns have either circular or oblong cross-sections and different longitudinal reinforcement. Figure 3.7 shows the different column cross-sections and reinforcement plans.

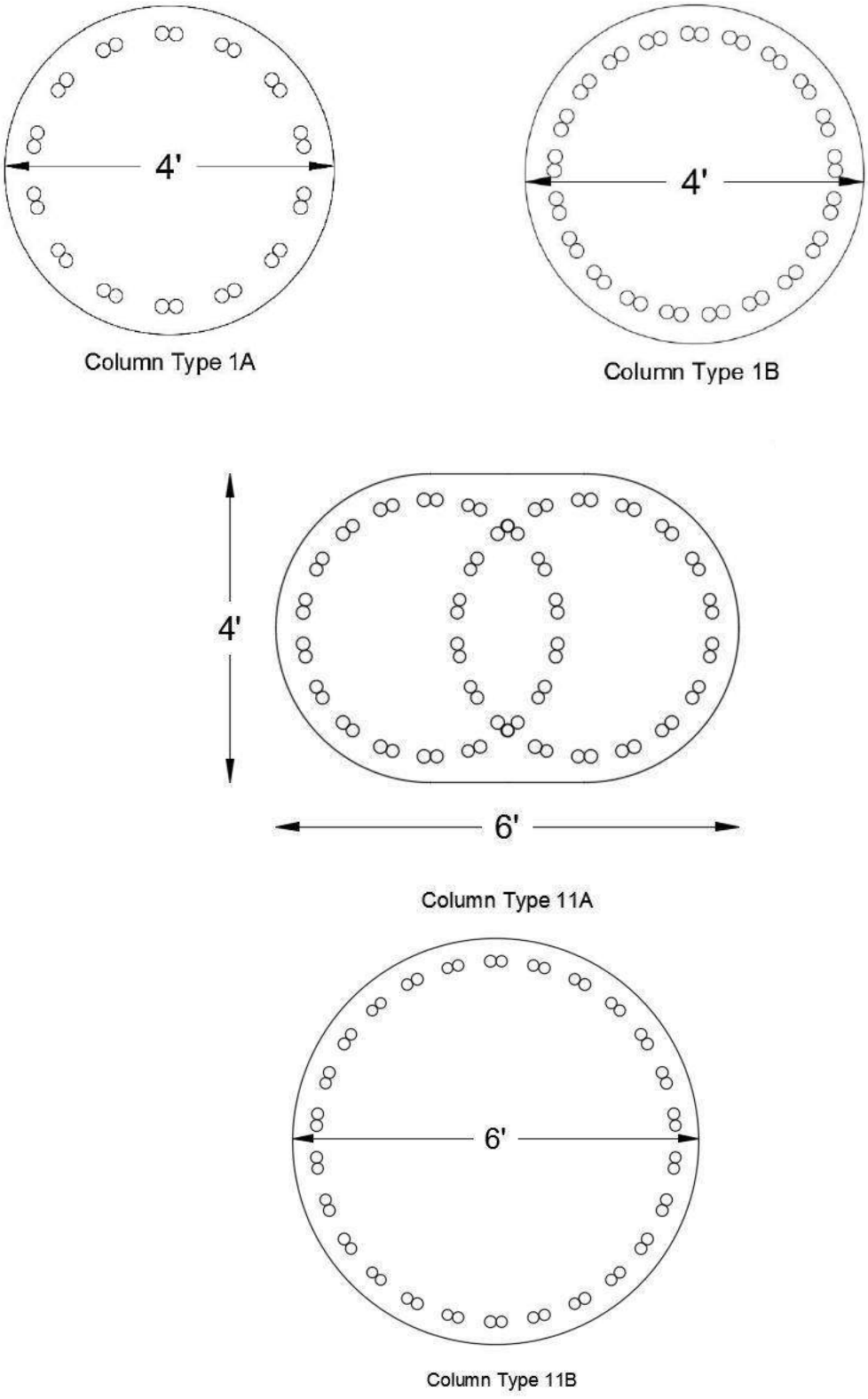

Figure 3.7 Column cross-sections

Column 1A was a circular column with a diameter of 4 feet and 28 #10 bars for longitudinal reinforcement. The reinforcement was bundled into 14 pairs. The compressive and tensile strengths of column 1A were calculated as -11,543 kips and 2,134 kips. Figure 3.8 shows the axial push-pull results from OpenSees, which provided a compressive strength of -11,470 kips and a tensile strength of 2,134 kips. Figure 3.9 shows the bending moment-rotation behavior obtained from OpenSees. With no axial force, OpenSees gave a moment capacity of 40,150 K-in while Response-2000 gave a moment capacity of 39,504 K-in.

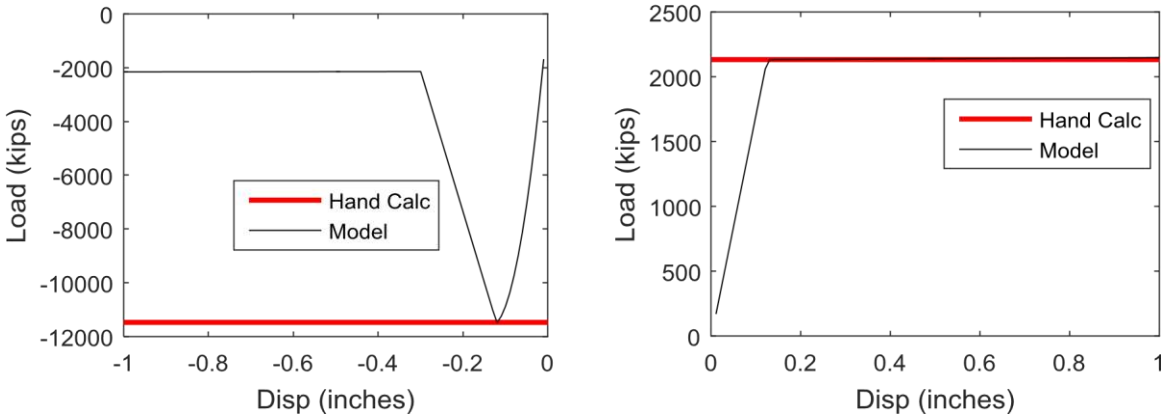

Figure 3.8 Axial push-pull behavior of Column 1A section. Compression (left) and tension (right).

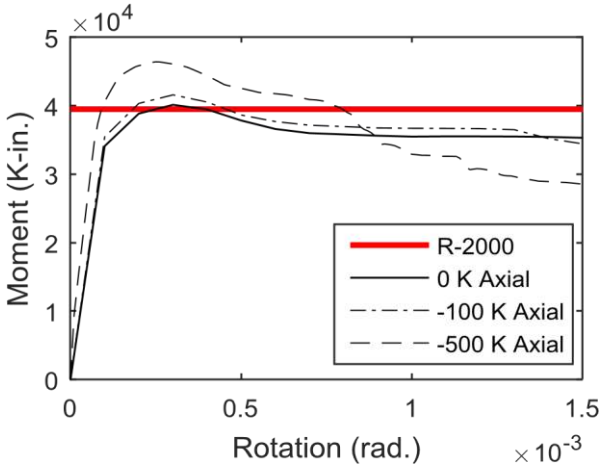

Figure 3.9 Moment-rotation behavior of Column 1A section.

Type 1B was a 4-foot diameter circular column with 42 #10 bars for longitudinal reinforcement, bundled in 21 pairs. The calculated compressive strength was -12,610 kips and the calculated tensile strength was 3,200 kips. From OpenSees, the compressive strength was -12,500 kips and the tensile strength was 3,201 kips, as shown in figure 3.10. The moment-rotation behavior of column 1B is shown in figure 3.11. OpenSees gave a moment capacity of 57,080 Kin with no axial load applied, while Response-2000 gave a moment capacity of 55,308 K-in.

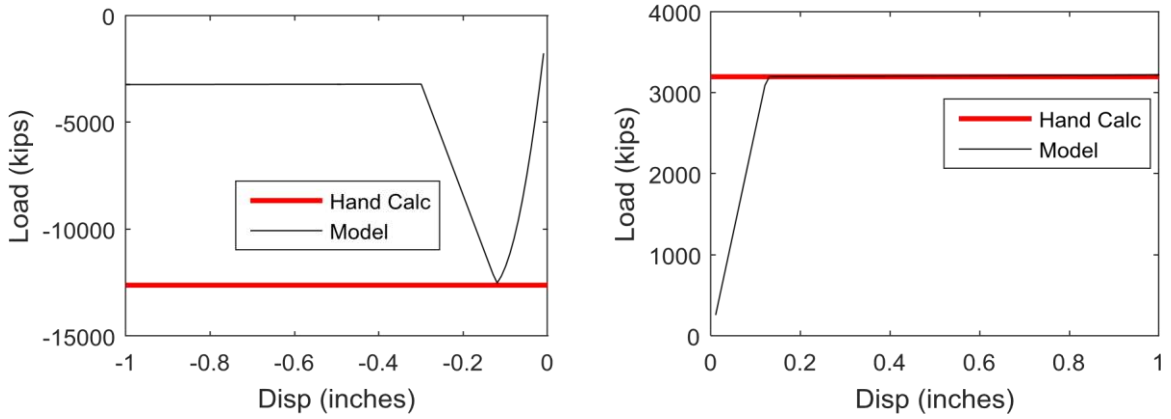

Figure 3.10 Axial push-pull behavior of Column 1B section. Compression (left) and tension (right).

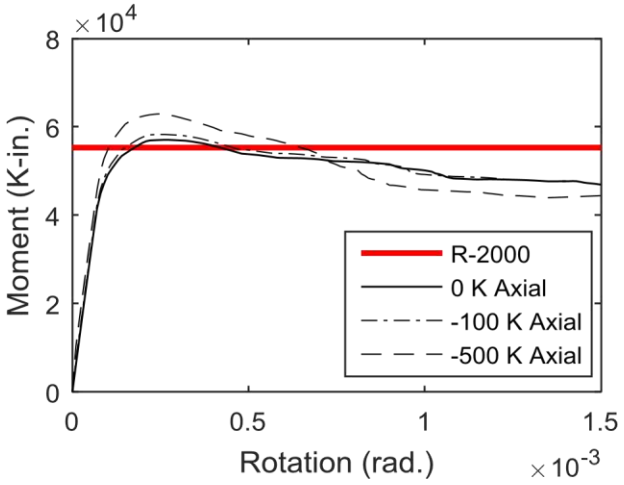

Figure 3.11 Moment-rotation behavior of Column 1B section.

Column Type 11A was a 4-foot by 6-foot oblong column with 72 # 10 bars as longitudinal reinforcement. The bars were bundled into 36 pairs. The compressive strength was

calculated as -20,887 kips and the tensile strength as 5,486 kips. Figure 3.12 shows that the compressive strength obtained from OpenSees was -20,700 kips and the OpenSees tensile strength was 5,487 kips. Figure 3.13 shows the moment-rotation behavior for column 11A. With no axial force, OpenSees gave a moment capacity of 136,600 K-in while Response-2000 gave a moment capacity of 135,048 K-in.

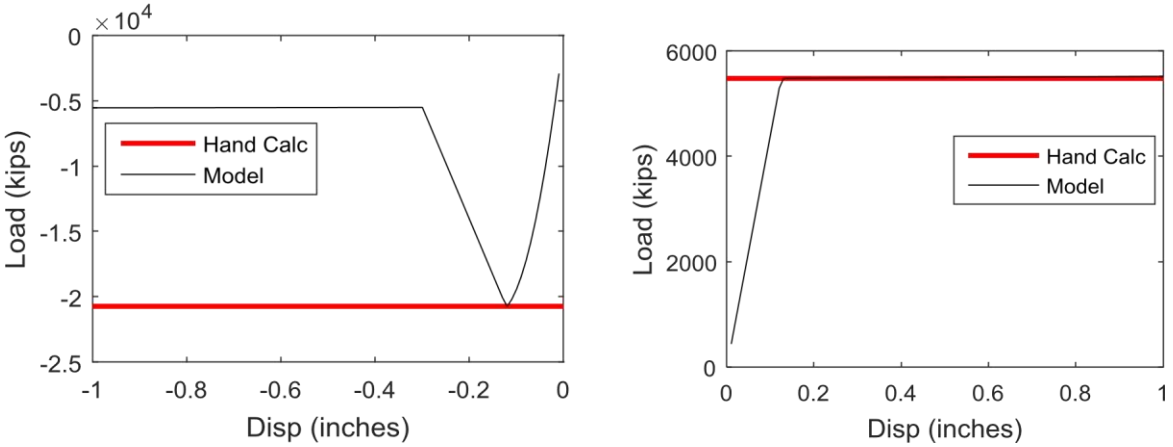

Figure 3.12 Axial push-pull behavior of Column 11A section. Compression (left) and tension (right).

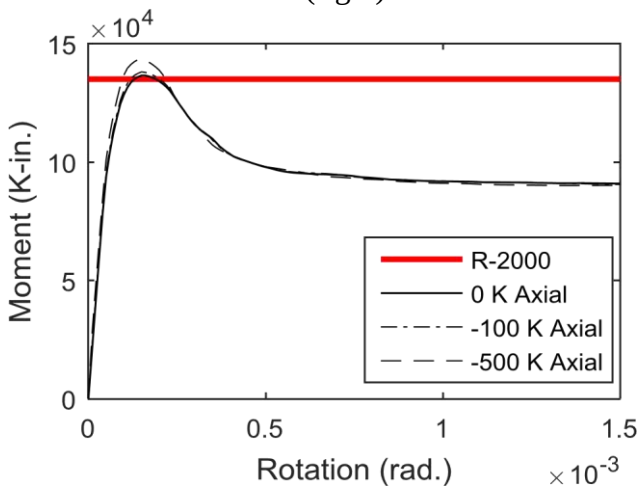

Figure 3.13 Moment-rotation behavior of Column 11A section.

Type 11B was a 6-foot diameter circular column with 52 #10 bars for longitudinal reinforcement, bundled in 26 pairs. The calculated compressive strength was -26,039 kips and the calculated tensile strength was 4,867 kips. From OpenSees, the compressive strength was -

25,880 kips and the tensile strength was 4,867 kips, as shown in figure 3.14. The moment-rotation behavior of column 1B is shown in figure 3.15. Response-2000 gave 131,016 K-in as the moment capacity, while OpenSees gave a moment capacity of 133,500 K-in with no axial force.

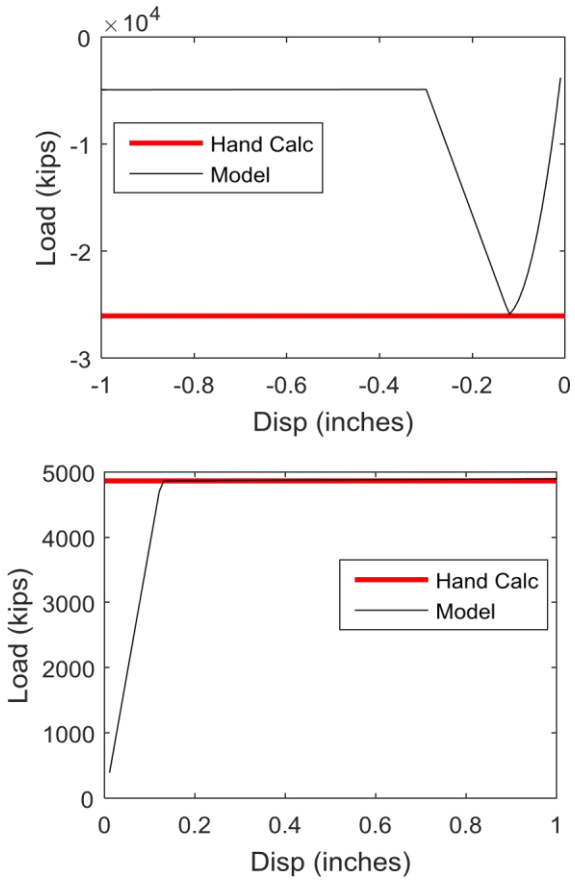

Figure 3.14 Axial push-pull behavior of Column 11B section. Compression (left) and tension (right).

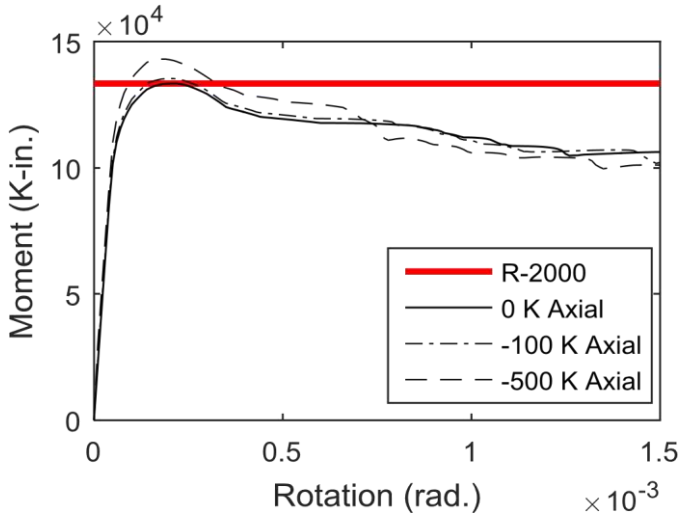

Figure 3.15 Moment-rotation behavior of Column 11B section.

Table 3.3 summarizes the results of these push-pull validation tests for all four column sections and the deck section. The final columns show the percentage of error between the hand calculations and OpenSees model strengths. For the column sections, the percentage of error was less than 1 percent in all cases, and the error was less than 5 percent for the deck section.

Table 3.3 Tension and compression strengths of model sections

Section	Hand Tension (Kips)	Hand Compression (Kips)	OpenSees Tension (Kips)	OpenSees Compression (Kips)	% Error Tension	% Error Compression
Col 1A	2134	-11543	2134	-11470	**0.00**	**0.63**
Col 1B	3200	-12610	3201	-12500	**0.03**	**0.87**
Col 11A	5486	-20887	5487	-20700	**0.02**	**0.90**
Col 11B	4867	-26039	4867	-25880	**0.00**	**0.61**
Deck	7584	-52387	7278	-51650	**4.03**	**1.41**

Table 3.4 summarizes the moment capacity results for all four column sections. The right most column shows the percentage of error between the Response-2000 results and the OpenSees results. For each section, the error was less than 5 percent.

Table 3.4 Moment capacity of the column sections

Section	Response-2000 (K-in)	OpenSees (K-in)	% Error

1A	39,504	40,150	**1.6**
1B	55,308	57,080	**3.1**
11A	135,048	136,600	**1.15**
11B	131,016	133,500	**1.9**

3.4 Abutments

The roller abutment used for this project was modeled by releasing longitudinal translation at the deck end nodes. A single point constraint was applied at each end node to constrain displacement in the vertical direction and rotation about the longitudinal axis of the deck.

The spring abutment model was more complex, and was meant to represent different behaviors in the longitudinal and transverse directions. In the longitudinal direction, the response represented the behavior of the elastomeric bearing pads, abutment wall and piles, and soil backfill material. In the transverse direction, the response was based on the elastomeric bearing pads, concrete shear keys, abutment piles, wing walls, and backfill material (Mackie et al., 2008). To create these responses in the OpenSees models of this project, steel01 and elastic uniaxial materials were defined and then combined by using a parallel uniaxial material. Figure 3.16 shows the resulting behavior of the materials defined for the spring abutment model used in this research, which closely matched the desired behavior.

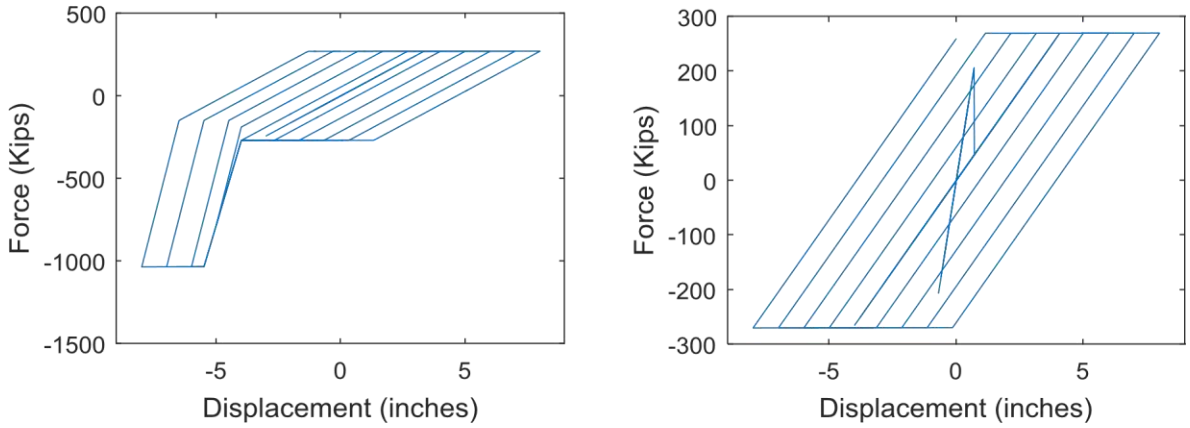

Figure 3.16 Modeled spring abutment longitudinal (left) and transverse (right) response in kips and inches.

The roller abutment was applied to the models by using a zero-length element at the deck end nodes connecting the deck to a fixed node. This zero-length element was defined by using the parallel uniaxial materials that represent the longitudinal and transverse responses shown in figure 3.16.

3.5 Connections

The connection between the tops of the columns and the deck was modelled by using a zero length element and the OpenSees equalDOF command. A zero length element was used to model the behavior of the neoprene bearings that support the deck. There was a bearing pad under each of the three box webs of the deck section. A uniaxial steel material model was used to define the stiffness and behavior of these bearing pads, and the zero length element was defined with this material in the longitudinal and transverse directions. For the vertical direction, the equalDOF command was used to constrain the column and deck node to the same vertical displacement.

3.6 Damping

Rayleigh damping was applied to the models, with a 2 pecent damping ratio. Rayleigh damping applies factors to the mass and stiffness-proportional damping matrices of a structure and combines them to form a damping matrix. For this model, stiffness proportional Rayleigh damping was used and a factor of zero was applied to the mass matrix. The factor on the stiffness matrix was based on the first mode natural circular frequency and the damping ratio. The Rayleigh damping command in OpenSees assigned the resulting damping matrix to all previously defined nodes and elements.

Chapter 4 Structural Response

Ground motions were selected and run on all eight models to determine relationships between strain readings and drift limit states. This chapter describes the analysis and structural response of the bridge models.

4.1 Gravity Load

The gravity load is applied as point loads at the deck nodes. It was calculated on the basis of a concrete weight of 150 lb/ft^3 and a steel weight of 480 lb/ft^3. Using the cross-sectional areas of steel and concrete in the deck and a 10-foot tributary length, this resulted in a vertical gravity load of 96.7 kips at each deck node.

A static analysis was used to apply the gravity load in ten steps. The Newton algorithm was used, and the load controlled integrator applies the load in increments. Figure 4.1 shows the displaced shape of bridge 1Ar under gravity load alone. The deck deflected vertically and symmetrically, as expected. The deflection was about 0.7 inches, which is reasonable for the span lengths of this bridge.

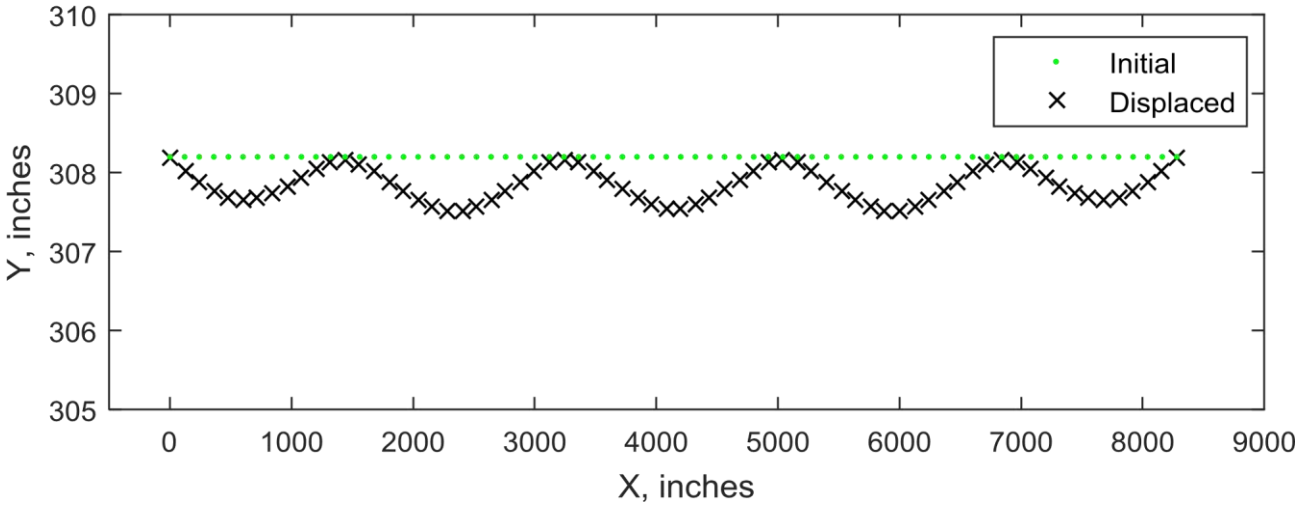

Figure 4.1 Displaced shape of Bridge 1Ar deck under gravity load

4.2 Ground Motions

A suite of 20 ground motions was run through each model, at 10 different scale factors. The ground motions used came from a SAC suite of earthquakes representative of the Seattle region. The SAC Steel Project is a group funded by FEMA to solve problems identified with steel frame structures after the 1994 Northridge Earthquake, and they provide several ground motion suites. The ground motions chosen were 2 in 50-year probability earthquakes. Table 4.1 lists each of the 20 ground motions used with a description, magnitude, distance from the epicenter, and the peak ground acceleration (PGA) of the record. Included in the suite were both fault normal (fn) and fault parallel (fp) records, and both simulated and actual earthquake records. Time history plots of each of the ground motions used can be found in the Appendix.

Table 4.1 Ground motion suite information

EQ code	Description	Earthquake Magnitude	Distance (km)	PGA (g's)
SE 21	fn 1992 Mendocino	7.1	8.5	0.76
SE 22	fp 1992 Mendocino	7.1	8.5	0.49
SE 23	fn 1992 Erzincan	6.7	2.0	0.61
SE 24	fp 1992 Erzincan	6.7	2.0	0.54
SE 25	fn 1949 Olympia	6.5	56.0	0.90
SE 26	fp 1949 Olympia	6.5	56.0	0.82
SE 27	fn 1965 Seattle	7.1	80.0	1.76
SE 28	fp 1965 Seattle	7.1	80.0	1.39
SE 29	fn 1985 Valpariso	8.0	42.0	1.64
SE 30	fp 1985 Valpariso	8.0	42.0	1.57
SE 31	fn 1985 Valpariso	8.0	42.0	1.27
SE 32	fp 1985 Valpariso	8.0	42.0	0.90
SE 33	fn Deep Interplate (simulation)	7.9	65.0	0.80
SE 34	fp Deep Interplate (simulation)	7.9	65.0	0.65
SE 35	fn 1978 Miyagi-oki	7.4	66.0	0.61
SE 36	fp 1978 Miyagi-oki	7.4	66.0	0.78
SE 37	fn Shallow Interplate (simulation)	7.9	15.0	0.56
SE 38	fp Shallow Interplate (simulation)	7.9	15.0	0.53
SE 39	fn Shallow Interplate (simulation)	7.9	15.0	0.58
SE 40	fp Shallow Interplate (simulation)	7.9	15.0	0.75

These ground motions were applied to the models by using the uniform excitation load pattern in OpenSees. This load pattern applied the acceleration files to the model in the direction specified. Each ground motion was run in both the longitudinal and transverse directions. The Newmark integrator was used to apply the load pattern, with a gamma factor of 0.5 and a beta factor of 0.25. These factors represented the average acceleration method. If convergence was not achieved with this method, then analysis parameters were changed and different algorithms

were tried until convergence was achieved. The transient analysis command was used to perform a transient analysis with a constant time step, equal to the time step of the input acceleration file.

Each ground motion was scaled to peak ground accelerations ranging from 0.15g to 1.5g, in increments of 0.15g. This provided a wide range of intensities and characteristics of ground motions, which resulted in a wide range of model behaviors. Running these ground motions at different PGAs allowed the full range of responses to be analyzed, from elastic behavior to the onset of collapse.

4.3 Recorders

Displacement recorders were placed at all nodes of the model. Each of the translational degrees of freedom was recorded at each time step in the analysis. Reaction recorders were placed at each of the constrained nodes. These were the fixed nodes at the column bases and the nodes at the abutments at each end of the deck. The reaction recorder command recorded the nodal reactions in the degrees of freedom specified.

Strain recorders were placed using engineering judgment at points where strain would likely be highest. These were chosen on the basis of where axial forces and moments were greatest. These critical points were determined to be at the column tops and bases, and in the deck near the connections and at midspan. At these critical points in the column, four recorders are placed along the outer fibers of the cross-section. They were placed at quadrant points aligning with the transverse and longitudinal directions. In the deck, recorders were placed at the top and bottom most fiber at the critical points. The OpenSees strain recorder reported the stress and strain at the specified fiber at each step of the analysis. Figure 4.2 shows the approximate locations of the strain recorders on the model, as red circles.

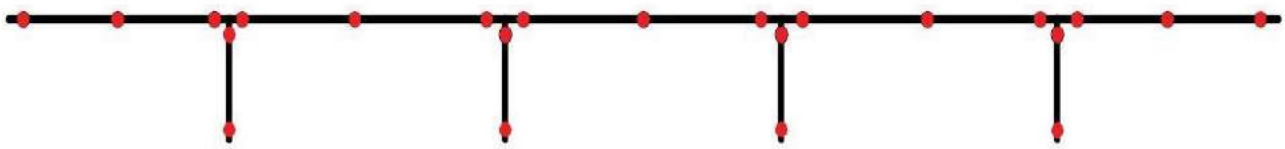

Figure 4.2 Approximate strain recorder locations

4.4 IDA Plots

IDA plots ere created for each bridge once all of the runs had been completed. These plots were created by using the maximum column drift for each run. The IDA plot for each bridge showed a line for each of the 20 ground motions, with 10 points on each line. Each of the 10 points represented the run of a scaled record of each ground motion, ranging from PGAs of 0.15g to 1.5g. These IDA plots were useful to see the relationship between the defined drift limits and the behavior of the structure. Figure 4.3 shows the IDA plot for Bridge 11Ar. The red line represents the average of the PGA values at each drift limit, and vertical dotted lines show each of the maximum drift limits. This average line makes it clear that the structure incurred some damage around the second maximum drift limit (1.64 precent drift), and failed around the third and fourth drift limits. This is consistent with the damage state definitions corresponding to the maximum drift limits. Based on these data, the drift limits proposed by Mackie et al. (2008) were valid for the models used in this work. These limits were used to determine strain limits that related to each damage state, which is discussed in the following sections.

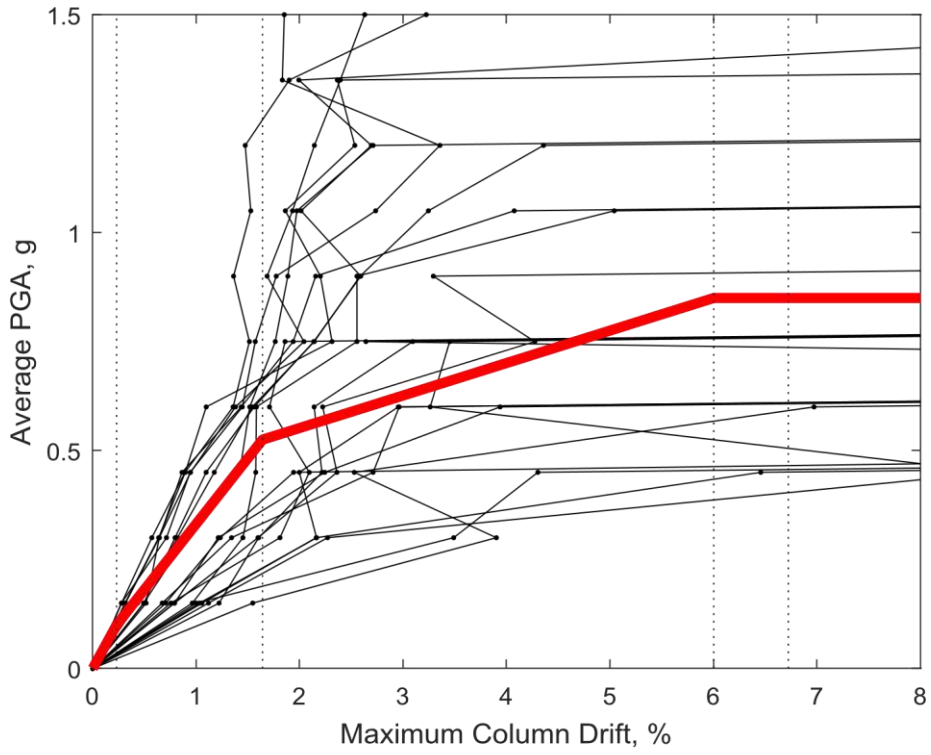

Figure 4.3 IDA Plot for Bridge 11Ar.

4.5 Strain Response

After all of the ground motions were run on each of the eight models at each PGA level, the strain and displacement data were plotted to determine a relationship between strain recordings and drift limits. Maximum and residual drift limits are provided in the paper by Mackie et al. (2008) so both were investigated. The drift was found by using the displacement recorded at the top node of each column, and the strain was taken from the recorder at the base of the column. The strains at the column bases were found to be higher than at the tops of the columns, so the column base strains were used for the plots.

Maximum drifts and strains were plotted by finding the maximum points from each run and then plotting them together for each bridge model in each direction. The drift and strain data from each of the four columns were plotted together. The drift limits related to damage states were plotted as vertical dotted lines. For each of the maximum drift plots, a bi-linear relationship

was observed. A linear curve was fit for each of the two linear regions. Figure 4.4 shows the maximum strain versus maximum drift plot for bridge 1Ar, with the ground motion in the longitudinal direction.

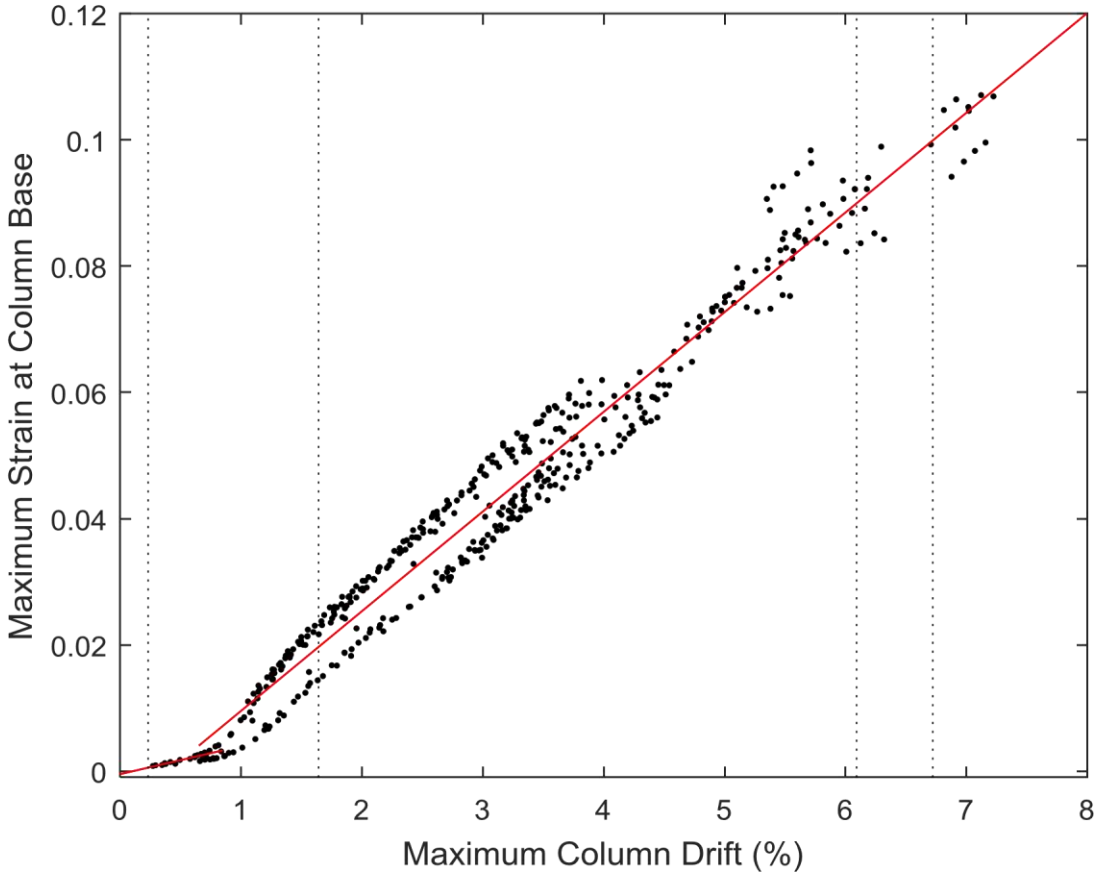

Figure 4.4 Maximum strain vs. maximum drift for Bridge 1Ar with ground motion in the longitudinal direction.

With the ground motion run in the transverse direction, a similar behavior was observed. Figure 4.5 shows the maximum strain versus maximum drift plot for bridge 1Ar, with the ground motion in the transverse direction.

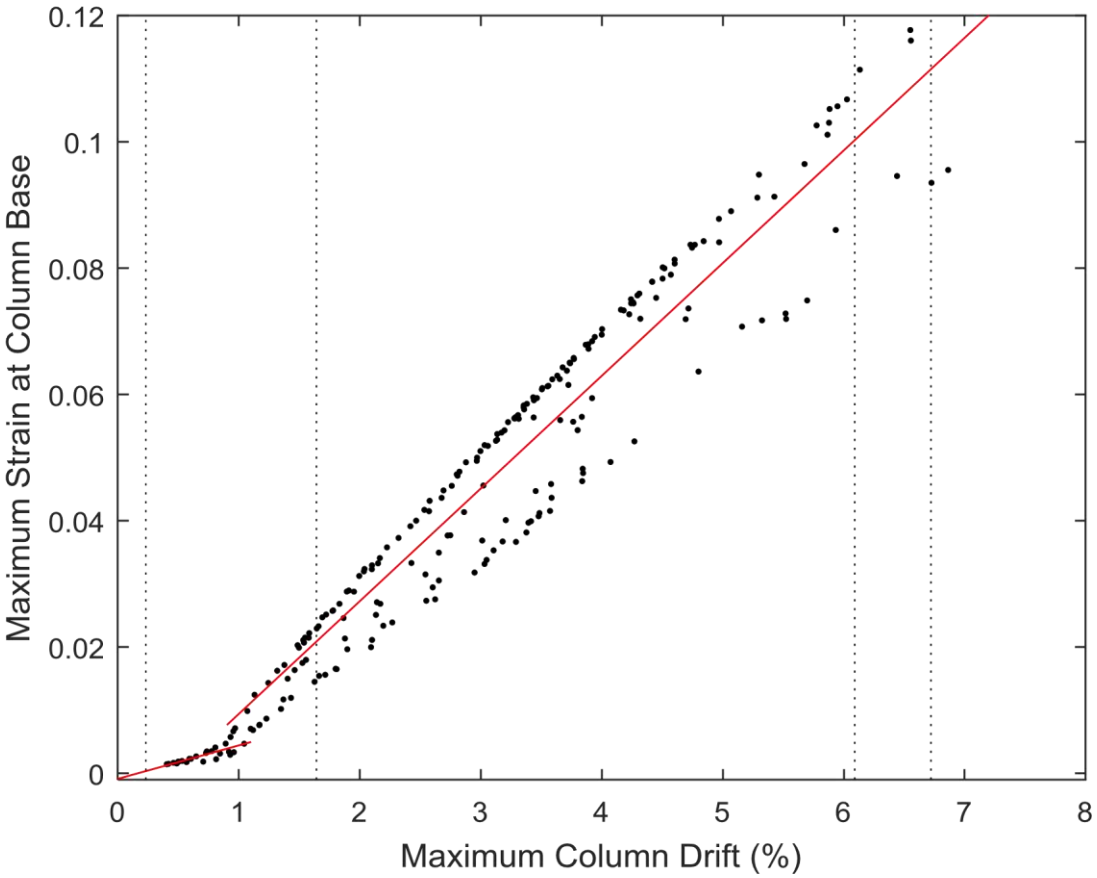

Figure 4.5 Maximum strain vs. maximum drift for Bridge 1Ar with ground motion in the transverse direction.

The resulting plots for the maximum strain in the other seven bridges showed similar behavior. For all of the Type 1 bridges, the strain values intersecting with the drift limits were relatively similar. However, the strain values for Type 11 bridges were not consistent with those of the Type 1 bridges. Figure 4.6 shows the maximum strain versus maximum drift plot for bridge 11Ar, with the ground motion in the longitudinal direction. For the Type 11 bridges, a similar bi-linear behavior was observed, but the strain values corresponding with the drift limits appeared to be lower.

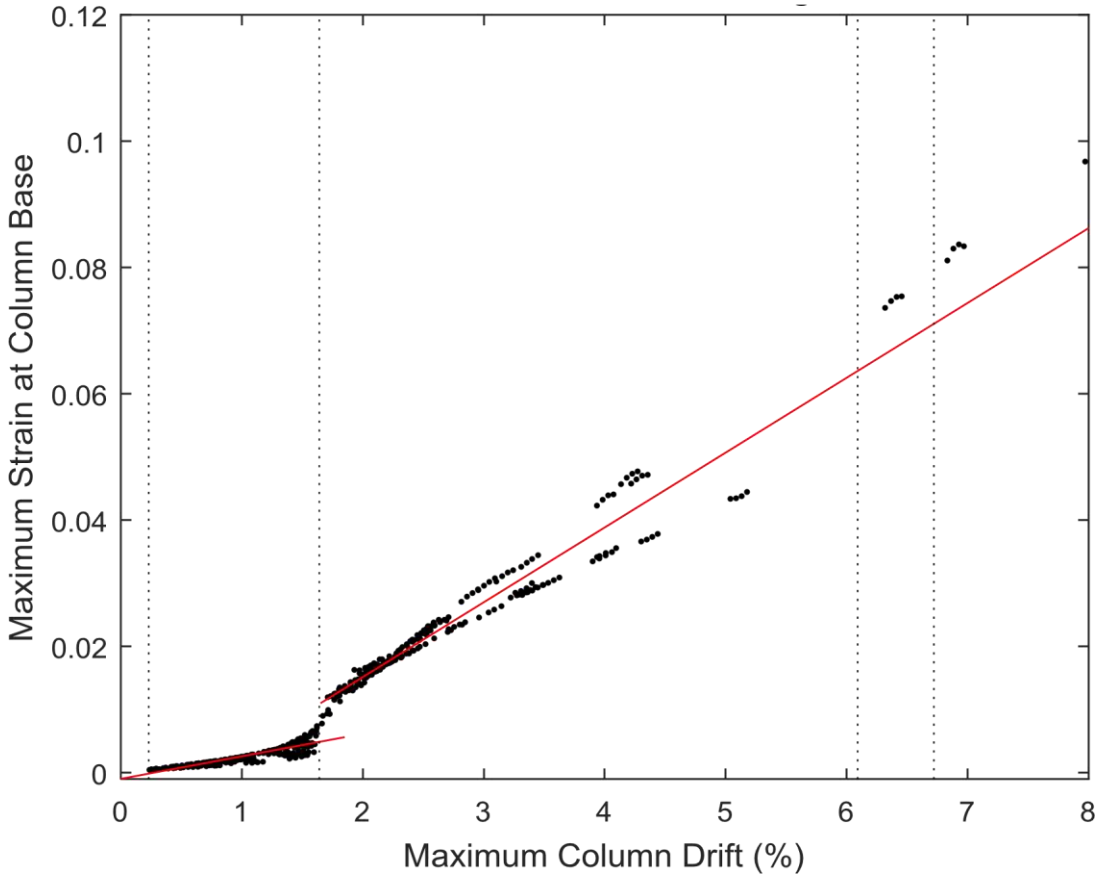

Figure 4.6 Maximum strain vs. maximum drift for Bridge 11Ar with ground motion in the longitudinal direction

Figure 4.7 shows the maximum strain versus maximum drift for Bridge 11Ar with the ground motion in the transverse direction. A similar bi-linear behavior was observed, again with lower strain values than those of the corresponding plot for Bridge 1Ar.

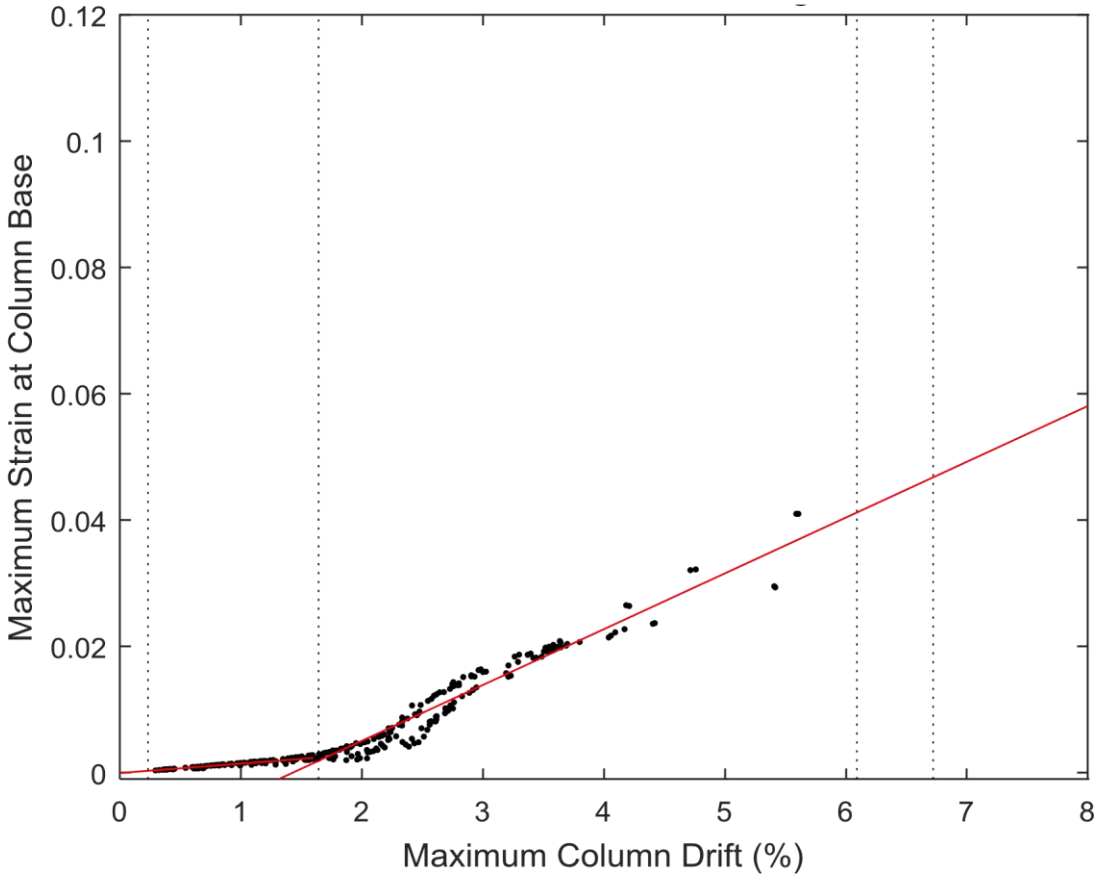

Figure 4.7 Maximum strain vs. maximum drift for Bridge 11Ar with ground motion in the transverse direction

For the residual strain limits, residual drift and strain were plotted for each bridge and in both ground motion directions. To determine the residual drift and residual strain, an average was taken of the values over the last natural period of the analysis. Each ground motion was run only to the end of the acceleration file, and the structure was not allowed to vibrate without the input, so the residual drift could not be read directly from the output data. However, the ground motions flattened out at the end of the time history, so an average over the last several values was an appropriate estimate of the residual value.

A linear relationship was observed for each of the residual strain versus drift plots. A line was fit to the data for each bridge. Figure 4.8 shows the residual strain versus residual drift for Bridge 1Ar in the longitudinal direction.

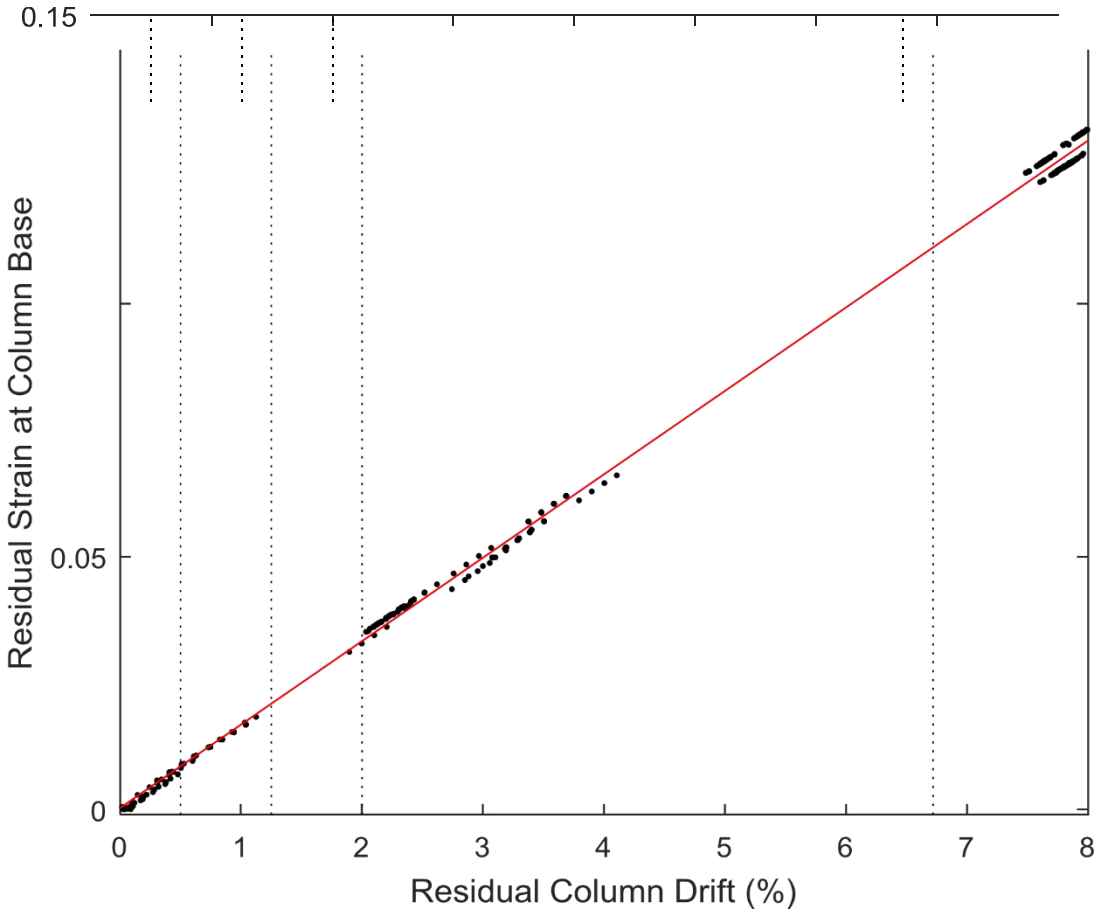

Figure 4.8 Residual strain vs. residual drift for Bridge 1Ar with ground motion in the longitudinal direction

Similar behavior was observed with the ground motion in the transverse direction, as shown in figure 4.9.

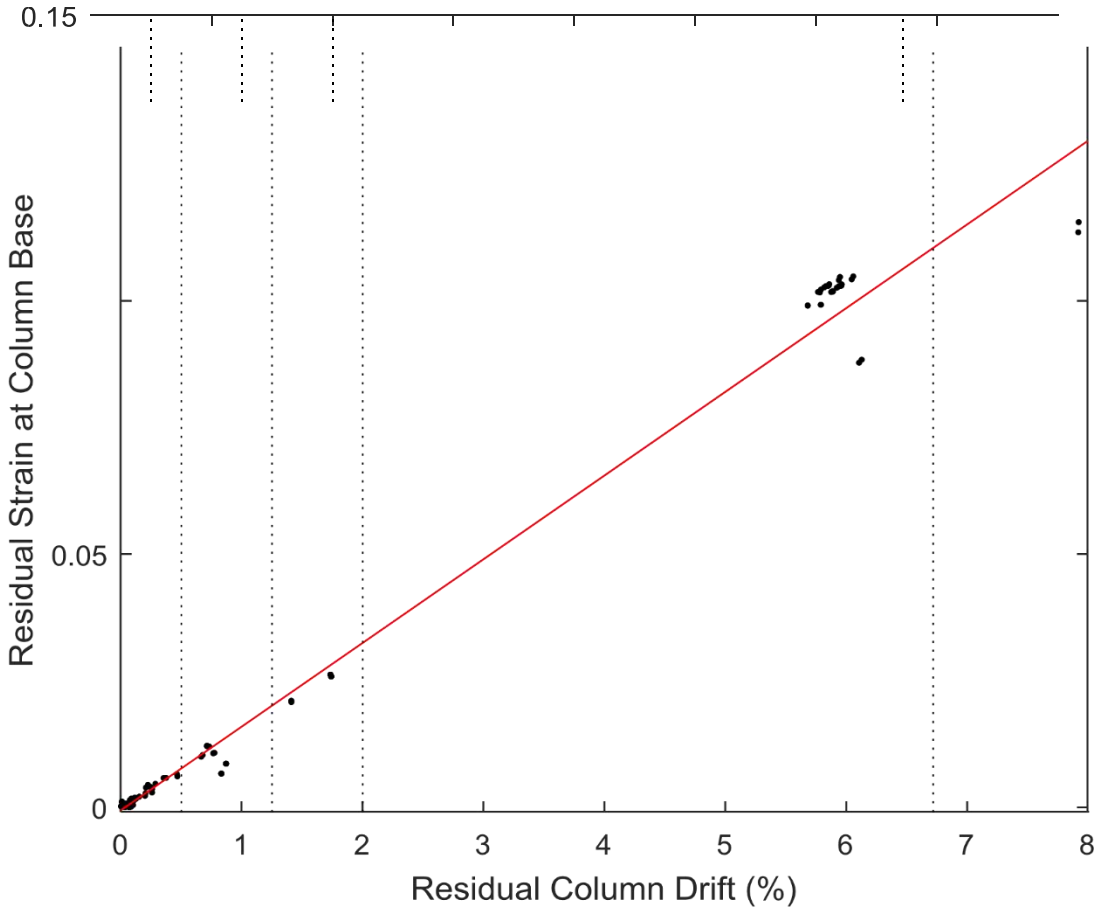

Figure 4.9 Residual strain vs. residual drift for Bridge 1Ar with ground motion in the transverse direction

As with the maximum drift and strain plots, the Type 11 bridges displayed behavior similar to that of the Type 1 bridges, but the strain values that corresponded to the residual drift limits were lower than those for the Type 1 bridges. Figure 4.10 shows the residual strain versus residual drift for Bridge 11Ar in the longitudinal direction.

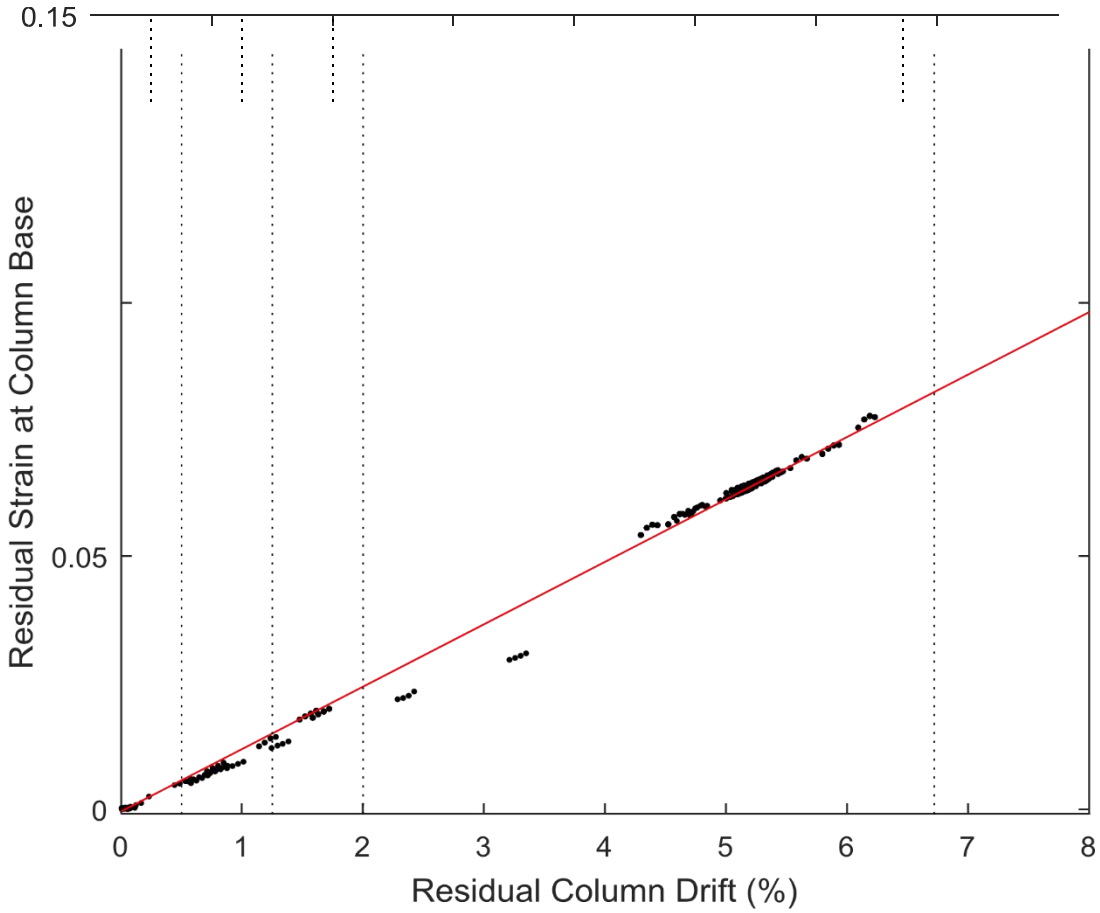

Figure 4.10 Residual strain vs. residual drift for Bridge 11Ar with ground motion in the longitudinal direction

Figure 4.11 shows similar behavior for Bridge 11Ar with the ground motion in the transverse direction.

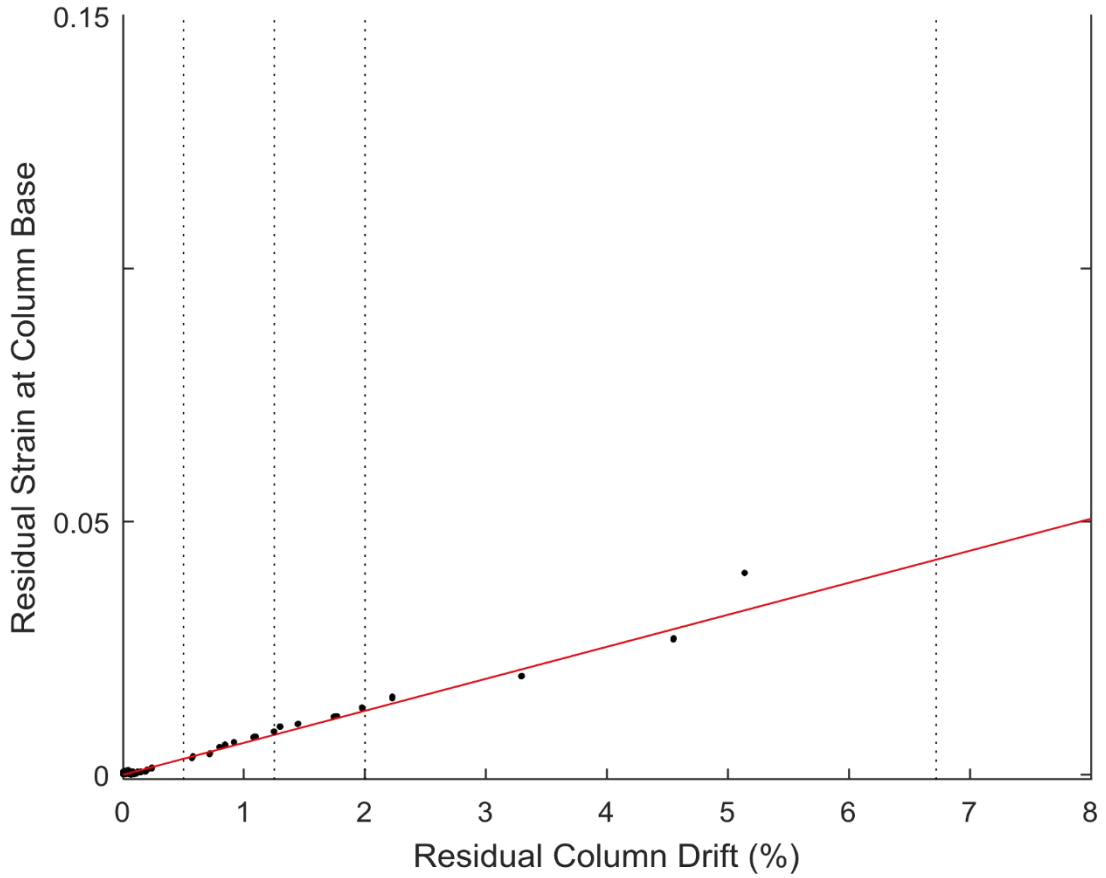

Figure 4.11 Residual strain vs. residual drift for Bridge 11Ar with ground motion in the transverse direction

The resulting plots for the remaining bridges displayed similar behavior and can be found in the Appendix. The following chapter discusses the results and the strain limits corresponding to the drift limits in more detail.

4.6 Hand Calculations for Strain

Hand calculations were performed to estimate both the elastic and plastic strain responses of each column. Figure 4.12 shows the hand calculations for Bridge 1Br, as well as the data obtained from the OpenSees model. This plot makes clear that the hand calculations for strain were not a good representation of the behavior of the bridge, especially once it had moved past the elastic range.

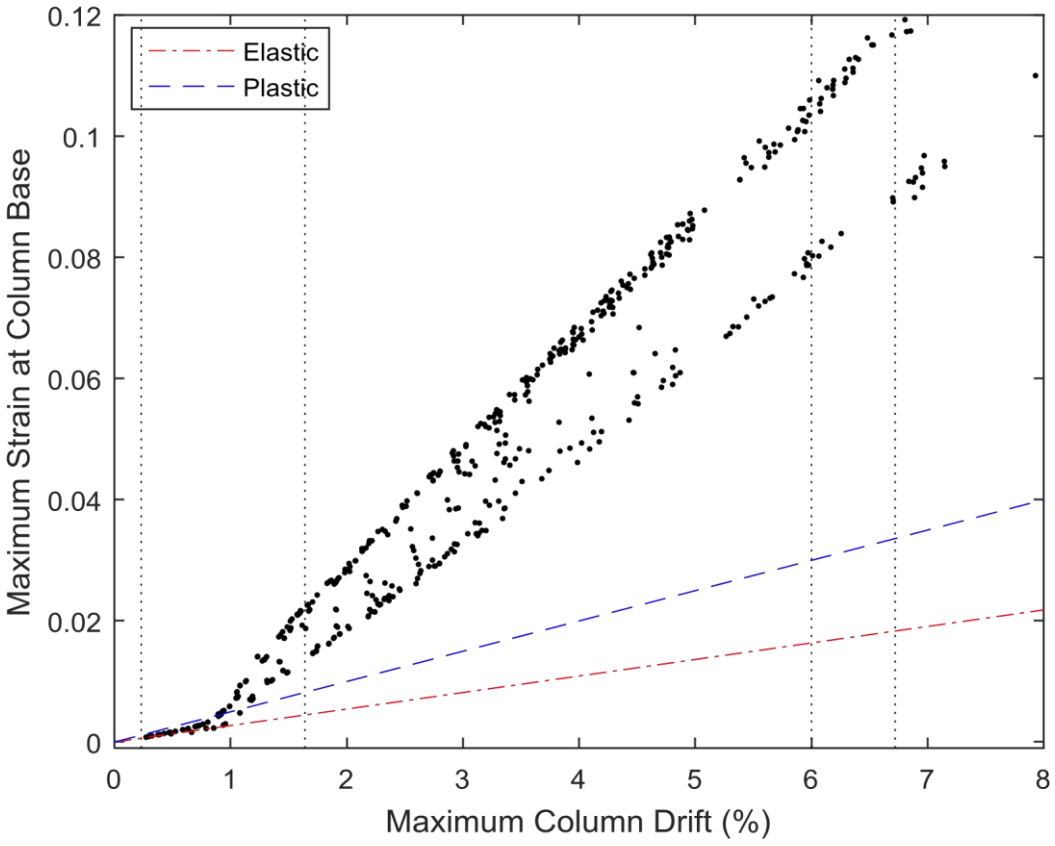

Figure 4.12 Hand calculations for strain plotted with 1Br model data

Figure 4.13 shows the same plot, focused on the elastic region. Here, the hand calculation for elastic strain represented the model data fairly well. Therefore, while hand calculations may provide good estimates for elastic behavior, the plastic behavior of a bridge pier is more difficult to determine by hand and can be better found by modeling the structure.

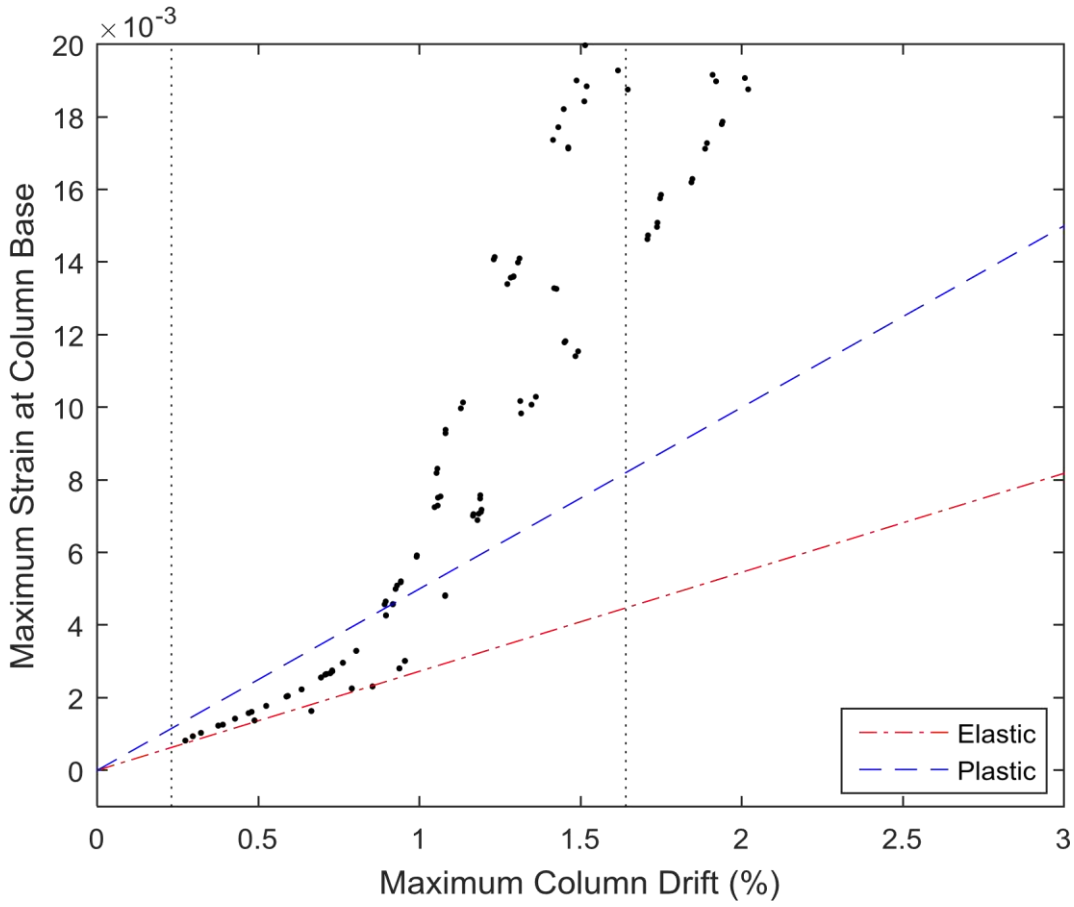

Figure 4.13 Hand calculations for strain of model 1Br in elastic region

Chapter 5 Damage State Detection Utilizing Strain Measurements

This chapter describes the determination of strain limits from drift limits, based on the strain data obtained from the OpenSees models. Recommendations are made based on the damage states corresponding to each limit.

5.1 Strain Limits

From the intersection of the drift limits and the lines of fit for the data obtained from the models, strain limits corresponding to each drift limit were calculated. Different limits were determined for Type 1 and Type 11 bridges for both maximum and residual column drift limits, with the ground motion applied in both the longitudinal and the transverse directions. The average maximum and residual strain limits for types 1 and 11 bridges are discussed in this section, as well as the standard deviations for those limits.

The maximum drift limits were 0.23 percent for the damage state designated as DS0, 1.64 percent for DS1, 6 percent for DS2, and 6.72 percent for DS3, from Mackie et al. (2008). The first damage state (DS0) drift limit is associated with the column cracking moment and marks the onset of initial cracking and negligible damage. DS1 marks the onset of concrete cover spalling. Longitudinal reinforcing bars first begin buckling at DS2, and column failure is initiated at DS3.

The average strain limits based on these maximum drift limits for Type 1 bridges are shown in table 5.1. Initial column cracking occurs at a strain of 0.053 percent, and 1.93 percent strain marks the onset of concrete cover spalling. The longitudinal reinforcing bars begin to buckle at 9.43 percent strain, and collapse is initiated at 10.49 percent strain. The standard deviations for each of these limits were relatively low, which means these average limits are a good representation of the data.

Table 5.1 Maximum strain limits for Type 1 bridges

Drift:	*0.23%*	*1.64%*	*6%*	*6.72%*
	DS0	**DS1**	**DS2**	**DS3**
Average	0.00053	0.0193	0.0943	0.1049
Std. Dev.	0.00018	0.0014	0.0044	0.0049

The average strain limits based on the maximum drift limits for Type 11 bridges are shown in table 5.2. These limits are a bit lower than the limits found for the Type 1 bridges. 0. Initial column cracking begins at 022 percent strain, the onset of concrete cover spalling occurs at 0.45 percent strain, reinforcing bars begin buckling at 5.77 percent strain, and collapse is initiated at 6.47 percent residual strain.

Table 5.2 Maximum strain limits for Type 11 bridges

Drift:	*0.23%*	*1.64%*	*6%*	*6.72%*
	DS0	**DS1**	**DS2**	**DS3**
Average	0.00022	0.0045	0.0577	0.0647
Std. Dev.	0.00018	0.0012	0.0090	0.0098

The residual drift limit states provided by Mackie et al. (2008) are 0.5 percent drift for DS0, 1.25 percent drift for DS1, 2 percent drift for DS2, and 6.72 percent drift for DS3. The limit for DS0 was based on the onset of significant damage; DS1 was calculated as the damage state at which the pier needs to be thickened and a jacket needs to be installed; DS2 marked the damage state where re-centering of the column is required; and DS3 marked the onset of column failure.

Table 5.3 shows the average strain limits corresponding to these residual drift damage states for the Type 1 bridge models. Again, the standard deviations shown are relatively small, so the average values are a good representation of the strain limits that correspond to the different

residual drift damage states.

Table 5.3 Residual strain limits for Type 1 bridges

Drift:	*0.50%*	*1.25%*	*2%*	*6.72%*
	DS0	**DS1**	**DS2**	**DS3**
Average	0.0074	0.0197	0.0319	0.1090
Std. Dev.	0.0016	0.0016	0.0016	0.0039

The average strain limits based on these residual drift limits for Type 11 bridges are shown in table 5.4. As with the maximum drift limits, the residual strain limits for Type 11 bridges were lower than the limits found for the Type 1 bridges.

Table 5.4 Residual strain limits for Type 11 bridges

Drift:	*0.50%*	*1.25%*	*2%*	*6.72%*
	DS0	**DS1**	**DS2**	**DS3**
Average	0.0048	0.0119	0.0190	0.0640
Std. Dev.	0.0010	0.0028	0.0046	0.0162

Using these strain limits, recommendations for action can be taken on the basis of strain sensor readings. Some of these recommendations are discussed in the following section.

5.2 Recommendations

For each damage state defined, Mackie et al. (2008) provided recommended repair actions. These recommended actions are based on the damage level associated with each limit and can help bridge officials make decisions. Both the maximum and residual strain limits and their implications should be considered by decision makers. In the case of a major natural

disaster, residual strain values may be more realistic since they will be easier to obtain. During the event, it is likely that data will be interrupted, and maximum values may not be measured or recorded. For continuous data collection between events, maximum strain limits can be helpful in deciding whether there is damage to a pier and whether a bridge inspector should be sent to look at the bridge.

For the maximum strain limit state DS1, cracks should be sealed and some minor removal and patching of concrete may be required. Cracks must be sealed and major patching will be required when the DS2 limit is reached. If the DS3 strain limit is reached, the column has failed and needs to be replaced.

If the residual strain limit state DS1 is reached, buckled reinforcement needs to be replaced and a steel column casing should be installed. The columns must be re-centered if the DS2 strain limit is recorded, and the column needs replacement if the DS3 residual strain limit has been reached.

Since the maximum strain and residual strain limit states provide different values and relate to different types of damage, monitoring strain recordings with both limits in mind will be helpful. If any of the limits are met, the owner should have information about what type of damage might exist and make decisions based on this information. During times when there is no significant seismic activity, maximum strain limits may be helpful, as they mark the onset of damage at a lower strain value. The data can be processed to show any recordings that exceed any of the limit states so that bridge officials can look into the condition of the bridge.

Chapter 6 Conclusions and Future Research

6.1 Wireless Sensor Networks

With recent advances in technology, widespread deployment of wireless sensor networks to monitor bridges is becoming more feasible. Off the shelf platforms can be adapted to create affordable systems that are easy to install and can be deployed for several years without replacement. Having wireless sensor networks monitoring lifeline bridges in the region will make the Pacific Northwest much more resilient to a large natural disaster. However, there is a need for an efficient framework for interpreting the data recorded by SHM systems.

Computer models are a powerful tool for determining relationships between data that can be recorded and damage states that can be calculated. Since limit state design has been used for many years, a wealth of knowledge has been gathered and resources are available for determining damage limit states. Relating these limit states to recorded data, and relaying the information about what types of damage correspond to different sensor reading limits, can make SHM systems more useful for owners and decision makers. This project provided the results from relating strain data to drift limit states for certain types of bridges. By relating recordable data to known limit states, sensor data can be used to directly determine the state of a bridge.

The data collected by strain sensors in a wireless sensor network can be displayed in real time to give bridge officials a current overview of the bridges in a region. Making this information immediately available, and flagging bridges with readings that surpass the limit states, can allow a community to be highly resilient and efficient after a natural disaster. First responders can be provided with information about what routes are inaccessible and which are the most efficient for reaching different areas. Visual inspections after an event can be prioritized

on the basis of severity of sensor readings, and officials can work to reopen buildings quickly and create the least negative impact on the community.

Creating a framework to use with advanced wireless sensor network technology will give the SHM community the potential to profoundly affect communities after disasters. The technology has already become advanced enough to make the sensor network deployment realistic, but a gap must be filled between the recorded data and providing useful information to decision makers.

6.2 Future Research

Determining the relationship between strain data and damage limit states provides a framework for relaying useful information from strain gauge data. The relationships and strain limits found in this research showed that the same percentage of drift limits correspond to different percentage of strain limits for the two types of bridges considered. The major difference between the Type 1 and Type 11 bridges studied was column height, so there may be a relationship between the height of a bridge and the strain limits. More work needs to be done before these strain limits can be applied in wireless sensor networks on a broad range of bridges.

To determine the strain limits for bridges in the region, a survey of bridges in the Pacific Northwest needs to be obtained, and the bridges need to be classified into several categories. Analyses similar to the ones done in this research can be performed for each bridge category to determine strain limit values. These limits can then be tested on different column types and on full-scale bridges.

Once an effective framework is in place for relaying sensor information and an inexpensive and easily installed wireless sensor network has been developed, the wireless system can be deployed throughout a large region. With all of the lifeline bridges instrumented and

relaying useful information, bridge officials can make better informed decisions about both regular bridge maintenance and actions to take directly following a natural disaster.

References

Berry, M. P. and Eberhard, M. O. (2005). “Practical Performance Model for Bar Buckling. *ASCE J. Eng. Structures.*, 2005; 131(7): 1060-70.

Bentz, Evan. “Response-2000.” *University of Toronto, Toronto, Ontario Canada*. <http://www.ecf.utoronto.ca/~bentz/r2k.htm>

Caltrans (2004). *Seismic Design Criteria 1.3*. California Department of Transportation, Sacramento, CA.

Choi, H., Choi, S. and Cha H. "Structural Health Monitoring System based on Strain Gauge Enabled Wireless Sensor Nodes", INSS: International Conference on Networked Sensing Systems, Kanazawa, Japan, June 17- 19, 2008: p211-214.

Chang, Peter C, Flatau, Alison, and Liu, S.C. (2003). "Review Paper: Health Monitoring in Civil Infrastructure." *Sage Publications. Structural Health Monitoring, 2003 Vol 2(3): 0257267.*

Chung, Wonseok and Sotelina, Elisa D. (2006). “Three-Dimensional Finite Element Modeling of Composite Girder Bridges.” *J. Eng. Structures.*, 28, 63-71.

Jang 2013

Jang, Shinae et al. (2010). "Structural Health Monitoring of a Cable-Stayed Bridge Using Smart Sensor Technology: Deployment and Evaluation." *Smart Structures and Systems, Vol. 6, No. 5-6, 2010, 439-459.*

Ketchum, M., Chang, V., and Shantz, T. (2004). “*Influence of Design Ground Motion Level on Highway Bridge Costs*.” Report No. Lifelines 6D01, University of California, Pacific Earthquake Engineering Research Center, Berkeley CA.

Ko, J.M., and Ni, Y.Q. (2005). "Technology Developments in Structural Health Monitoring of Large-Scale Bridges." *ScienceDirect. Engineering Structures 27, 2005, 1715-1725.*

Kramer, S. L., Arduino, P., and Shin, H. (2008). “*Performance-based evaluation of bridges on liquefiable soils using OpenSees”*. Report No. 2008/xx, forthcoming, University of California Berkeley, Pacific Earthquake Engineering Research Center, Berkeley CA.

Ledezma, C. A. and Bray, J. D. (2008). “*Performance-based earthquake engineering design evaluation procedure for bridge foundations undergoing liquefaction-induced lateral spreading*.” Report No. 2007/xx, forthcoming, University of California Berkeley, Pacific Earthquake Engineering Research Center, Berkeley CA.

Lee,W. K. and Billington, S. L. (2008). "*Performance-based earthquake engineering assessment of self-centering post-tensioned concrete bridge systems"*. Report No. 2008/xx, forthcoming, University of California Berkeley, Pacific Earthquake Engineering Research Center, Berkeley CA.

Lynch, Jerome Peter. (2007). "An Overview of Wireless Structural Health Monitoring for Civil Structures." *Philosophical Transactions of the Royal Society, 2007, 345-372.*

Mackie, K. R. and Stojadinovic´, B. (2007). "Performance of Benchmark Bridge Structures." In *Proc., ASCE Structures Congress*, Long Beach, CA, May 16-19.

Mackie, K. R., Wong, J.M., and Stojadinovic´, B. (2008). "Integrated Probabilistic PerformanceBased Evaluation of Benchmark Reinforced Concrete Bridges." Report No. 2007/09, University of California Berkeley, Pacific Earthquake Engineering Research Center, Berkeley CA.

Mander, John B. et al. (2007). "Incremental Dynamic Analysis Applied to Seismic Financial Risk Assessment of Bridges." *ScienceDirect. Engineering Structures 29, 2007, 26622672.*

Mander, John B. (1999). "Fragility Curve Development for Assessing the Seismic Vulnerability of Highway Bridges." *Multidisciplinary Center for Earthquake Engineering Research, Research Progress and Accomplishments, July 1999, p 91-100.*

Mazzoni, S., McKenna F., Scott, M. H., and Fenves, G. L. (2006) "Open System for Earthquake Engineering Simulation User Command-Language Manual." Version 1.7.3. *University of California, Berkeley, CA.*
<http://opensees.berkeley.edu/OpenSees/manuals/usermanual/>

Scott, M. H., Kidarsa, A., and Higgins, C. (2008). "Development of Bridge Rating Applications Using OpenSees and Tcl." *ASCE. Journal of Computing in Civil Engineering, 2008, 22(4): 264-271.*

Simon, József. (2010). "Numerical Model Development for Seismic Assessment of Continuous Girder Bridges." *Conference of Junior Researchers in Civil Engineering, 2010, 216-224.*

Vamvatsikos, D. and Cornell, C. A. (2002). "Incremental Dynamic Analysis." *John Wiley & Sons, Ltd. Earthquake Enging Struct. Dyn., 2002, 31: 491-514.*

Wang, Y., Lynch, J. P., and Law, K. (2007). "A Wireless Structural Health Monitoring System with Multithreaded Sensing Devices: Design and Validation." *Structure and Infrastructure Engineering, Vol. 3, No. 2, June 2007, 103-120.*

Zhou, Guang-Dong and Yi, Ting-Hua. (2013). "Recent Developments on Wireless Sensor Networks Technology for Bridge Health Monitoring." *Hindawi Publishing Corporation, Mathematical Problems in Engineering, 2013.*

Bibliography

Aktan, E., Chase, S., Inman, D., and Pines, D. (2001). "Monitoring and Managing the Health of Infrastructure Systems." *Proceedings of the 2001 SPIE Conference on Health Monitoring of Highway Transportation Infrastructure, SPIE, March 6-8, 2001*.

Choi, E., DesRoches, R. and Nielson B. "*Seismic fragility of typical bridges in moderate seismic zones",* Engineering Structures, Volume 26, Issue 2, January 2004, Pages 187-199.

Esch, G., Scott, M.H., and Zhang, E. (2009). "Graphical 3D Visualization of Highway Bridge Ratings." *ASCE. Journal of Computing Engineering, 2009, 23(6): 355-362.*

Kalkan, Erol, and Kwong, Neal S. (2011) "Documentation for Assessment of Modal PushoverBased Scaling Procedure for Nonlinear Response History Analysis of "Ordinary Standard" Bridges." *U.S. Geological Survey Open-File Report 2010-1328, 58 p.* <http://pubs.usgs.gov/of/2010/1328/>.

Lynch, J. P., and Loh, K. J. (2006). "A Summary Review of Wireless Sensors and Sensor Networkds for Structural Health Monitoring." *The Shock and Vibration Digest, 2006, 38; 91*.

Mackie, K. R. and Stojadinovic´, B. (2005). "*Fragility basis for California highway overpass bridge seismic decision making."* Report No. 2005/02, University of California Berkeley, Pacific Earthquake Engineering Research Center, Berkeley CA.

McKenna, F., Fenves, G. L., and Scott, M. H. (2000). Open System for Earthquake Engineering Simulation. University of California, Berkeley, CA. <http://opensees.berkeley.edu>

Ramanathan, K., DesRoches, R., and Padgett, J. E. (2010). "Analytical Fragility Curves for Multispan Continuous Steel Girder Bridges in Moderate Seismic Zones." *Transportation Research Record: Journal of the Transportation Research Board, 2010, No. 2202, pp 173-182.*

Scott, M. H. (2008). "Extensions of OpenSees for Bridge Management Applications." ASCE. *Structures Congress 2008 – 18th Analysis and Computation Specialty Conference.*

Sommer, A. M., Nowak, A. S., and Thoft-Christensen, P. (1993). "Probability-Based Bridge Inspection Strategy." *ASCE. J. Struct. Eng., 1993, 119(12), 3520-3536.*

Wang, Y., Loh, K. J., Lynch J. P., Fraser, M., Law, K., and Elgamal, A. (2006). "Vibration Monitoring of the Voigt Bridge using Wired and Wireless Monitoring Systems." *The Proceeding of 4th China-Japan-US Symposium on Structural Control and Monitoring. Oct. 16-17, 2006.*

Appendix A. Ground Motion Suite

Ground Motion Time History Plots

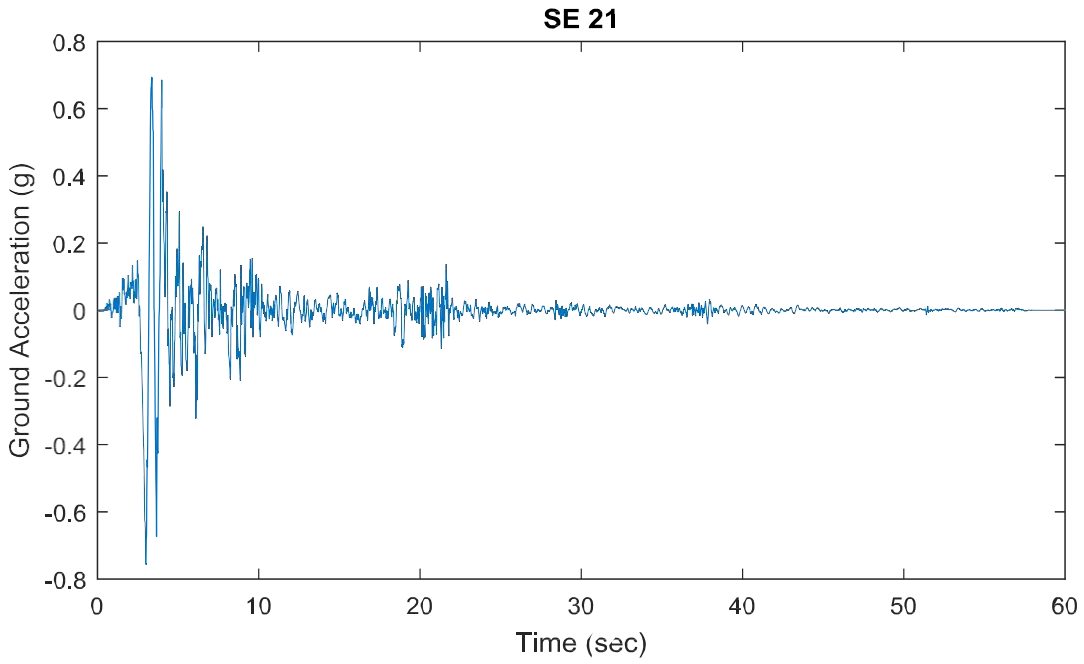

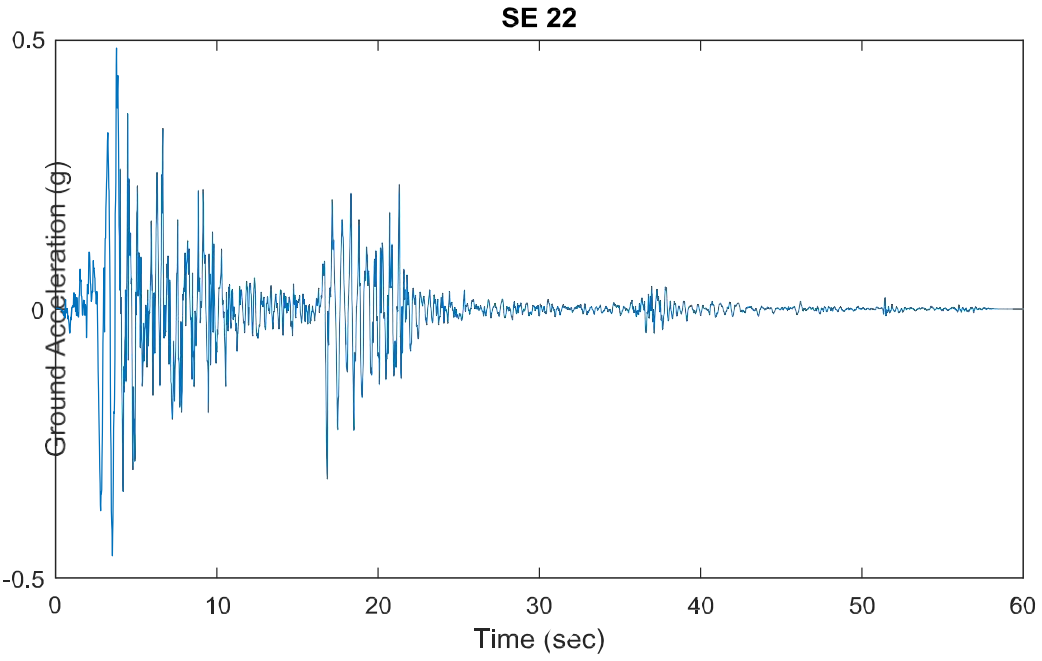

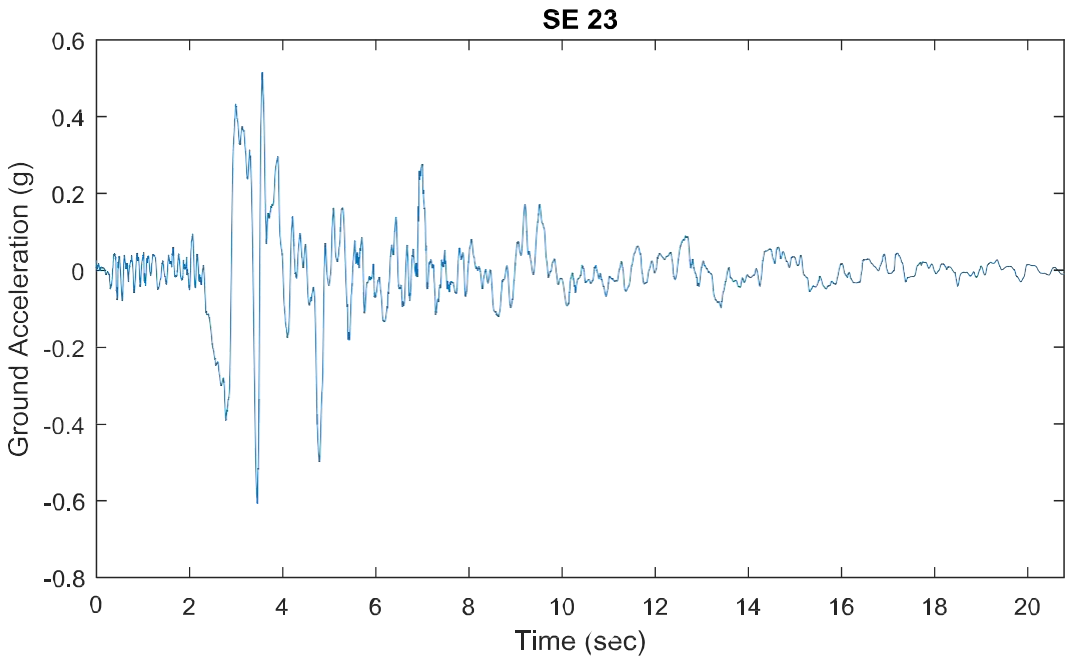
SE 23
Ground Acceleration (g)
Time (sec)
0.6
0.4
0.2
0
-0.2
-0.4
-0.6
-0.8
0
2
4
6
8
10
12
14
16
18
20

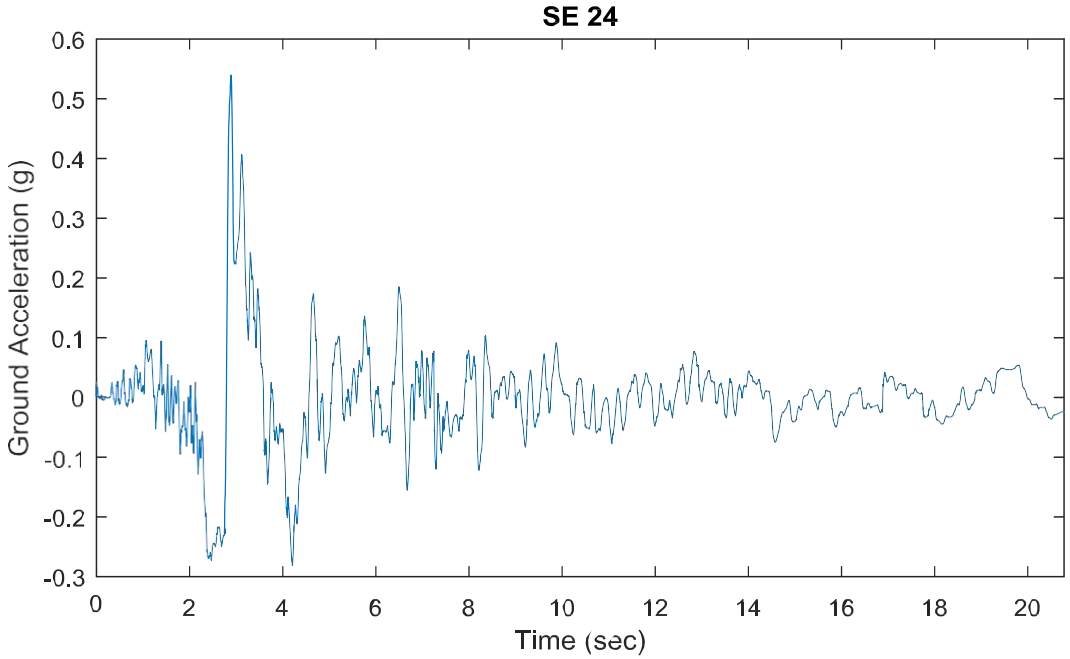
SE 24
Ground Acceleration (g)
Time (sec)
0.6
0.5
0.4
0.3
0.2
0.1
0
-0.1
-0.2
-0.3
0
2
4
6
8
10
12
14
16
18
20

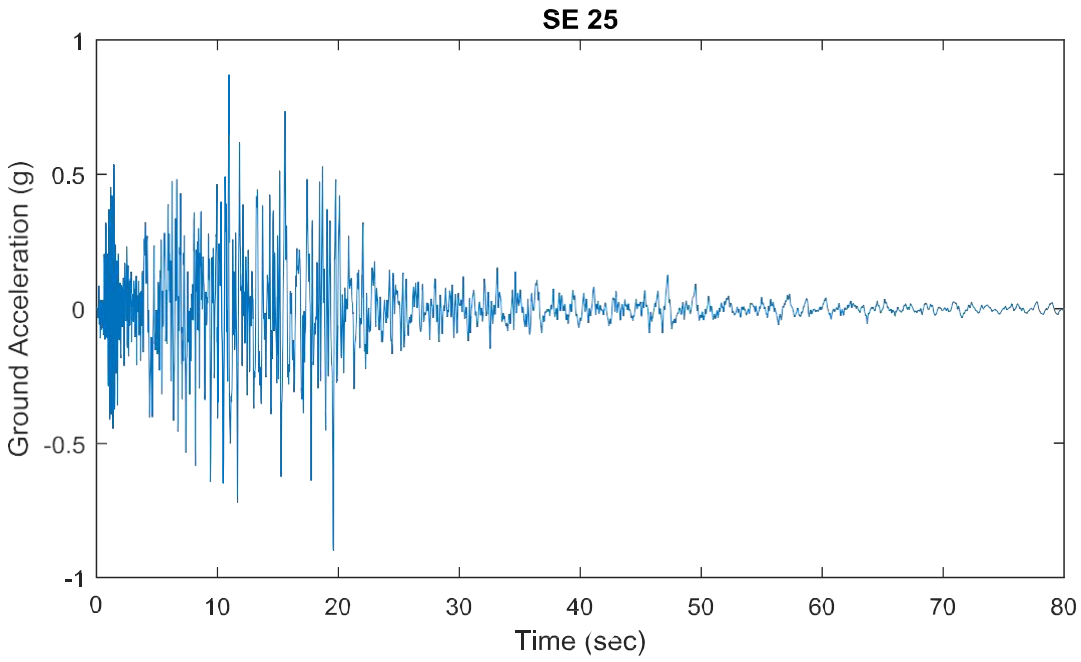
SE 25
Ground Acceleration (g)
1
0.5
0
-0.5
-1
0
10
20
30
40
50
60
70
80
Time (sec)

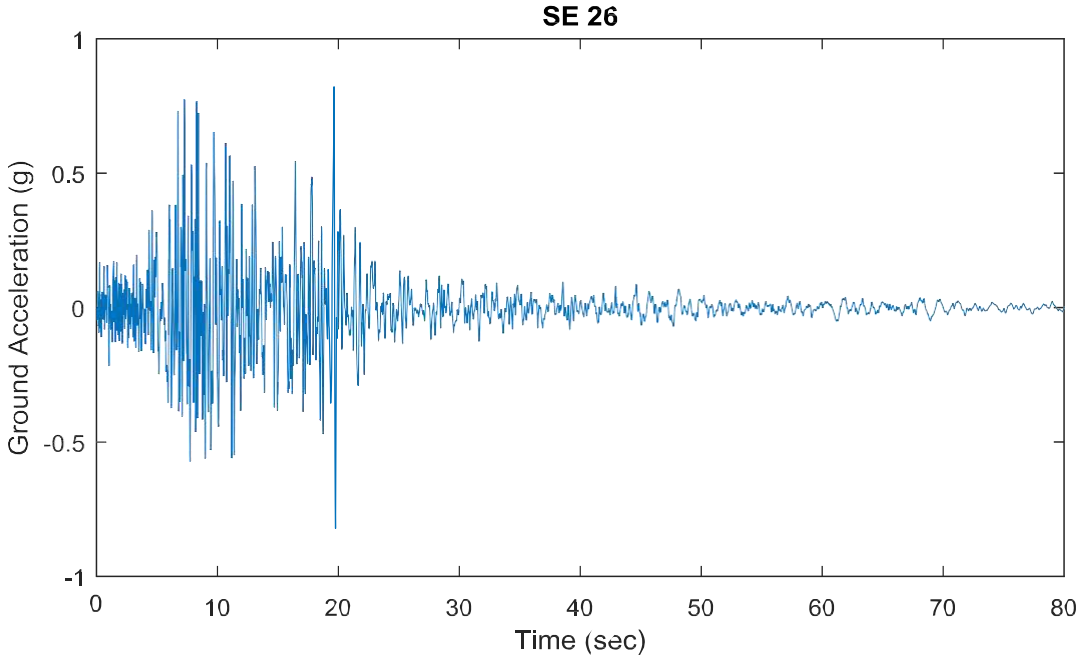
SE 26
Ground Acceleration (g)
1
0.5
0
-0.5
-1
0
10
20
30
40
50
60
70
80
Time (sec)

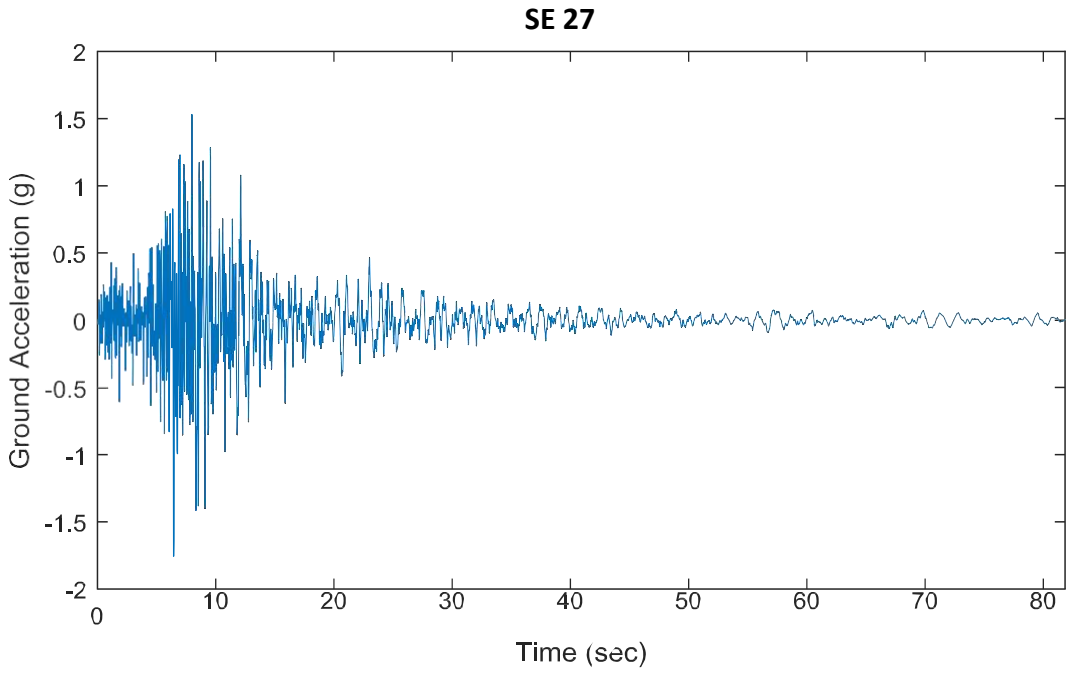
SE 27
Ground Acceleration (g)
Time (sec)
2
1.5
1
0.5
0
-0.5
-1
-1.5
-2
0
10
20
30
40
50
60
70
80

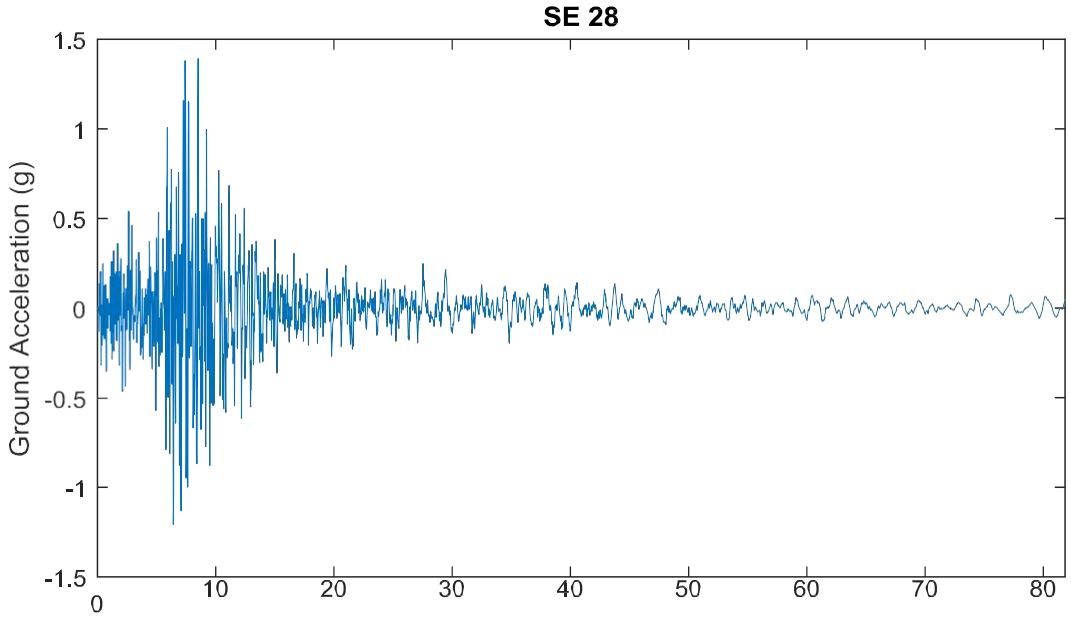
SE 28
Ground Acceleration (g)
1.5
1
0.5
0
-0.5
-1
-1.5
0
10
20
30
40
50
60
70
80

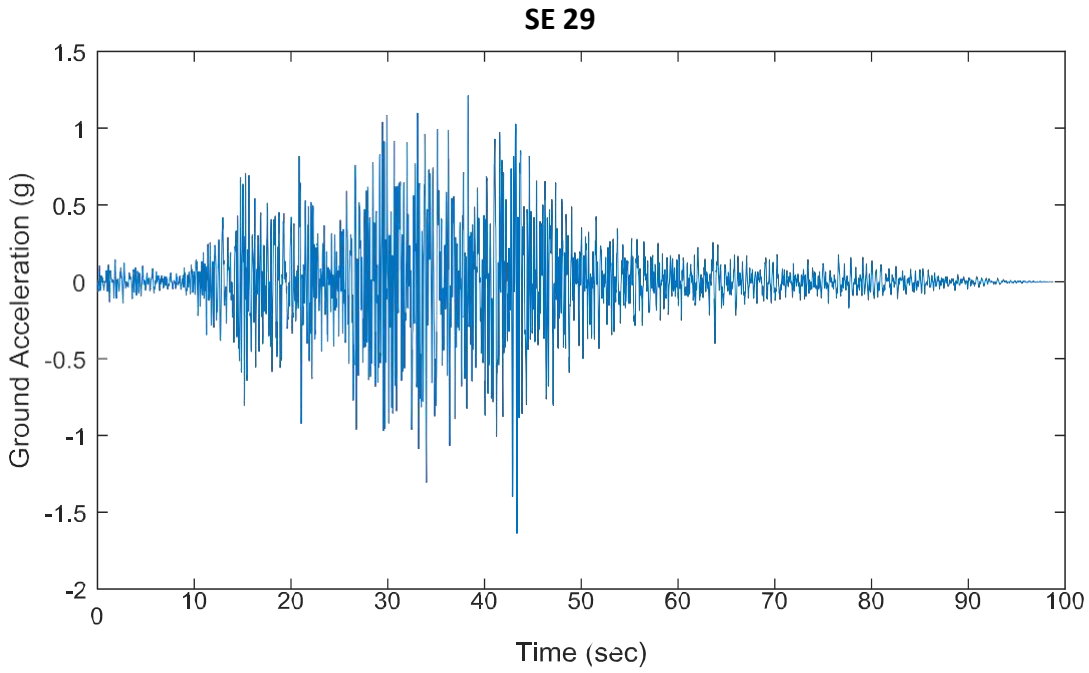
SE 29
Ground Acceleration (g)
Time (sec)
1.5
1
0.5
0
-0.5
-1
-1.5
-2
0
10
20
30
40
50
60
70
80
90
100

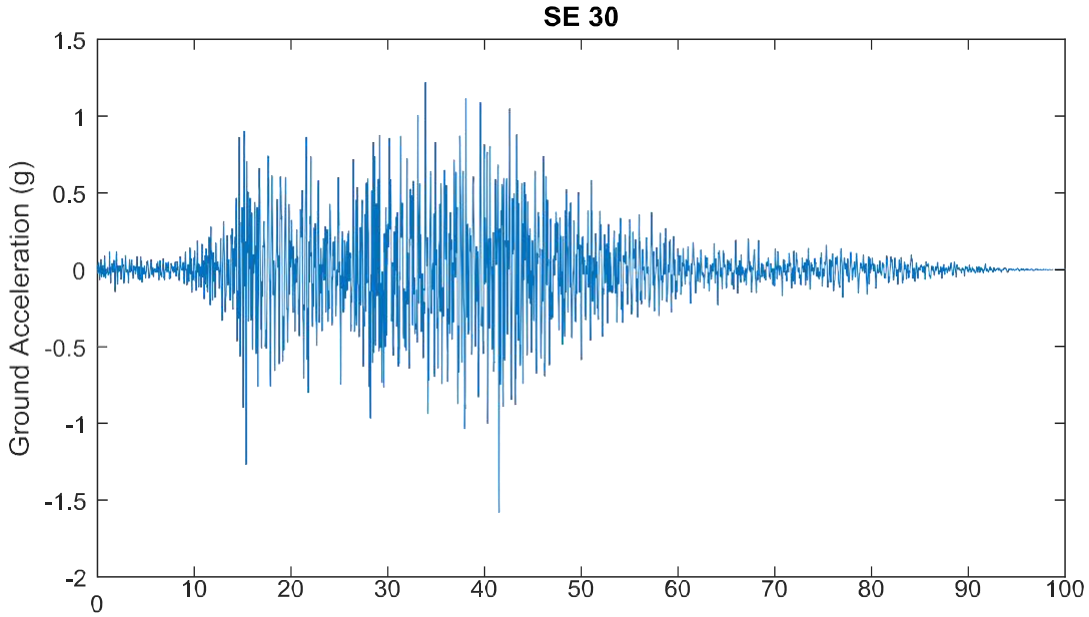
SE 30
Ground Acceleration (g)
1.5
1
0.5
0
-0.5
-1
-1.5
-2
0
10
20
30
40
50
60
70
80
90
100

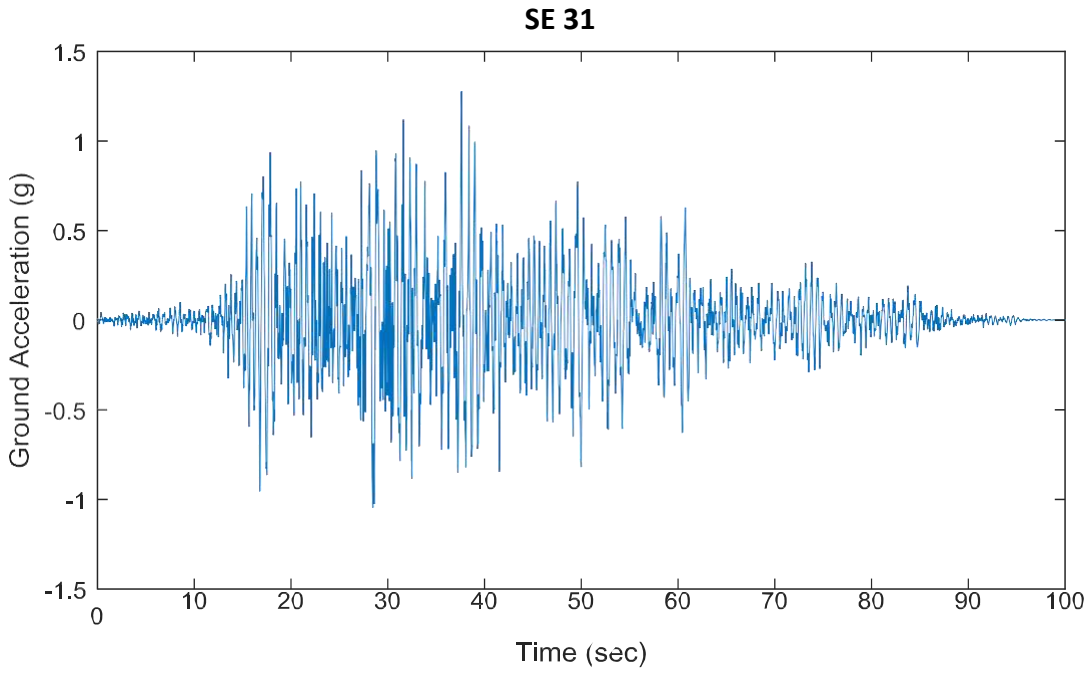
SE 31
Ground Acceleration (g)
Time (sec)
1.5
1
0.5
0
-0.5
-1
-1.5
0
10
20
30
40
50
60
70
80
90
100

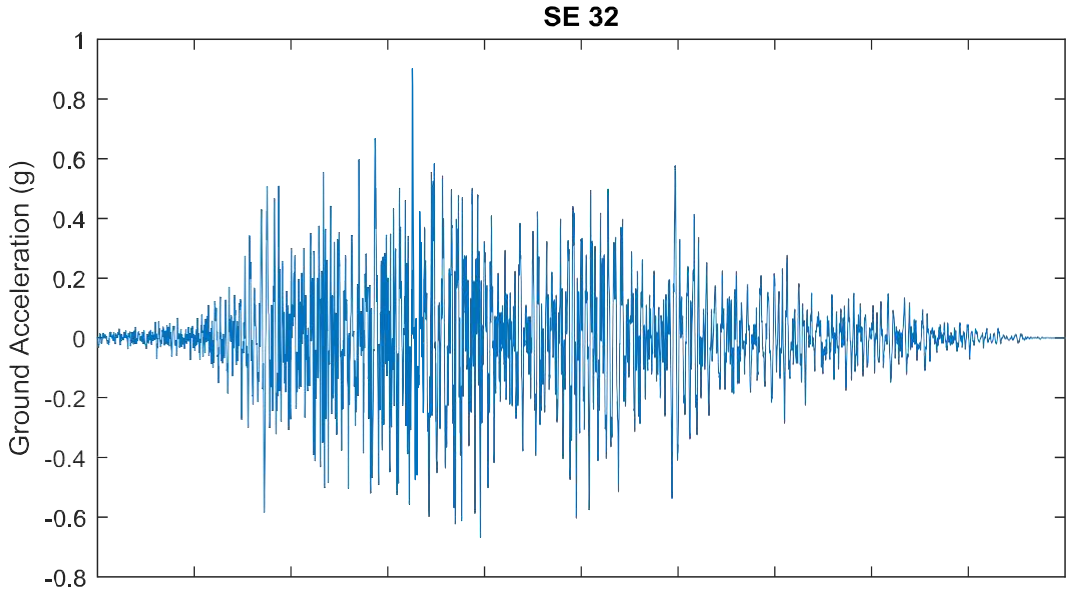
SE 32
Ground Acceleration (g)
1
0.8
0.6
0.4
0.2
0
-0.2
-0.4
-0.6
-0.8

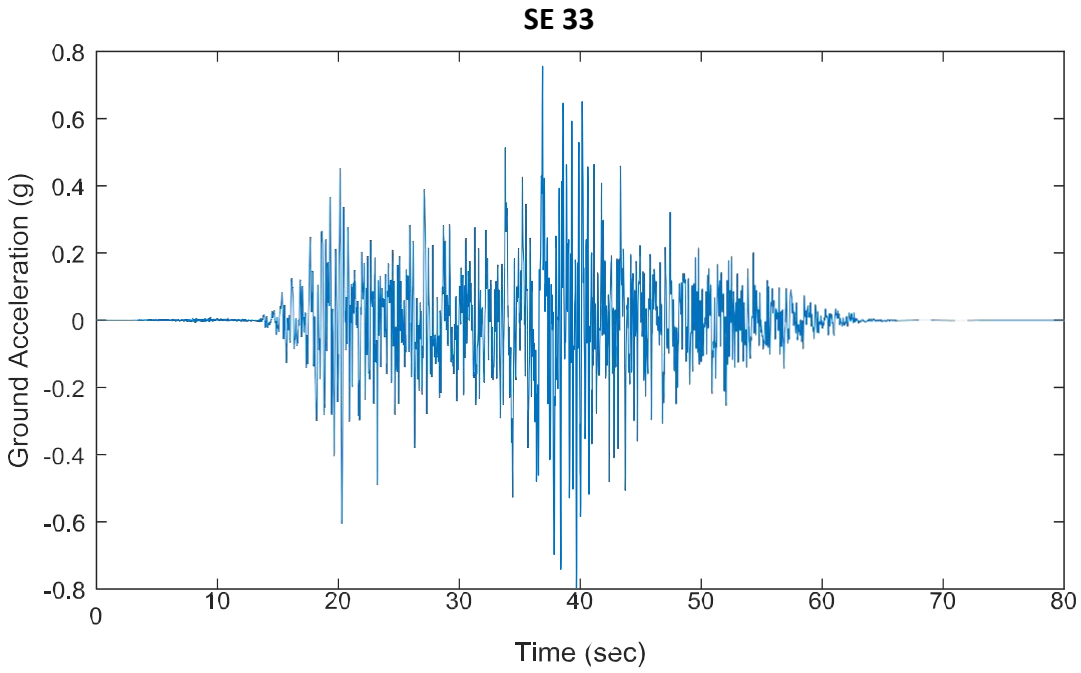
SE 33
Ground Acceleration (g)
Time (sec)
0.8
0.6
0.4
0.2
0
-0.2
-0.4
-0.6
-0.8
0
10
20
30
40
50
60
70
80

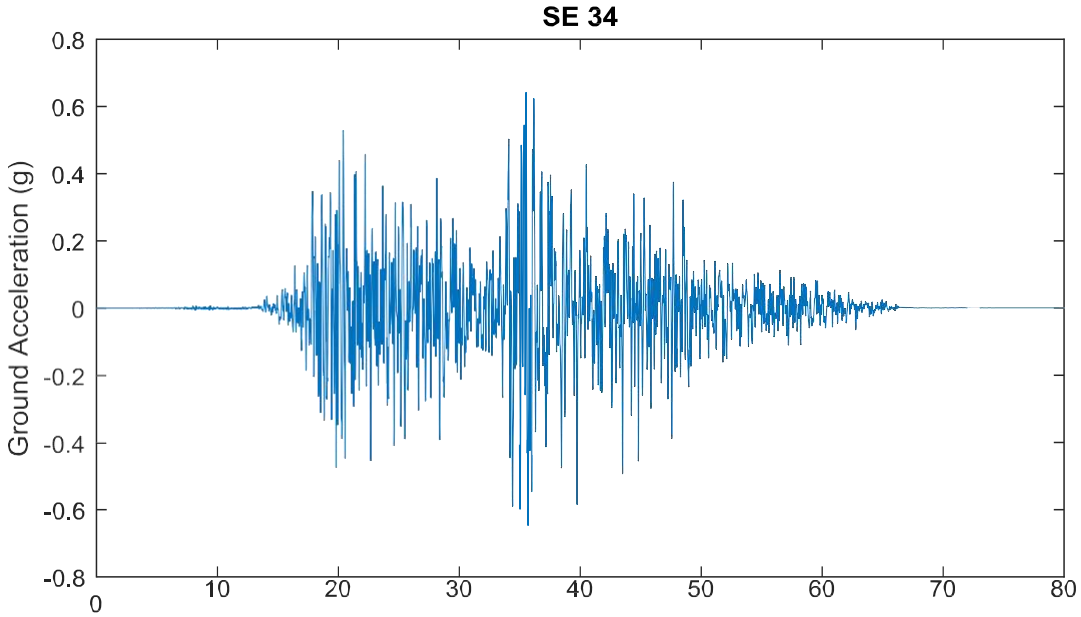
SE 34
Ground Acceleration (g)
0.8
0.6
0.4
0.2
0
-0.2
-0.4
-0.6
-0.8
0
10
20
30
40
50
60
70
80

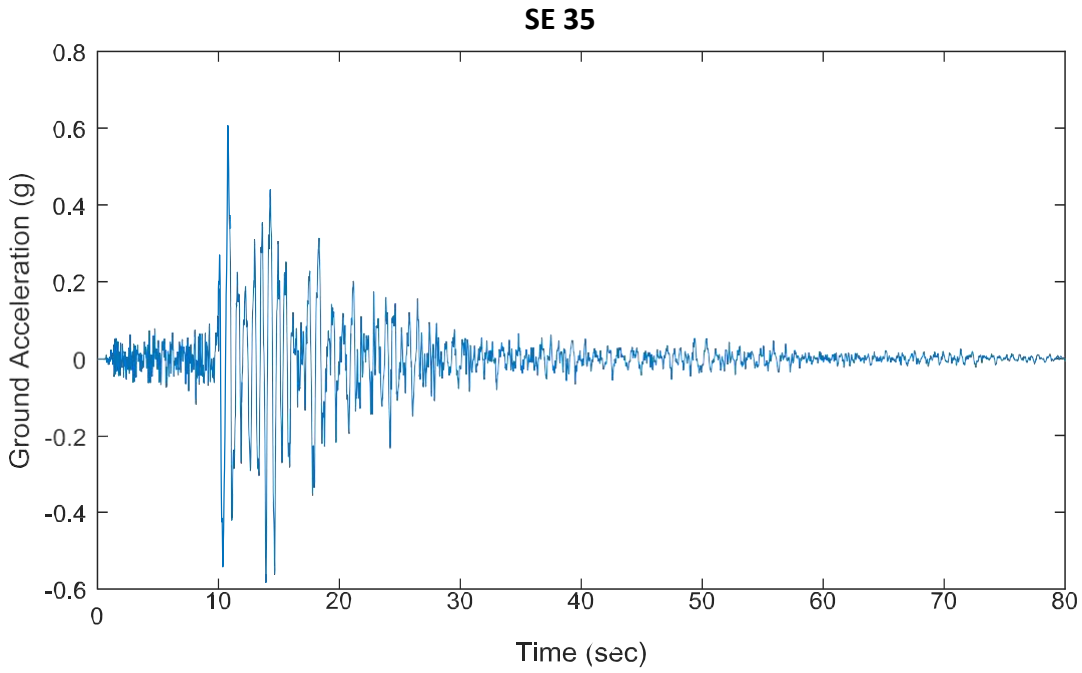
SE 35
Ground Acceleration (g)
Time (sec)
0.8
0.6
0.4
0.2
0
-0.2
-0.4
-0.6
0
10
20
30
40
50
60
70
80

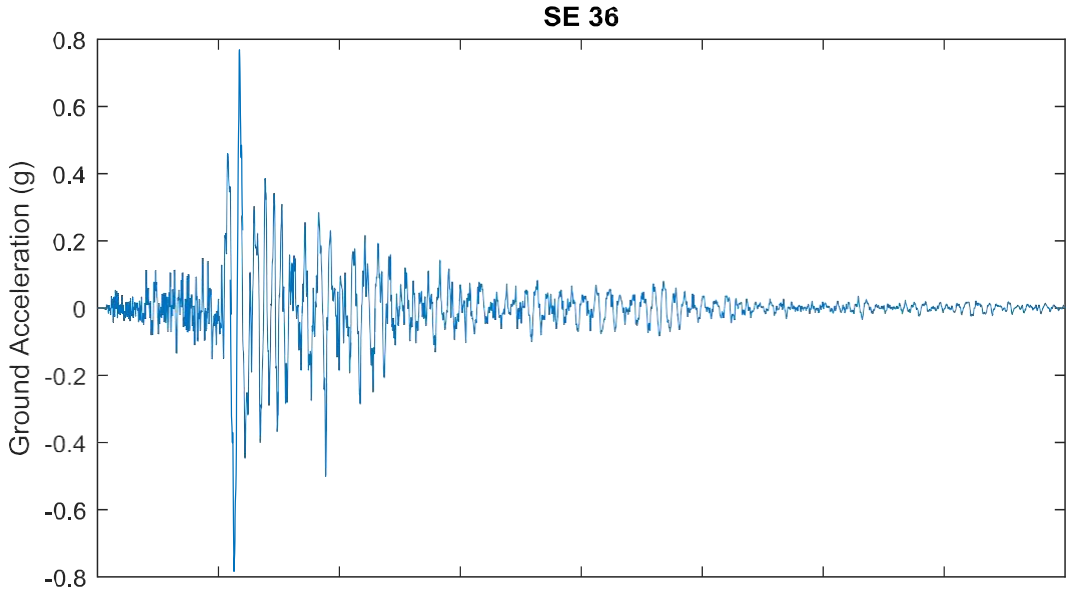
SE 36
Ground Acceleration (g)
0.8
0.6
0.4
0.2
0
-0.2
-0.4
-0.6
-0.8

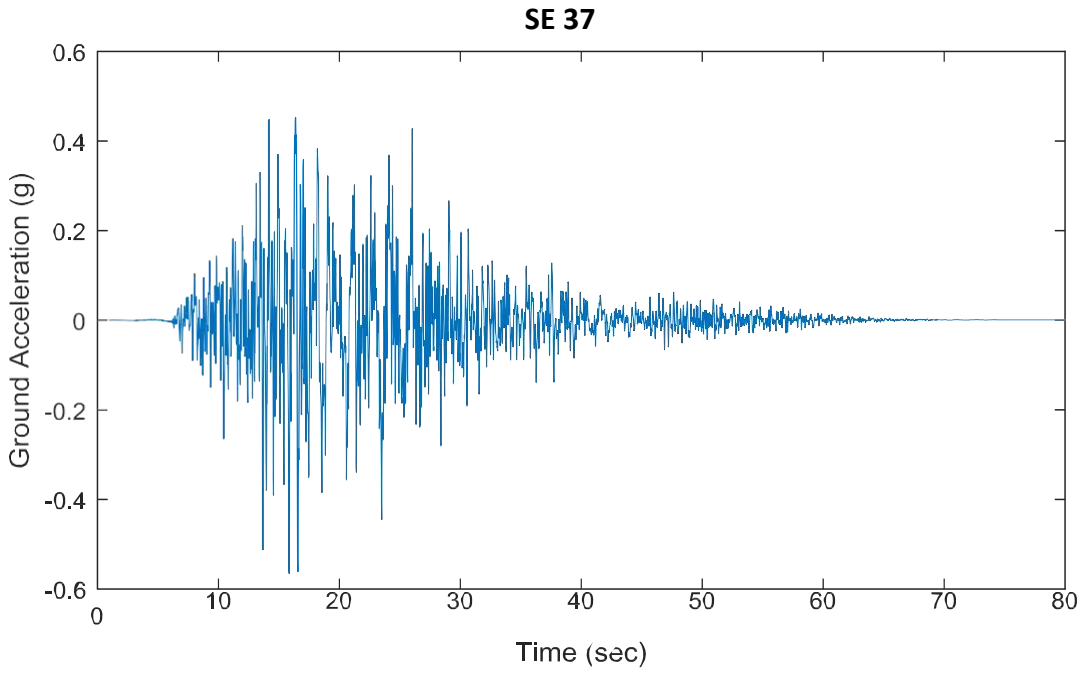
SE 37
Ground Acceleration (g)
Time (sec)
0.6
0.4
0.2
0
-0.2
-0.4
-0.6
0
10
20
30
40
50
60
70
80

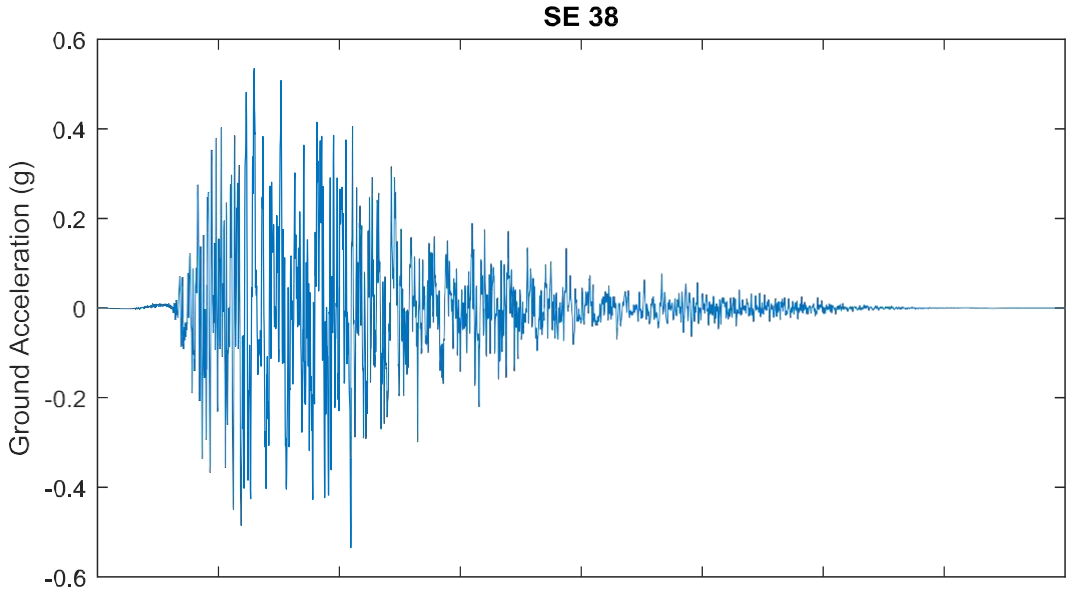
SE 38
Ground Acceleration (g)
0.6
0.4
0.2
0
-0.2
-0.4
-0.6

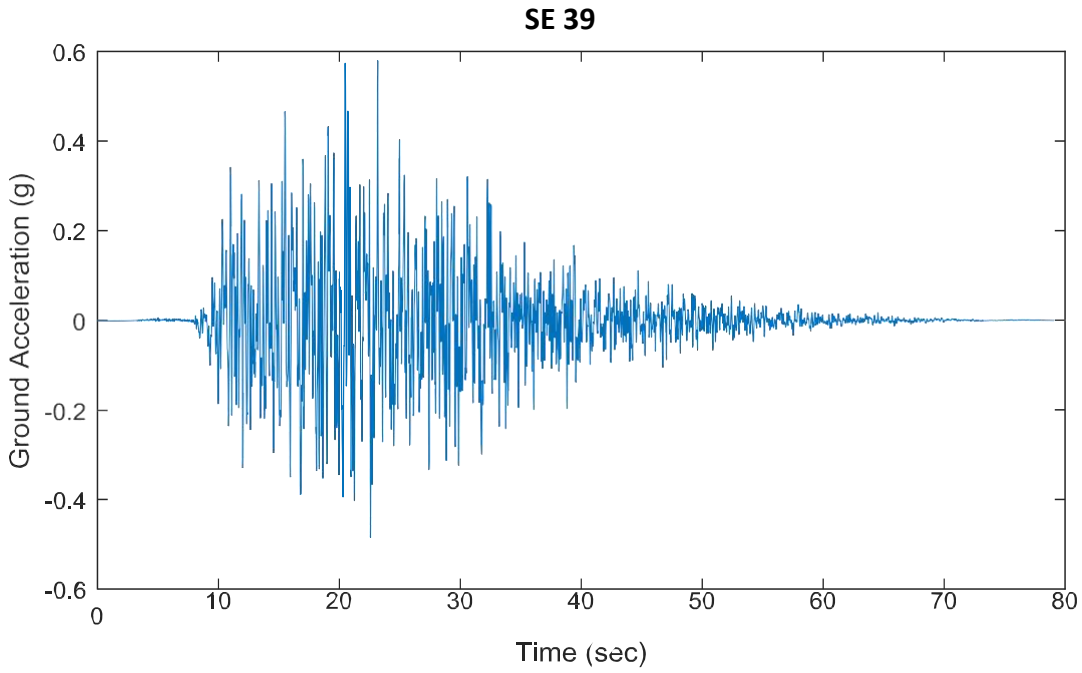
SE 39
Ground Acceleration (g)
Time (sec)
0.6
0.4
0.2
0
-0.2
-0.4
-0.6
0
10
20
30
40
50
60
70
80

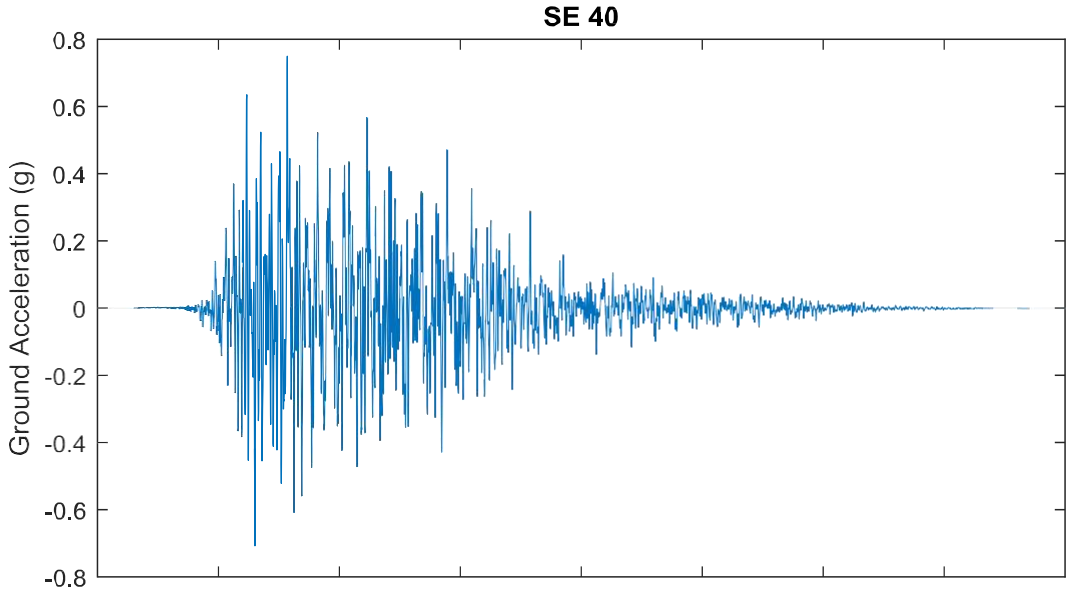
SE 40
Ground Acceleration (g)
0.8
0.6
0.4
0.2
0
-0.2
-0.4
-0.6
-0.8

Appendix B. Strain Data

Maximum Strain vs Maximum Drift Plots

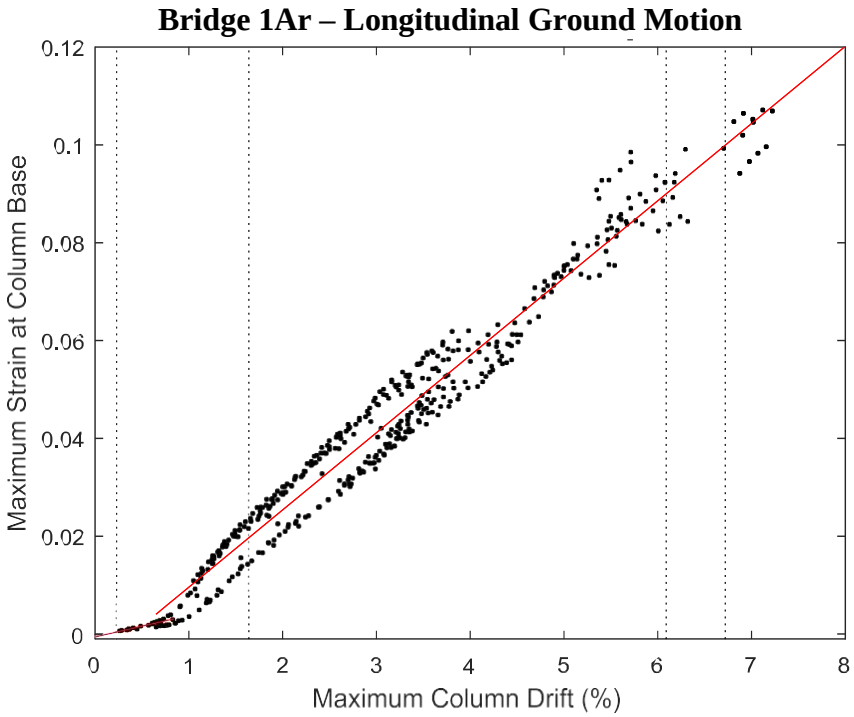

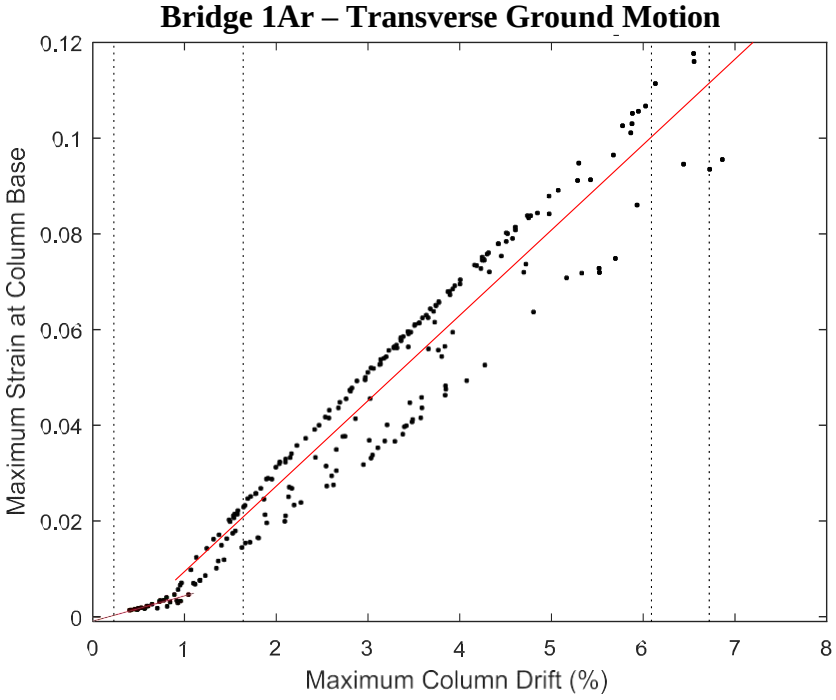

Bridge 1As – Longitudinal Ground Motion

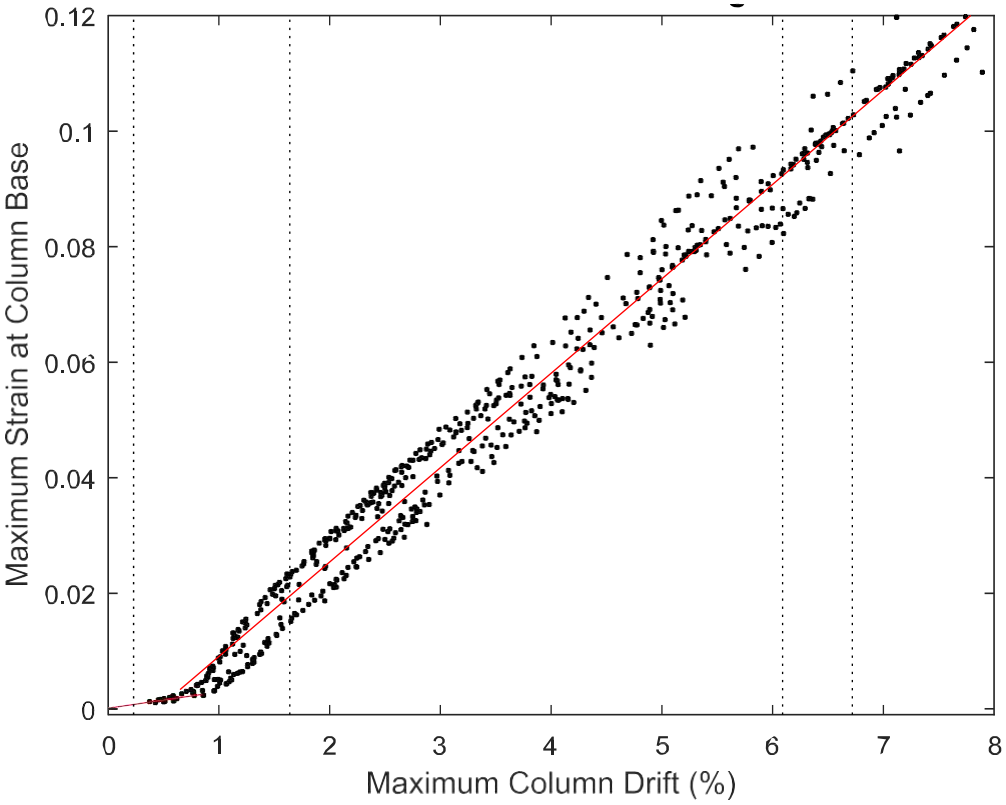

Bridge 1As – Transverse Ground Motion

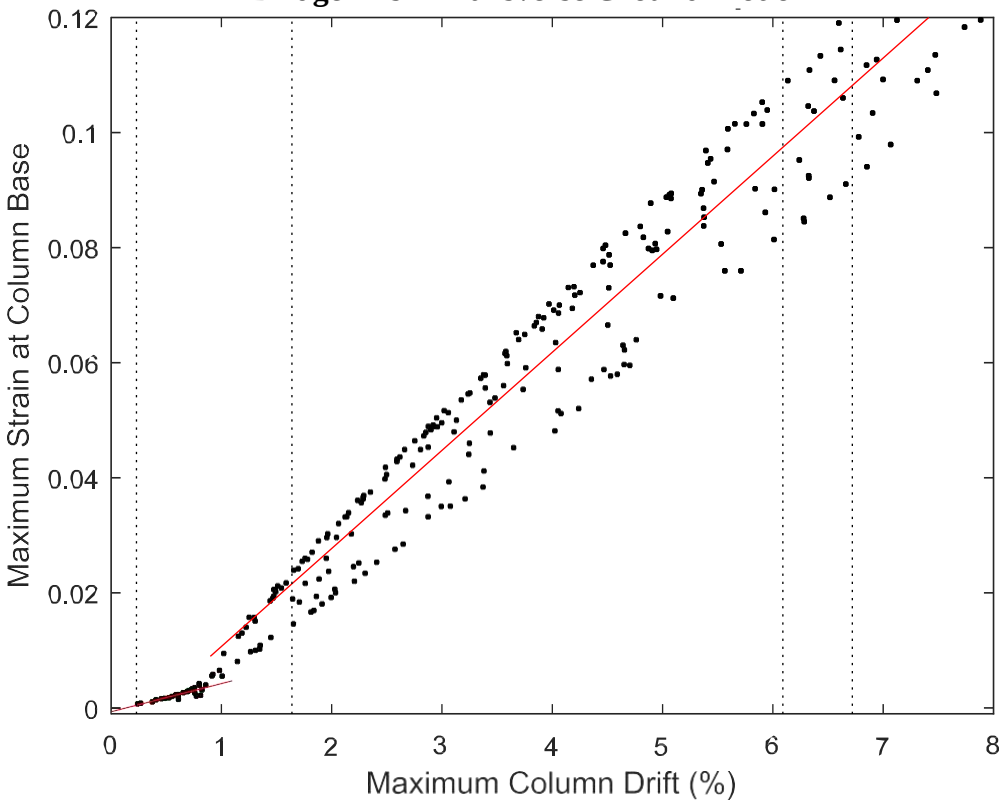

Bridge 1Br – Longitudinal Ground Motion

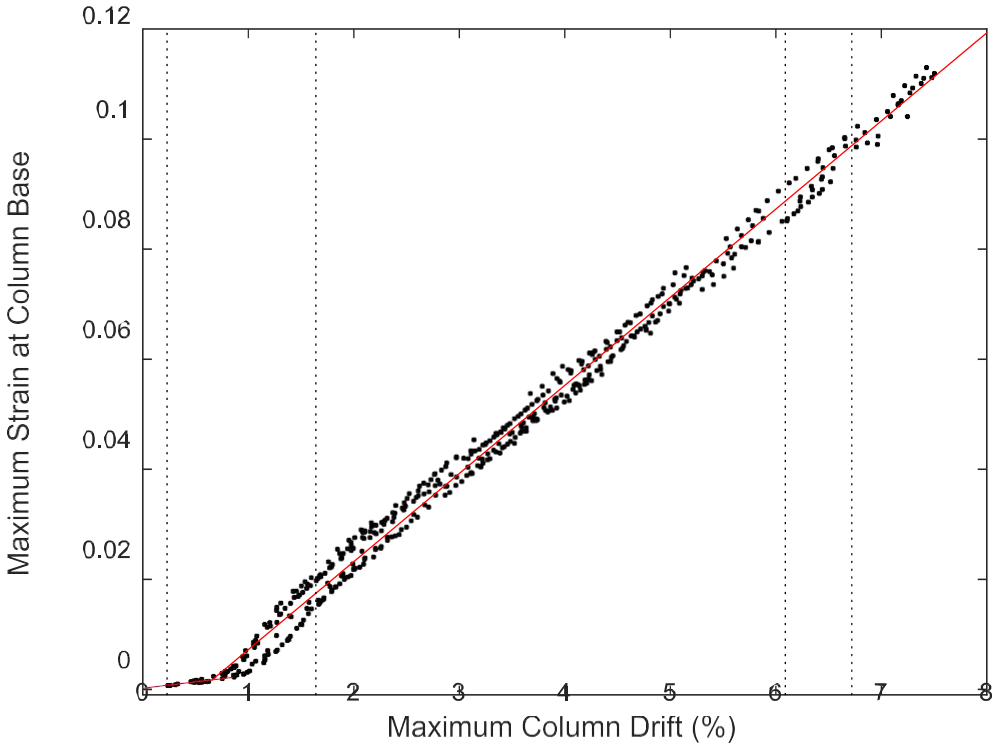

Bridge 1Br – Transverse Ground Motion

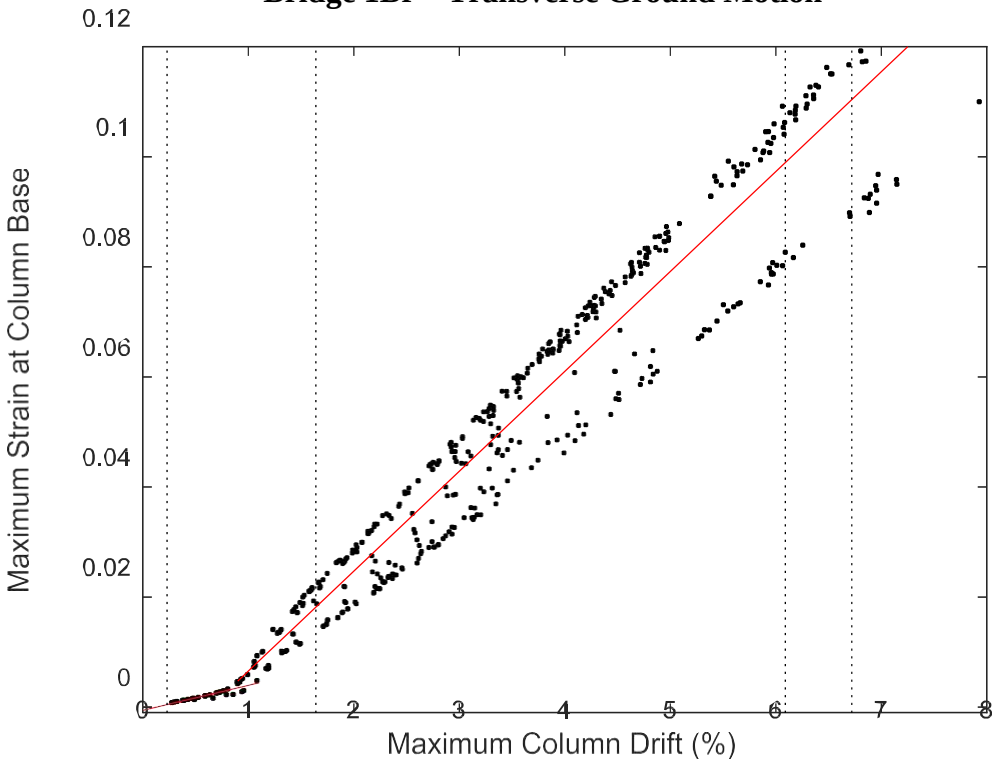

Bridge 1Bs – Longitudinal Ground Motion

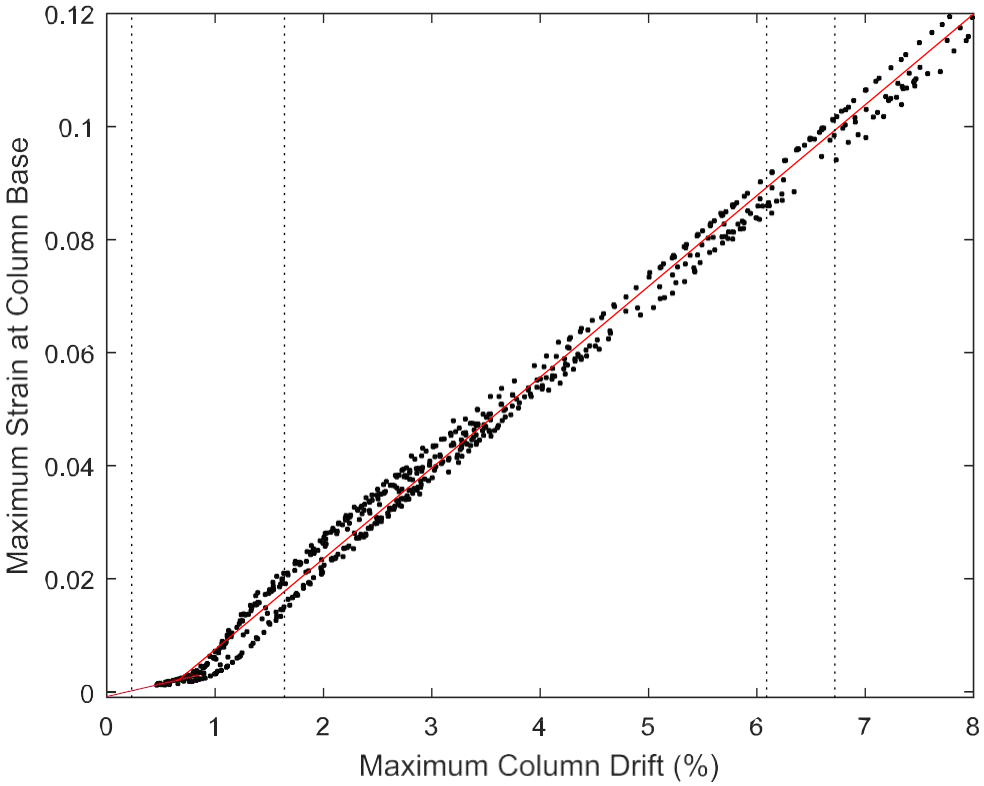

Bridge 1Bs – Transverse Ground Motion

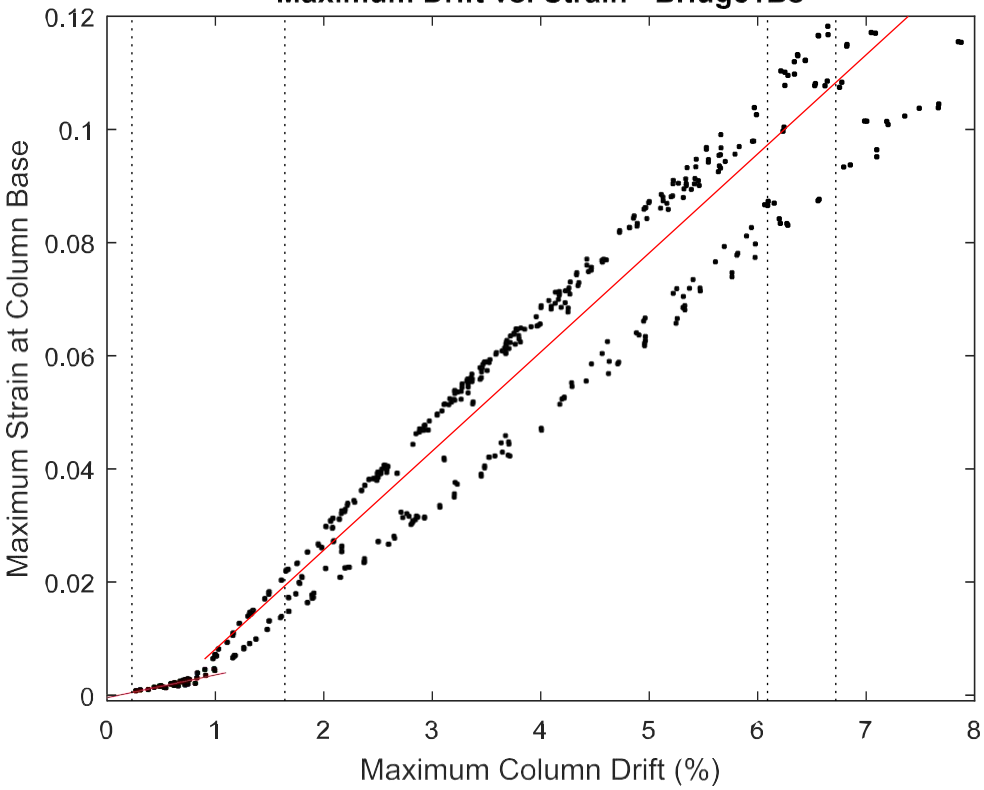

Bridge 11Ar – Longitudinal Ground Motion

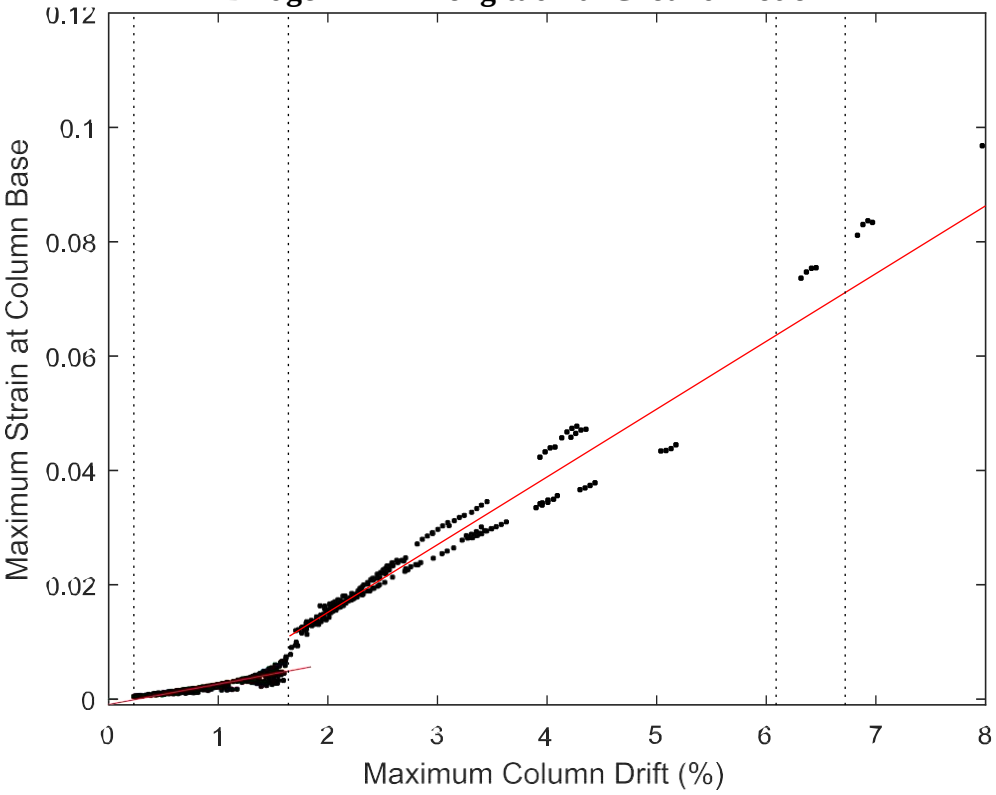

Bridge 11Ar – Transverse Ground Motion

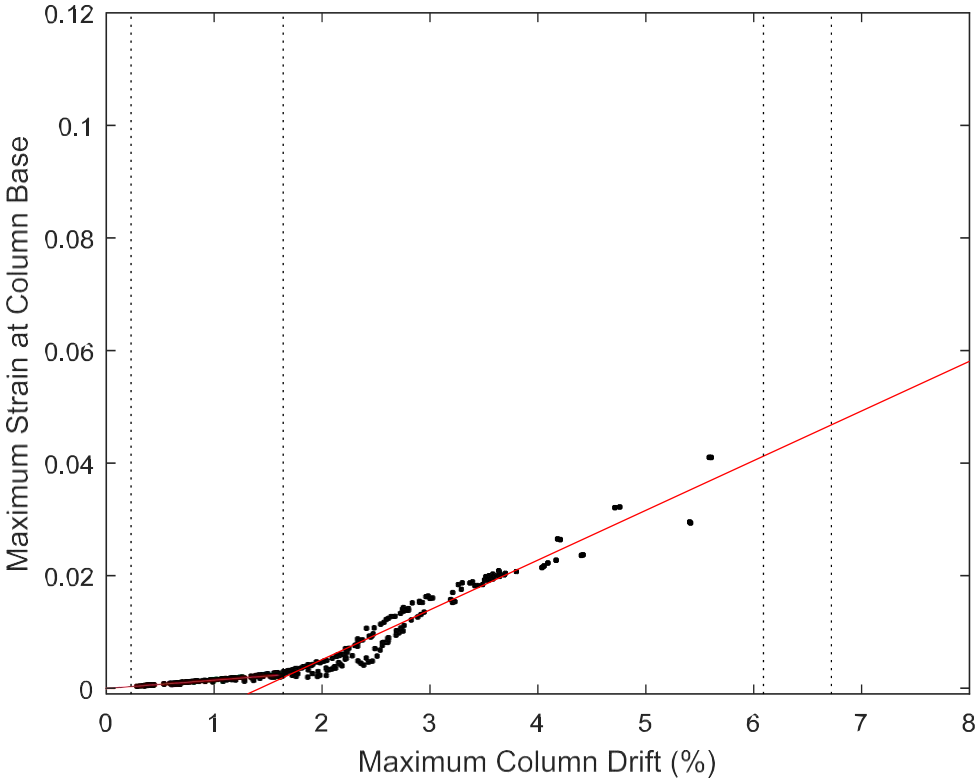

Bridge 11As – Longitudinal Ground Motion

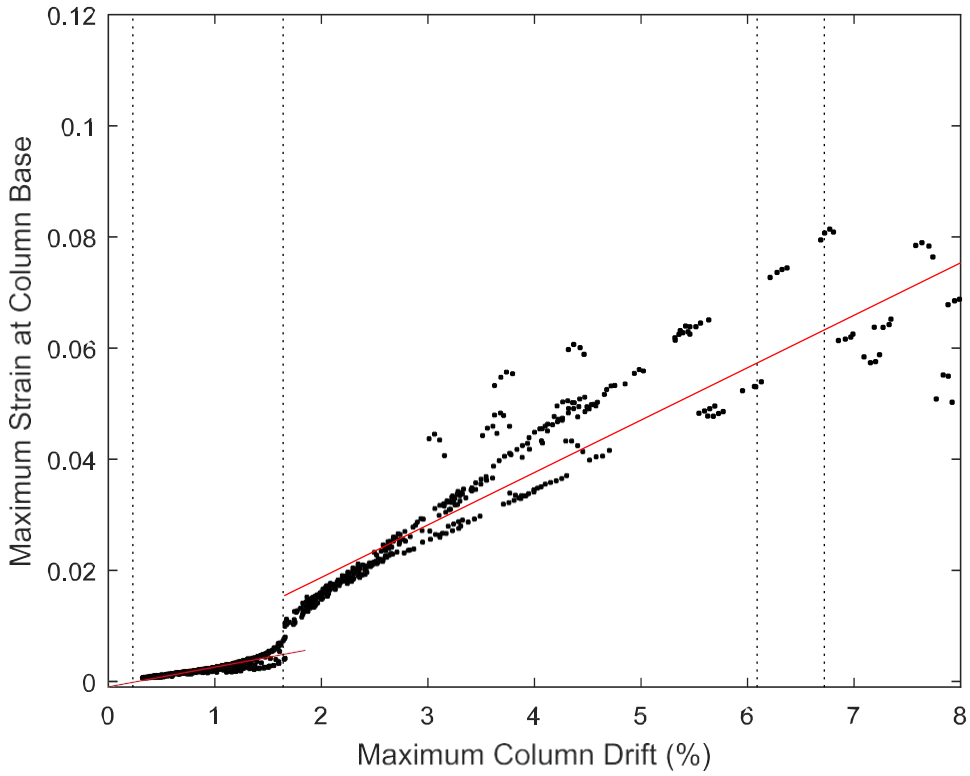

Bridge 11As – Transverse Ground Motion

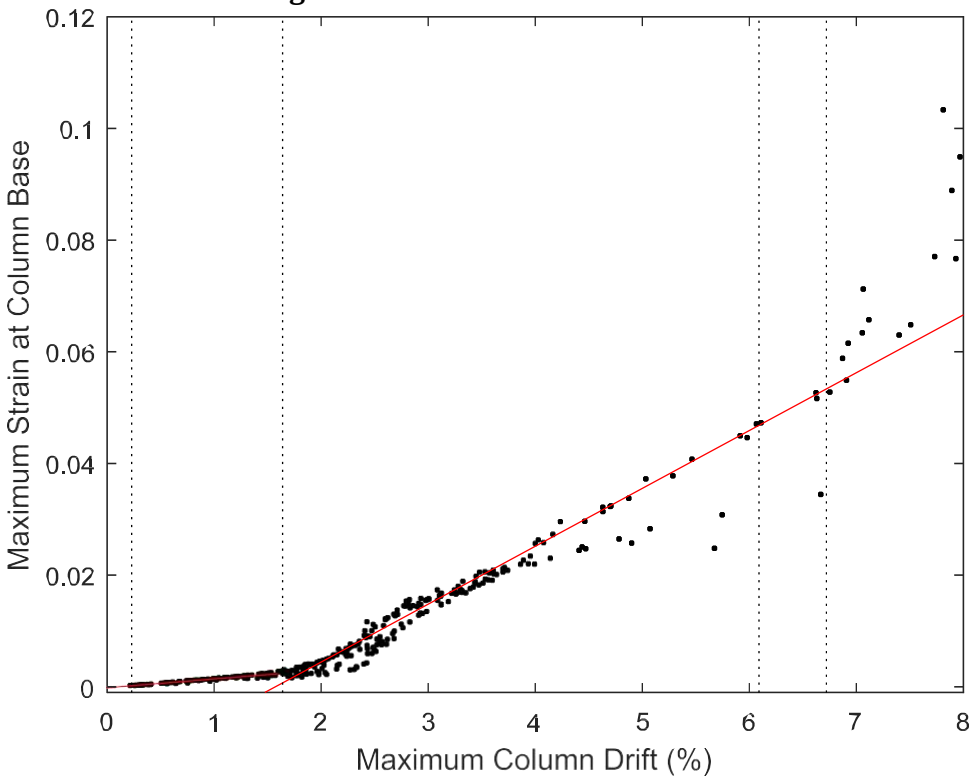

Bridge 11Br – Longitudinal Ground Motion

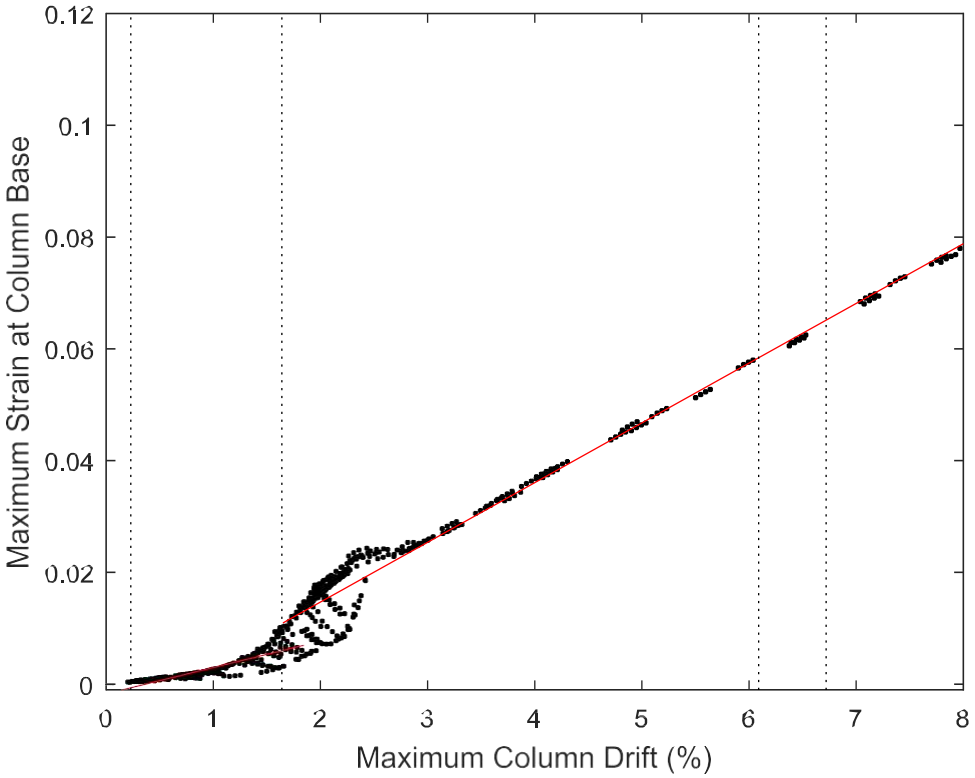

Bridge 11Br – Transverse Ground Motion

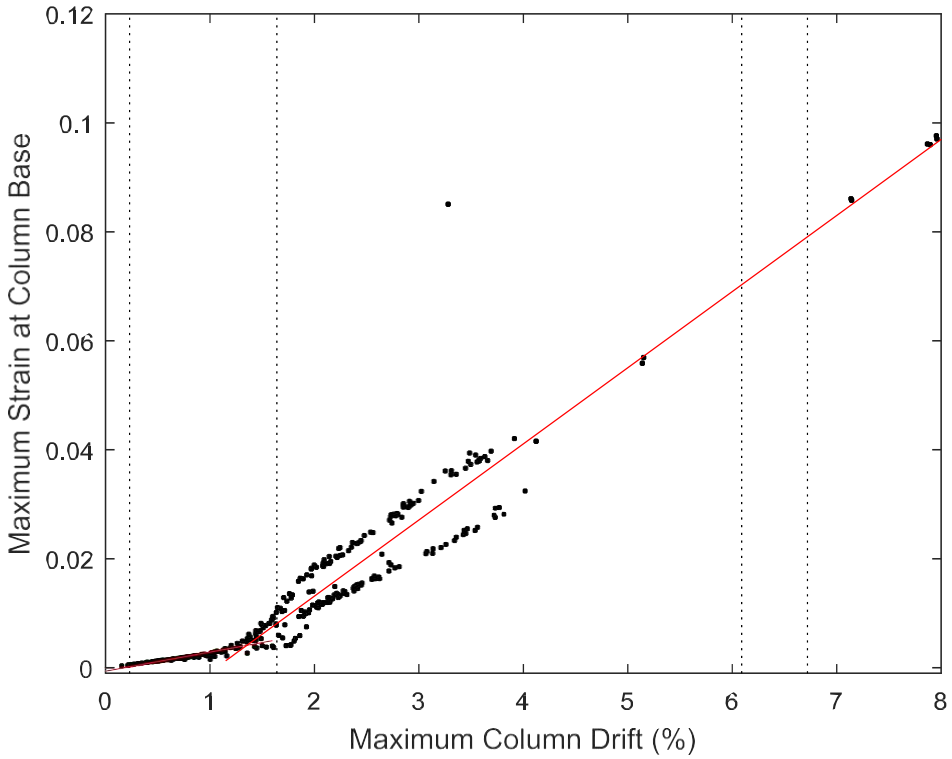

Bridge 11Bs – Longitudinal Ground Motion

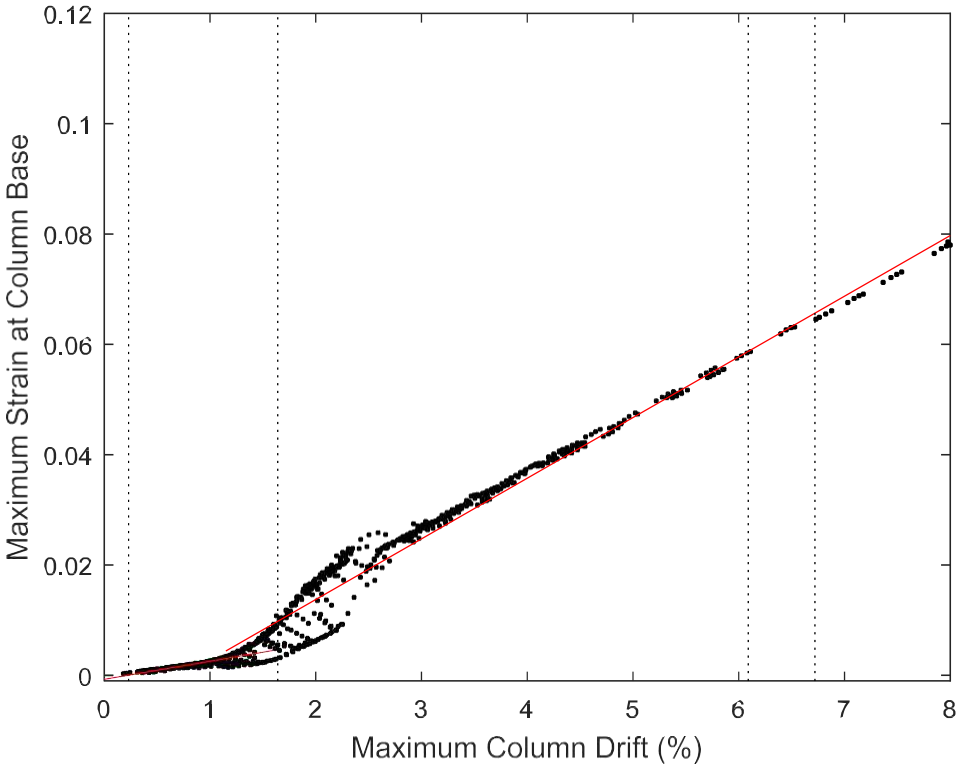

Bridge 11Bs – Transverse Ground Motion

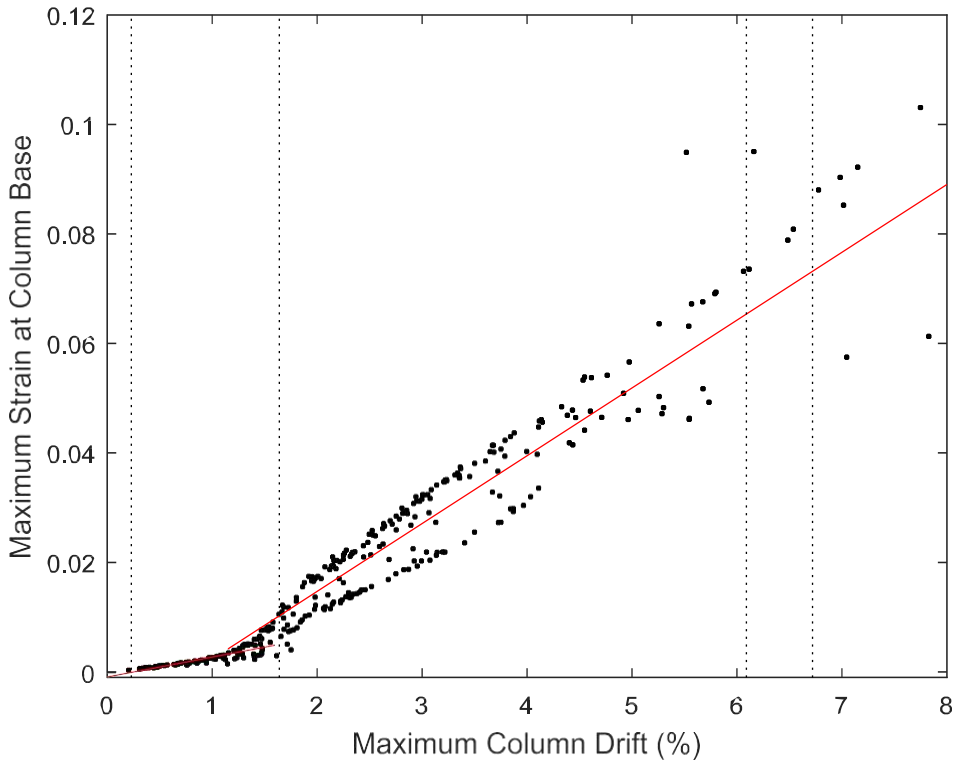

Residual Strain vs Residual Drift Plots

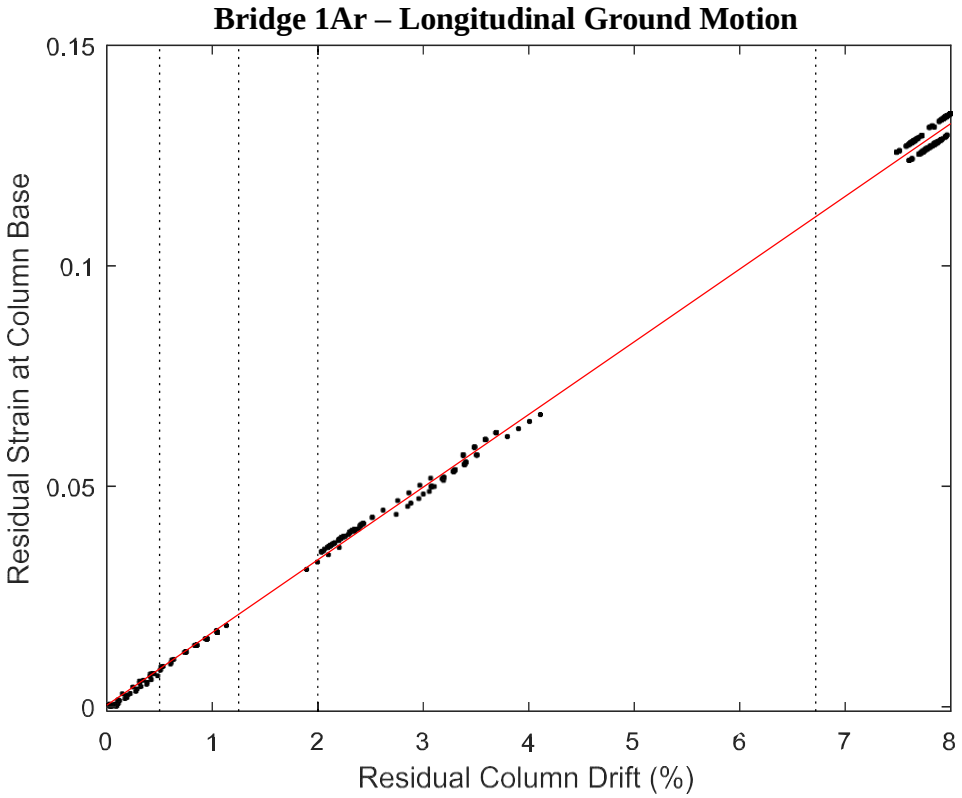

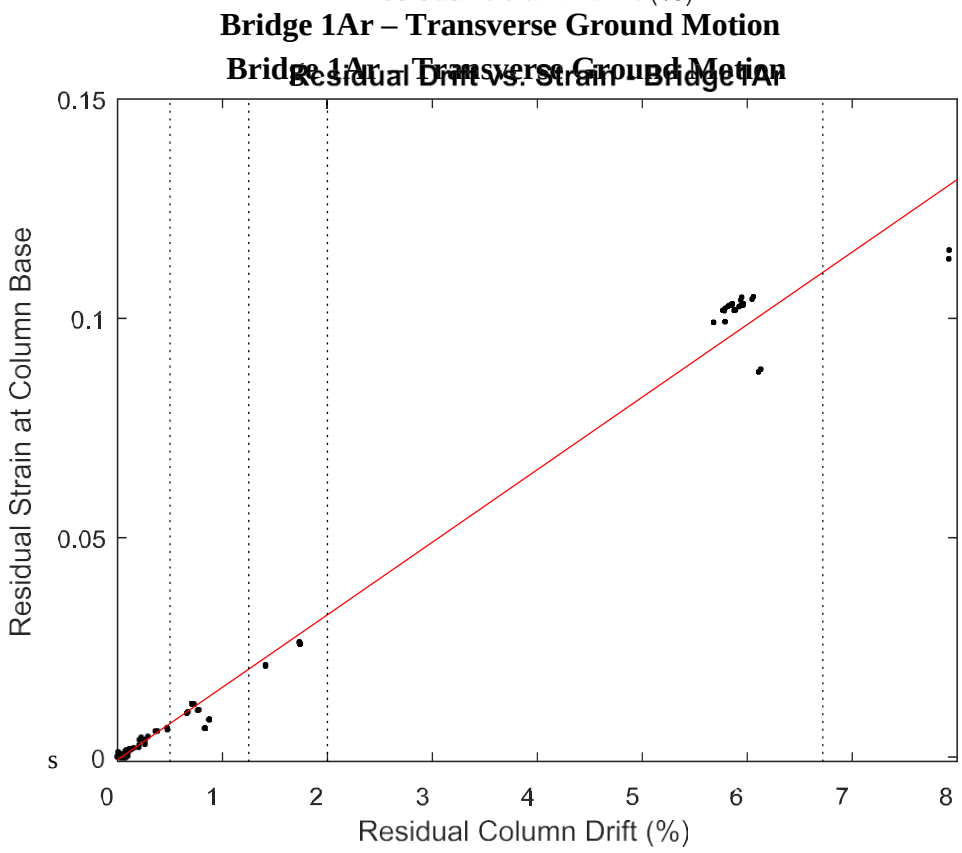

Bridge 1As – L Ground Motion

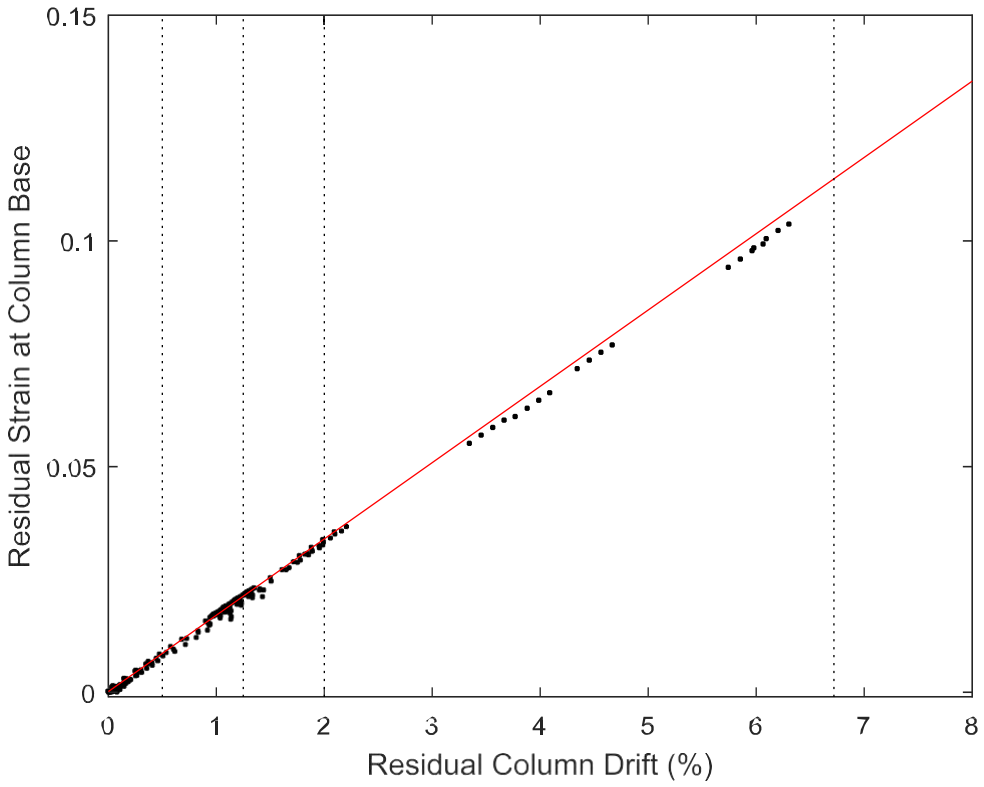

Bridge 1As – Transverse Ground Motion

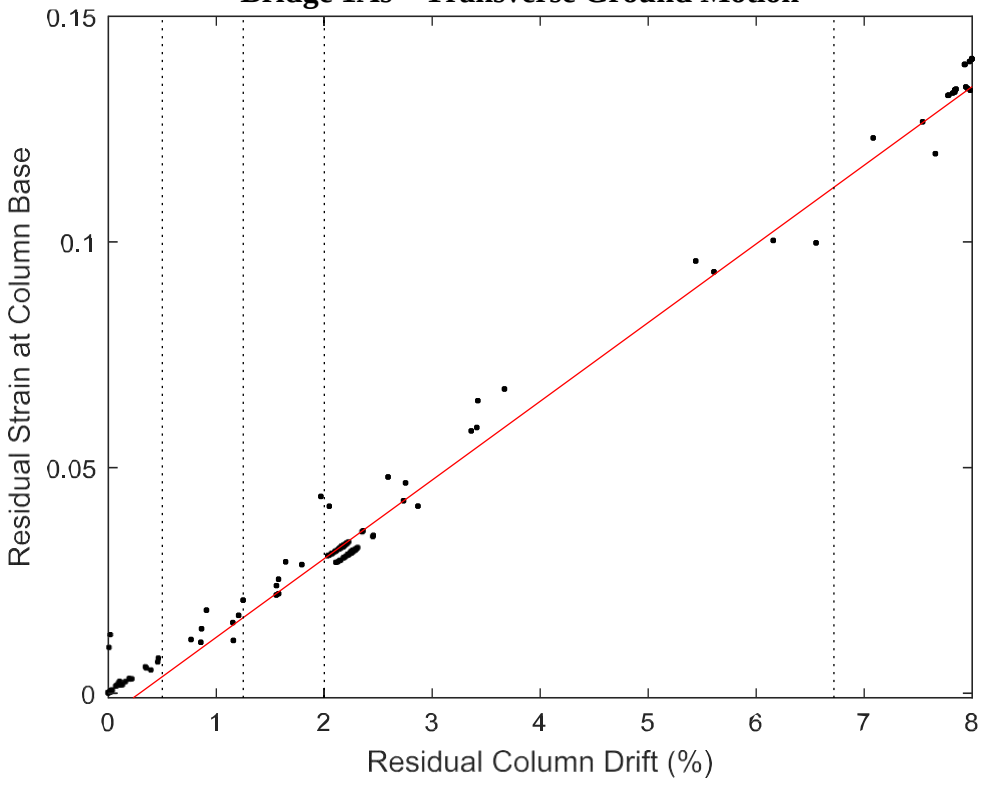

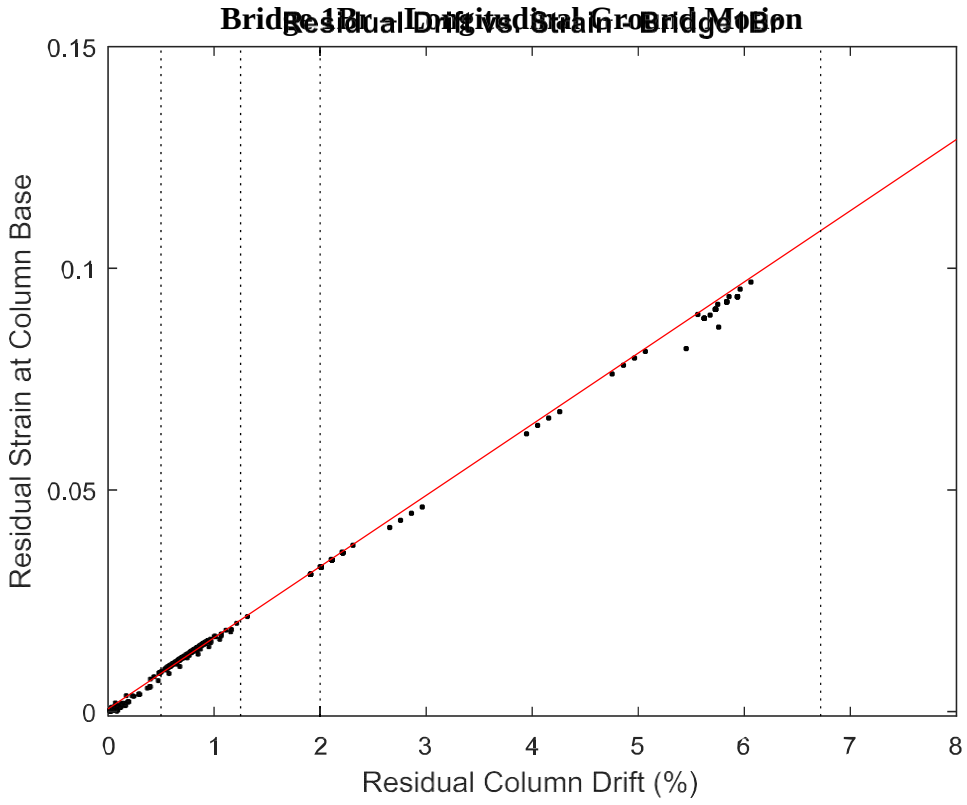
Residual Strain at Column Base
Residual Column Drift (%)
0
0.05
0.1
0.15
0
1
2
3
4
5
6
7
8

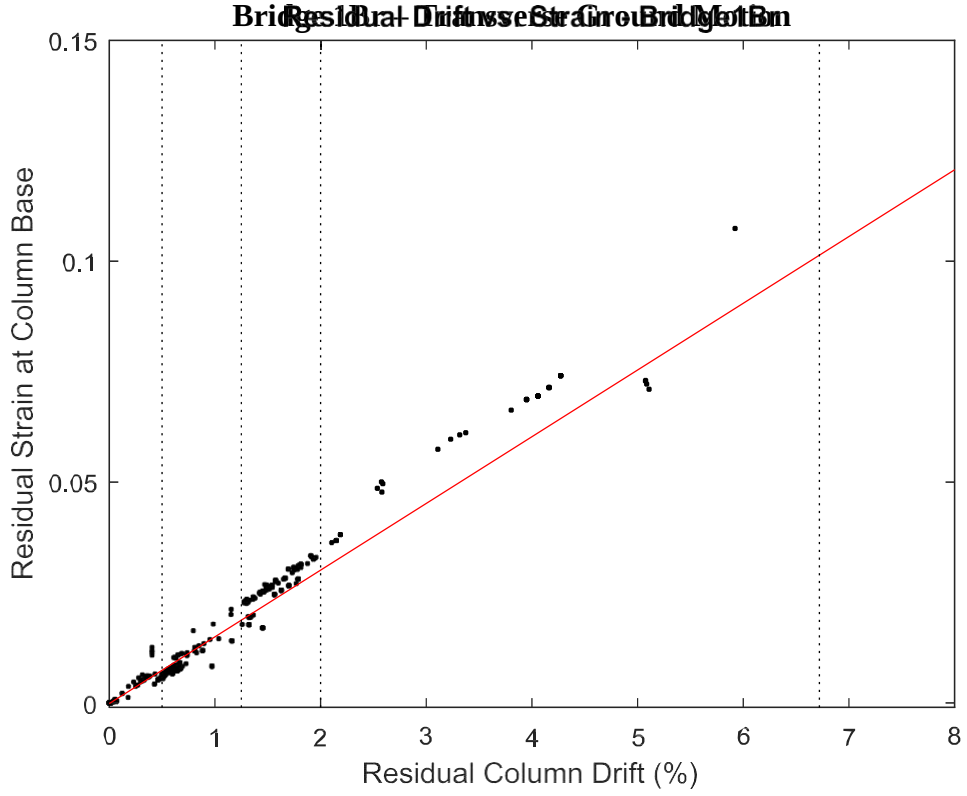
Residual Strain at Column Base
Residual Column Drift (%)
0
0.05
0.1
0.15
0
1
2
3
4
5
6
7
8

Bridge 1Bs – Longitudinal Ground Motion

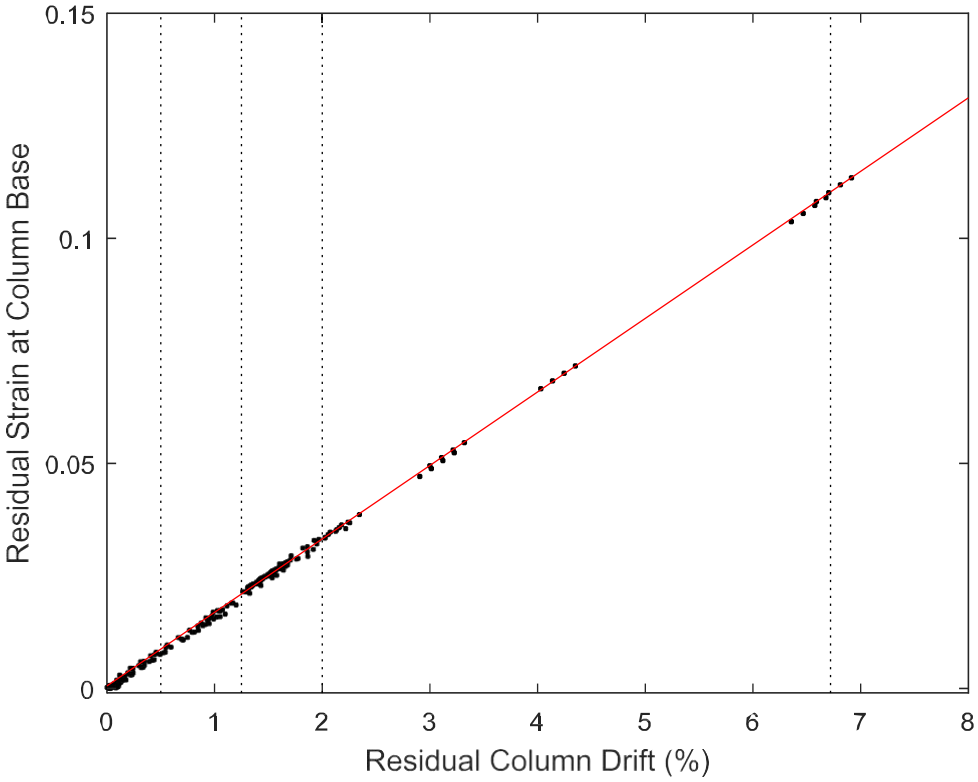

Bridge 1Bs – Transverse Ground Motion

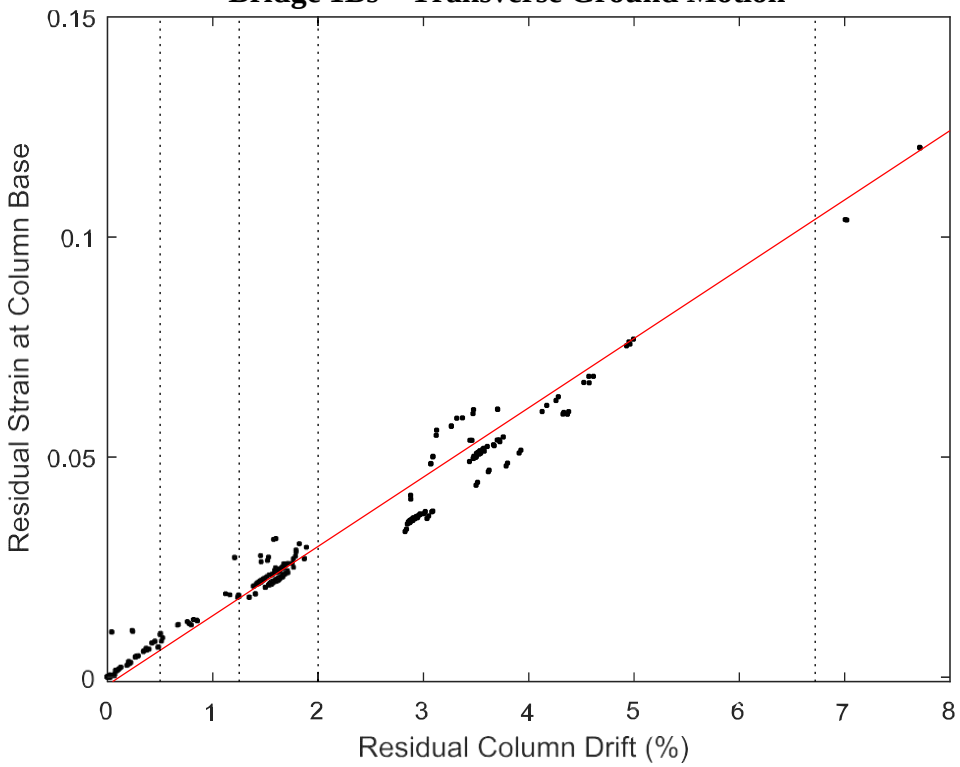

Bridge 11Ar – Longitudinal Ground Motion

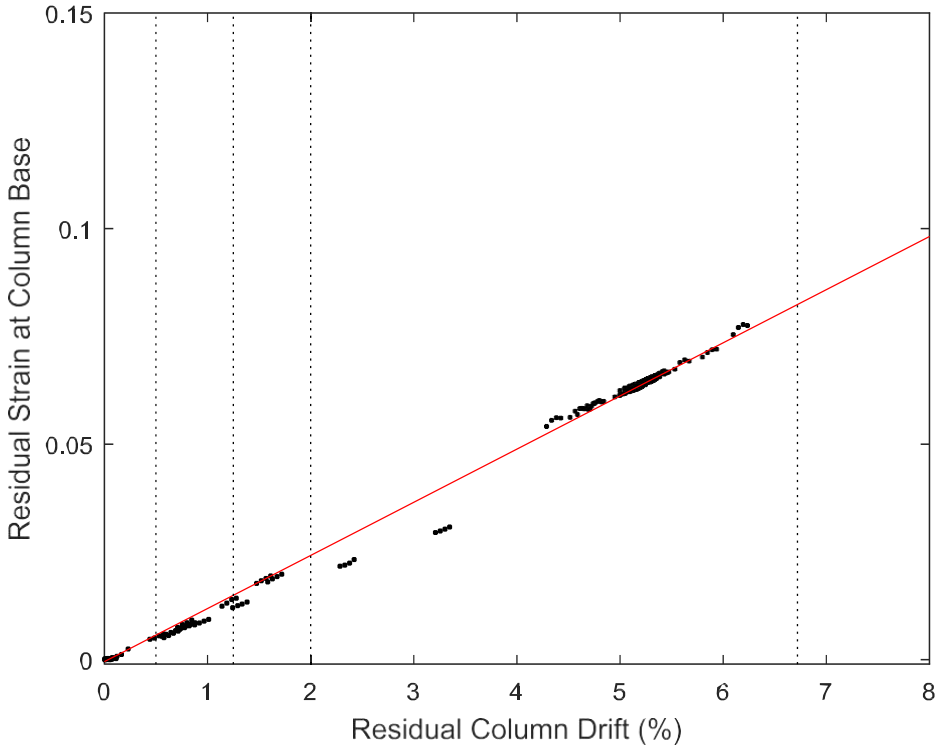

Bridge 11Ar – Transverse Ground Motion

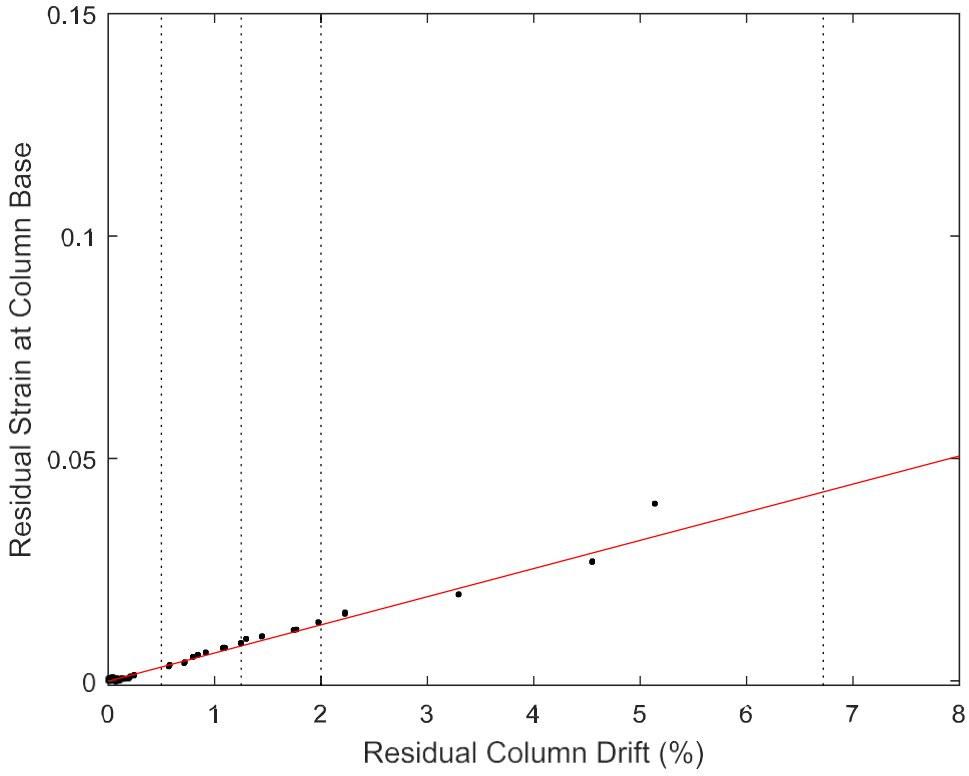

Bridge 11As – Longitudinal Ground Motion
Residual Drift vs. Strain – Bridge 11As

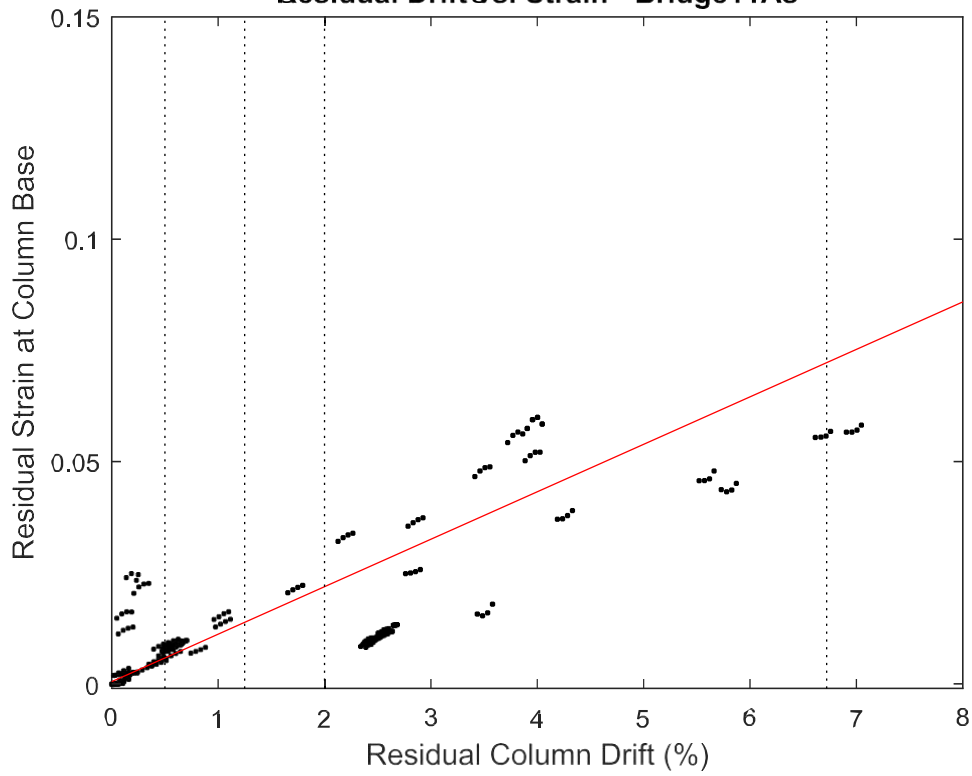

Bridge 11As – Transverse Ground Motion

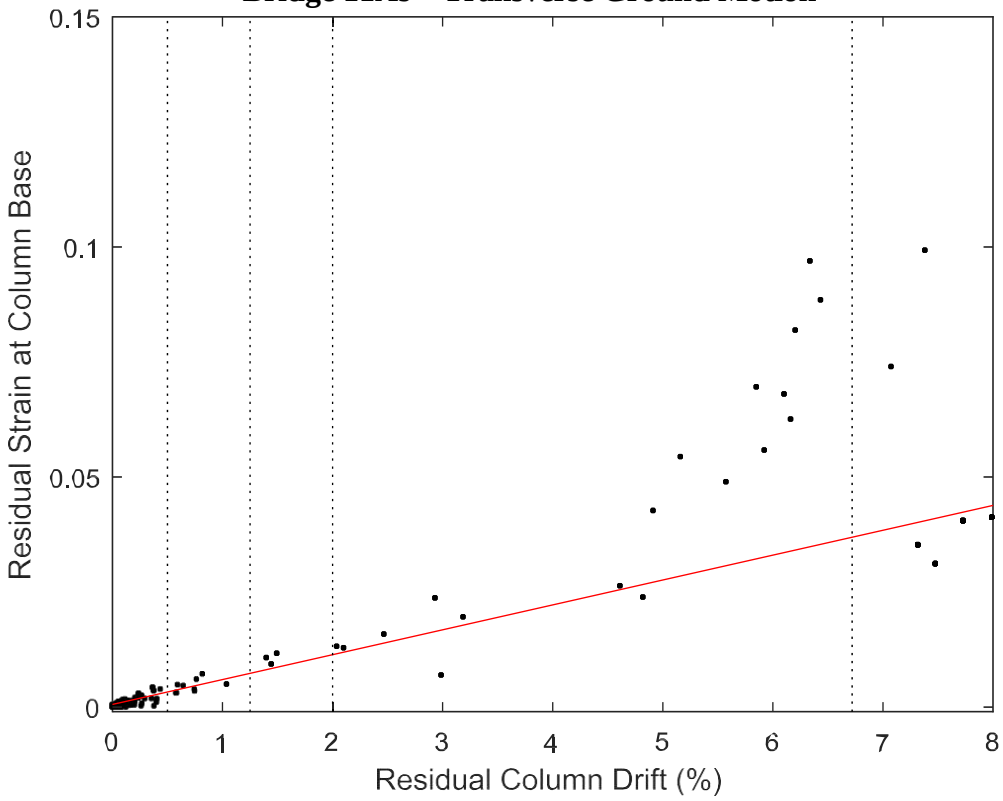

Bridge 11Br – Longitudinal Ground Motion

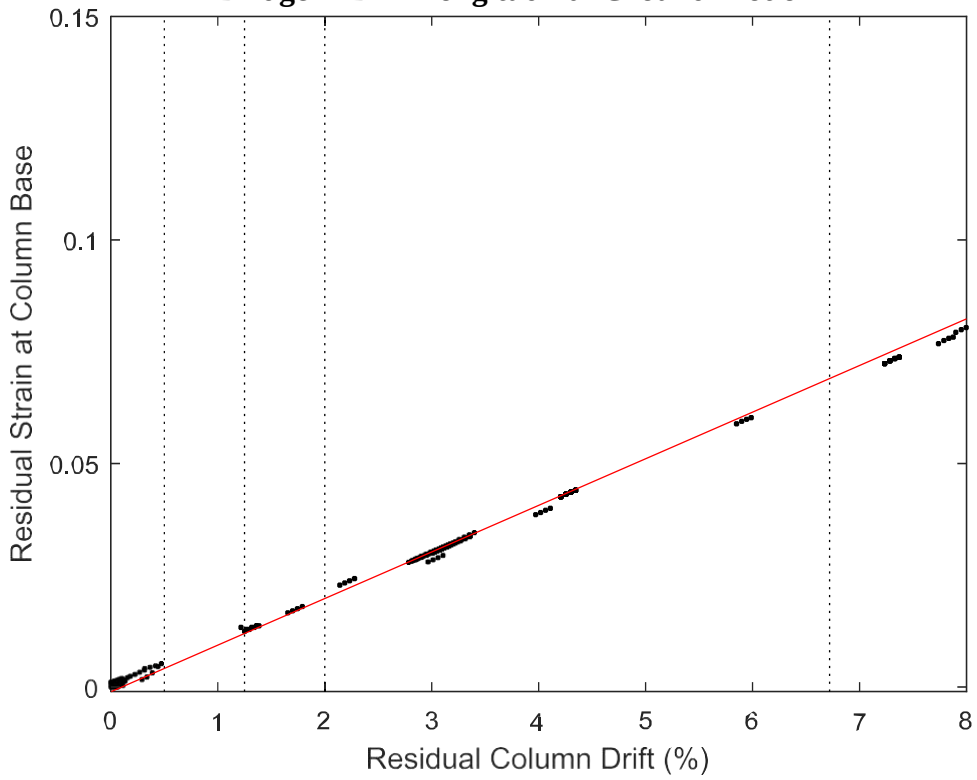

Bridge 11Br – Transverse Ground Motion

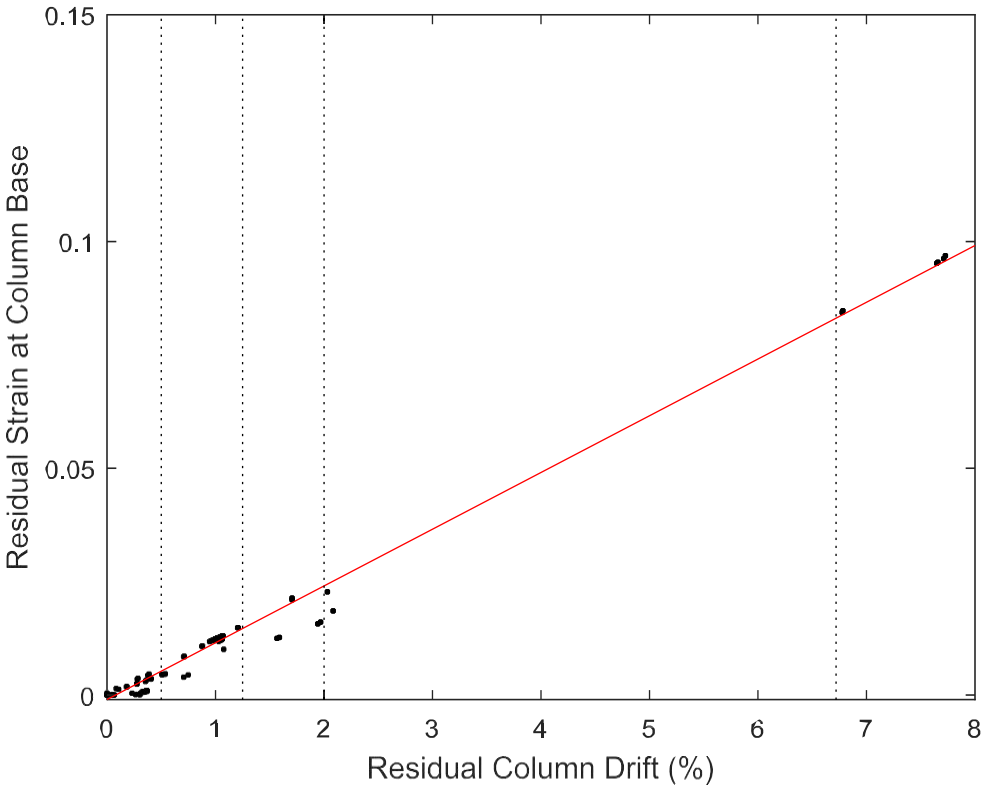

Bridge 11Bs – Longitudinal Ground Motion

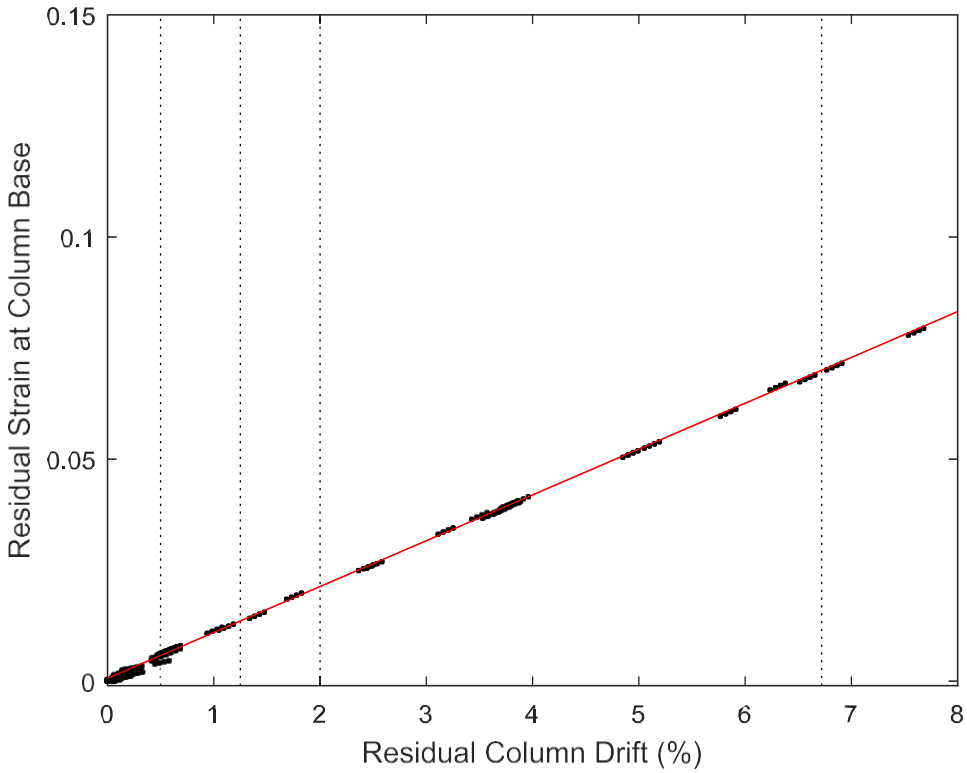

Bridge 11Bs – Transverse Ground Motion

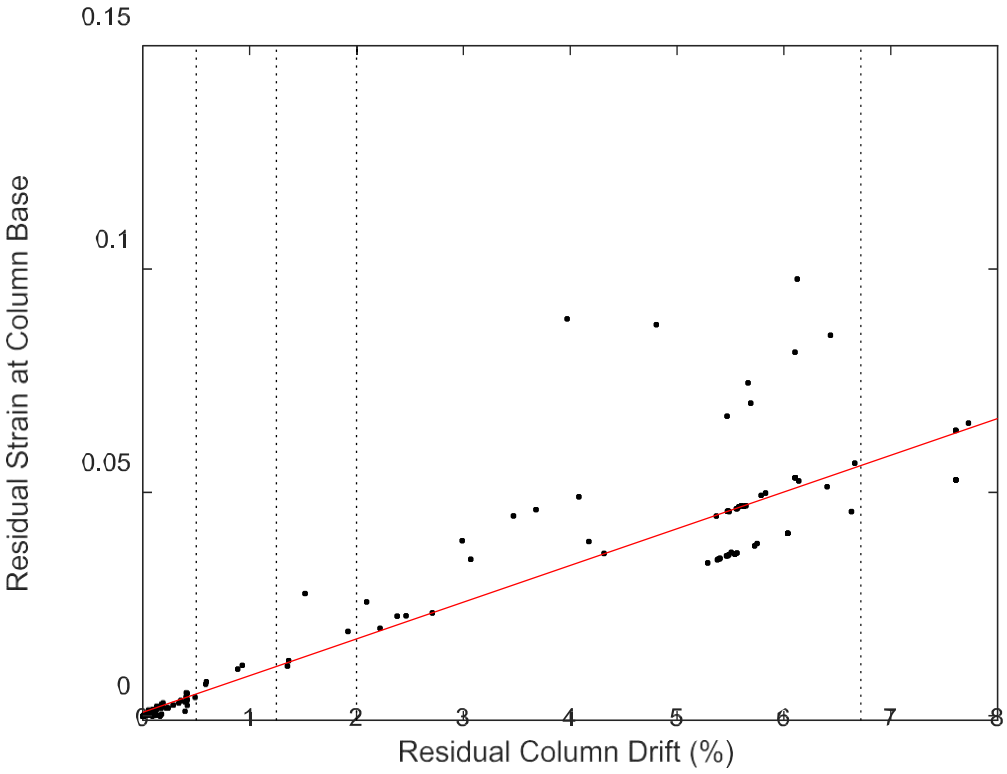

Maximum Strain Limit Values

Type 1 Bridges

Drift:	*0.23%*	*1.64%*	*6%*	*6.72%*
	DS0	**DS1**	**DS2**	**DS3**
Average	0.00053	0.0193	0.0943	0.1049
Std. Dev.	0.00018	0.0014	0.0044	0.0049

Longitudinal Ground Motion

Drift:	*0.23%*	*1.64%*	*6%*	*6.72%*
	DS0	**DS1**	**DS2**	**DS3**
1Ar	0.00055	0.0197	0.0900	0.0999
1As	0.00081	0.0195	0.0923	0.1025
1Br	0.00078	0.0175	0.0887	0.0988
1Bs	0.00027	0.0178	0.0892	0.0994

Transverse Ground Motion

Drift:	*0.23%*	*1.64%*	*6%*	*6.72%*
	DS0	**DS1**	**DS2**	**DS3**
1Ar	0.00035	0.0208	0.1002	0.1115
1As	0.00051	0.0216	0.0975	0.1082
1Br	0.00046	0.0182	0.0989	0.1104
1Bs	0.00050	0.0193	0.0973	0.1083

Type 11 Bridges

Drift:	*0.23%*	*1.64%*	*6%*	*6.72%*
	DS0	**DS1**	**DS2**	**DS3**
Average	0.00022	0.0045	0.0577	0.0647
Std. Dev.	0.00018	0.0012	0.0090	0.0098

Longitudinal Ground Motion

Drift:	*0.23%*	*1.64%*	*6%*	*6.72%*
	DS0	**DS1**	**DS2**	**DS3**
1Ar	0.00012	0.0049	0.0636	0.0711
1As	0.00014	0.0049	0.0573	0.0633
1Br	0.00062	0.0060	0.0584	0.0651
1Bs	0.00008	0.0047	0.0587	0.0656

Transverse Ground Motion

Drift:	*0.23%*	*1.64%*	*6%*	*6.72%*
	DS0	**DS1**	**DS2**	**DS3**
1Ar	0.00032	0.0024	0.0412	0.0468
1As	0.00030	0.0025	0.0468	0.0534
1Br	0.00015	0.0051	0.0703	0.0791
1Bs	0.00004	0.0051	0.0654	0.0732

Residual Strain Limit Values

Type 1 Bridges

Drift:	*0.50%*	*1.25%*	*2%*	*6.72%*
	DS0	**DS1**	**DS2**	**DS3**
Average	0.0074	0.0197	0.0319	0.1090
Std. Dev.	0.0016	0.0016	0.0016	0.0039

Longitudinal Ground Motion

Drift:	*0.50%*	*1.25%*	*2%*	*6.72%*
	DS0	**DS1**	**DS2**	**DS3**
1Ar	0.0086	0.0210	0.0333	0.1111
1As	0.0086	0.0213	0.0340	0.1138
1Br	0.0086	0.0207	0.0327	0.1085
1Bs	0.0087	0.0210	0.0332	0.1103

Transverse Ground Motion

Drift:	*0.50%*	*1.25%*	*2%*	*6.72%*
	DS0	**DS1**	**DS2**	**DS3**
1Ar	0.0077	0.0201	0.0325	0.1105
1As	0.0037	0.0168	0.0298	0.1121
1Br	0.0074	0.0187	0.0301	0.1014
1Bs	0.0061	0.0179	0.0297	0.1040

Type 11 Bridges

Drift:	*0.50%*	*1.25%*	*2%*	*6.72%*
	DS0	**DS1**	**DS2**	**DS3**
Average	0.0048	0.0119	0.0190	0.0640
Std. Dev.	0.0010	0.0028	0.0046	0.0162

Longitudinal Ground Motion

Drift:	*0.50%*	*1.25%*	*2%*	*6.72%*
	DS0	**DS1**	**DS2**	**DS3**
1Ar	0.0057	0.0149	0.0242	0.0824
1As	0.0058	0.0139	0.0219	0.0722
1Br	0.0042	0.0120	0.0198	0.0690
1Bs	0.0058	0.0136	0.0213	0.0700

Transverse Ground Motion

Drift:	*0.50%*	*1.25%*	*2%*	*6.72%*
	DS0	**DS1**	**DS2**	**DS3**
1Ar	0.0031	0.0078	0.0126	0.0425
1As	0.0033	0.0073	0.0114	0.0369
1Br	0.0053	0.0147	0.0240	0.0831
1Bs	0.0049	0.0110	0.0172	0.0560